Evaluation of the Relationship between Friction, Texture, and Noise Properties of Preservation Treatment

FINAL PROJECT REPORT

by

Jorge A Prozzi
The University of Texas at Austin

Sponsorship
Texas Department of Transportation

for

Center for Highway Pavement Preservation
(CHPP)

UNIVERSITY TRANSPORTATION CENTER for HIGHWAY PAVEMENT PRESERVATION

In cooperation with US Department of Transportation-Research and Innovative Technology Administration (RITA)

June 2021

Disclaimer

The contents of this report reflect the views of the authors, who are responsible for the facts and the accuracy of the information presented herein. This document is disseminated under the sponsorship of the U.S. Department of Transportation's University Transportation Centers Program, in the interest of information exchange. The Center for Highway Pavement Preservation (CHPP), the U.S. Government, and matching sponsor assume no liability for the contents or use thereof.

Technical Report Documentation Page

1. Report No. CHPP Report-UTA#7-2021	2. Government Accession No.	3. Recipient's Catalog No.

4. Title and Subtitle Evaluation of the Relationship between Friction, Texture, and Noise Properties of Preservation Treatments	5. Report Date 6. Performing Organization Code
7. Author(s) Christian Sabillon-Orellana, Ruohan Li, Joaquin B. Hernandez and Jorge A Prozzi	8. Performing Organization Report No.
9. Performing Organization Name and Address CHPP Center for Highway Pavement Preservation, Tier 1 University Transportation Center Michigan State University, 2857 Jolly Road, Okemos, MI 48864	10. Work Unit No. (TRAIS) 11. Contract or Grant No.
12. Sponsoring Organization Name and Address United States of America Department of Transportation Research and Innovative Technology Administration	13. Type of Report and Period Covered 14. Sponsoring Agency Code

15. Supplementary Notes
Report uploaded at http://www.chpp.egr.msu.edu/

16. Abstract
This research project used texture, friction, and noise data collected along a number of asphalt pavements with different surface types across Texas to explore the intercorrelation between the three measures, both within each surface type and across different types. The research team found that across all surface types, the entire frequency band of noise from 400 to 5000 Hz correlates the strongest with texture of wavelengths from 31.5 to 2.5 mm positively, indicating that regardless of the surface type, pavements with a higher texture level in the wavelength spectrum of 31.5 mm to 2.5 mm tend to generate a higher level of noise. When each one-third octave band frequency noise is analyzed individually, the strongest positive correlation is found between noise of 630 Hz and texture of 50 mm wavelength. A negative correlation, however, is found between higher frequency ($f > 1000$ Hz) noise and shorter wavelength ($\lambda < 10$ mm) texture. The slope of noise versus texture is similar across different pavements, but the intercept can be different, indicating that with a unit increase in texture level, the additional noise generated by different pavements is of similar magnitude, but they might be at different levels of loudness given the same texture level. Across all pavement types, when texture level is the same, pavements with a thin overlay mix (TOM) surface tend to generate a consistently lower level of noise at both high and low frequencies. While no strong correlation was found between noise and friction, this finding is consistent with the conclusions from studies by many previous researchers.

17. Key Words Friction, Skid, Texture, Noise, Pavement Preservation, Surface Treatments	18. Distribution Statement No restrictions.

19. Security Classification (of this report) Unclassified.	20. Security Classification (of this page) Unclassified.	21. No. of Pages	22. Price NA

Form DOT F 1700.7 (8-72) Reproduction of completed page authorized.

Table of Contents

List of Figures

List of Tables

List of Abbreviations

AIMS	Aggregate Imaging System
BPN	British Pendulum number
BPT	British Pendulum test
CHPP	Center of Highway Pavement Preservation
CPX	close-proximity
CTM	circular track meter
dB	decibel
dBA	A-weighted decibel
DFT	discrete Fourier transform
GN	Grip Number
IFI	International Friction Index
IRI	International Roughness Index
LFC	longitudinal friction coefficient
LLS	Line Laser Scanner
MDOT	Michigan Department of Transportation
MLR	multiple linear regression
MPD	mean profile depth
MTD	mean texture depth
OBSI	on-board sound intensity
PCC	Portland cement concrete
PFC	permeable friction course
PSD	power spectral density
RMS	root mean square
SN	skid number
SLR	simple linear regression
SPB	statistical pass-by
SPL	sound pressure level
SPT	sand patch test
SRI	Skid Resistance Index
SRTT	Standard Reference Test Tire
TLD	texture level distribution

TOM	thin overlay mix
WFT	water film thickness

Acknowledgments

This study was conducted as part of the U.S. Department of Transportation's University Transportation Centers Program, under the Center for Highway Pavement Preservation (CHPP) and co-sponsored by the Texas Department of Transportation. The authors want to thank the students who helped collect samples throughout Texas over the summer months. The guidance of Dr. Andre Smit in the topic of noise is deeply acknowledged, as well as Mr. John Wirth who lend us an OBSI equipment for capturing noise data.

Executive Summary

Federal, state, and local highway agencies are increasing the demands on the performance and functionality of preservation treatments. It is no longer sufficient to extend the structural performance of highway pavements. Now there are growing demands to provide higher surface friction, lower pavement noise, higher durability, and reduced splash and spray. The technical objective of this study was to evaluate roadway surface characteristics—namely, texture, friction and tire/pavement noise—and assess their relationships. Field sections were evaluated to establish meaningful relationships between friction and noise. The on-board sound intensity (OBSI), GripTester, and the UT Line Laser Scanner (LLS) were the primary noise, friction and texture measuring devices, respectively. Nonetheless, other technologies for measuring friction and texture were also used, evaluated, and compared against the main pieces of equipment. The analysis included empirical data collected around the Texas highway network of varying asphalt mixes.

Among the major findings, the empirical data suggested there is no unique relationship between noise and friction. However, the relationship both measures have with pavement texture was found to be significant. A trend in noise was found across all highways, independent of asphalt mix, resulting in a correlation being maximized or texture wavelengths from 50 mm to 2.5 mm. These wavelengths encompass the full first decade of macrotexture. The finding indicates that as texture level increases, the noise intensity level increases as well. When both noise and texture are analyzed at individual one-third octave band frequencies and wavelengths, respectively, different trends are found in two separate, and most likely independent spectra. Noise of 630 Hz frequency was found to have maximally positive correlation with texture level of 50 mm wavelength, while the negative correlation was spread over a wider domain of texture wavelengths and range of frequencies. Not a single point of maximally negative correlation could be established. Overall, low frequency noise (less than 1000 Hz) correlates positively with large-scale texture ($\lambda > 10$ mm), and high frequency noise correlates negatively with small-scale texture. Regarding friction, the authors found that the GripTester is an apt device for measuring friction as it does not require traffic control, operates at highway speeds, and has a good correlation with the surface texture indicator, the mean profile depth (MPD). The highest coefficient of determination values, when correlating the MPD with the Grip Number (GN), were obtained when the GN was collected at 70 km/h (43.5 mph).

Chapter 1. Introduction

Federal, state, and local highway agencies are increasing the demands on the performance and functionality of preservation treatments. It is no longer sufficient to extend the structural performance of highway pavements. Now there are growing demands to provide higher surface friction, lower pavement noise, higher durability, and reduced splash and spray. Domenichini et al. (1999) pointed out that pavement characteristics are to be designed to fulfill structural (capacity), environmental (noise and vibrations), and safety (friction, hydroplaning, splash and spray) requirements. Hoerner and Smith (2002) described the two components of pavement performance: structural performance (the ability to carry traffic loads) and functional performance (the ability to provide a smooth, safe, and comfortable ride to travelers). Flinsch et al. (2003) define a good level of ride quality as the combination of good friction, low levels of roughness, and low levels of noise. Ahammed and Tighe (2010) cited Descornet (1989) in identifying the characteristics to consider while designing an optimized pavement surface. These characteristics include safety (in terms of skid resistance, tire grip, splash and spray, and visibility of road and pavement markings); economy (in terms of fuel consumption, vehicle/tire wear, and extra dynamic loads on pavements); and comfort of drivers and nearby residents (in terms of noise and vibration both inside and outside the vehicle).

Traffic noise has become an increasingly concerning issue. As cities expand in both size and population, the level of traffic-induced noise increases as well. As time progresses, an increasing number of people are being exposed to high levels of traffic noise both at home and work. Traffic noise is considered an environmental pollutant that negatively affects human health. According to the World Health Organization (WHO) Guidelines for Community Noise, road traffic is the largest source of community noise in most cities, especially where traffic volumes and speeds are high (Berglund, 2000). Examples of health effects resulting from prolonged exposure to environmental noise include increased risk of ischemic heart disease, sleep disturbance, cognitive impairment among children, annoyance, stress-related mental health risks, and tinnitus (Ohiduzzaman et al., 2016, Berglund, 2000). Clearly, a lengthy exposure to high levels of traffic noise can have detrimental effects on the quality of life of people living or working in proximity to heavily trafficked roadways (Smit et al., 2016). The WHO also states that people in high-income European countries lose a total of more than 1 million healthy years of life to these risks combined. The European Union's Seventh Environment Action Programme (7th EAP) defines high noise levels as noise levels for L_{den} (annual average day, evening, and night exposure to noise) above 55 dB and for L_{night} (averaged across the night period) above 50 dB (EEA, 2019). In the European Union (EU), about 40% of the population is exposed to traffic noise over 55 A-weighted decibels (dBA) during daytime, and 20% to levels over 65 dBA. Even at night, more than 30% of the population are exposed to noise levels exceeding 55 dBA, a level that is disturbing to sleep. Though noise has not been given as much attention in the United States compared to the EU nations, in a study conducted in Fulton County, Georgia, Seong et al. (2011) found that 48% of the total county population (870,166 residents) are potentially exposed to noise levels 55 dBA or higher during daytime, while 32% are exposed to noise levels higher than 50 dBA at night, confirming that noise problems similar to those in the EU nations exist in the United States as well. For these reasons, transportation agencies around the world are focusing their efforts to develop a fundamental understanding of the main parameters that influence the noise levels on the roadways.

Braun et al. (2013) classified the noise sources into engine noise, intake and exhaust system noise, and tire/road noise. In 1974, Harland identified rolling noise as the dominant noise source for light vehicles traveling at high speeds, one that makes a measurable contribution to noise levels under many other conditions. However, Zeller (2009) pointed out that unlike other noise sources, tire/road noise has not been effectively reduced over the years. While efforts continue to reduce the noise emitted by vehicle power units, resulting in quieter engines, power trains, and exhaust systems, unchanged is the level of tire/road noise, which may vary more than 15 dB under the same speed with different tire/road combinations and remains a major contributor to overall traffic noise (Sandberg and Descornet, 1980, Chandler et al., 2003, Haider et al., 2007). Elsenaar et al. (1977) noted that rolling noise becomes the major part among all sources of traffic noise at speeds above 37.5 mph (60 km/h) for light vehicles. Heckl (1986) cited Sandberg (1982) stating that for passenger cars traveling at speeds above 31 to 37.5 mph (50–60 km/h) and trucks at speeds above 50 to 56 mph (80–90 km/h), tire noise tends to be the dominant source of traffic noise. Domenichini et al. (1999) pointed out that tire-road interaction contributes to 80–90% of the overall traffic noise at speeds higher than 44–50 mph (70–80 km/h). In 2005, researchers Van Keulen and Duskov found that tire/road noise exceeds engine noise and becomes the dominant source at speeds of 22 and 31 mph (35 and 50 km/h) or higher for light vehicle and heavy vehicles, respectively.

For speeds higher than 50 mph (80 km/h), propulsion noise is negligible for light vehicles, whereas for heavy vehicles, though propulsion noise does not become negligible, tire/road noise still accounts for a larger portion of the total traffic noise. In addition, multiple studies have been conducted to understand the interaction between the pavement texture and noise being generated by moving traffic, and while it is known that texture affects tire-pavement noise, the parameters that control this interaction are not yet fully understood (Smit et al., 2016).

Though friction and noise have traditionally been believed to be conflicting characteristics, plenty of studies have shown that do not necessarily have to be incompatible (Elsenaar, 1977, Sandberg and Descornet, 1980). Chandler et al. (2003), citing Abbott and Phillips (1996), noted that the relationship between road surface texture and tire noise differs depending on whether the surface texture is predominantly transverse (brushed concrete) or random (hot rolled asphalt or exposed aggregate concrete surface).

1.1 Objectives and Scope

The technical objective of this study is to evaluate surface treatments in terms of texture, friction, and pavement-noise. The study will evaluate the interrelation between the three measures.

Traditionally, research focused on correlating noise with texture tend to use summary parameters such as mean profile depth (MPD) or overall on-board sound intensity (OBSI) to conduct a statistical analysis and determined whether a correlation exists or not. This practice can be sometimes misleading, because two pavements that have the same MPD can have completely different textures. Likewise, in the case with roads of similar overall OBSI, it is unknown whether the largest component of that noise is coming from low or high frequencies. This work aims to contribute to the literature by taking a different approach to the way in which pavement texture and tire-pavement noise are analyzed, in the hopes of addressing this issue and providing a better understanding of how those parameters interact. This study will use spectral analysis to look at the distribution of data within the frequency domain for both texture and noise and determine whether a correlation exists between the two.

Furthermore, research focused on friction and noise has been attempted before but no significant findings have been discovered. Projects from Europe have devoted great energy to relating pavement parameters with findings only relevant to European equipment not commonly found in the US and not readily available. The GripTester, found in certain European countries, will be the primary friction technology used in the data analysis of this study and will be evaluated against other friction testing technologies found in the US. Recent advancements with electro-optical devices have improved the resolution, speed, and information extracted from asphalt surfaces. The Line Laser Scanner (LLS) will be used to extract texture data to compare with friction and noise.

1.2 ROSANNE Project

In recent years, the EU's ROSANNE project was conducted to harmonize measurement methods for rolling resistance, skid resistance, and noise emission measurement standards for road surfaces and prepare for standardization in European countries. However, skid and noise standards in Europe are different from those in the US. For example, in Europe the noise standards are based on the statistical pass-by (SPB) method and the close-proximity (CPX) method, whereas in the US, the preferred method is the OBSI. In terms of skid, the primary standard in Europe is based on the Sideway-force Coefficient Routine Investigation Machine (SCRIM) while in the US most states use the locked wheel tester. Therefore, there are very significant differences between the European standard and those in the US.

The ROSANNE project was organized into four work packages (WP), each containing several deliverables: WP1: "Skid Resistance"; WP2: "Noise Emission"; WP3: "Rolling Resistance"; and WP4: "Texture, Reference Tires and Reference Surfaces." The project used a variety of equipment provided by several countries to aid in the development of a standard that would harmonize all the different technologies and measurements into a common scale for skid, noise, rolling resistance, and texture (Greene, 2014).

1.2.1 Pavement Noise Characterization

The two test methods used to measure noise during the ROSANNE project were the SPB and CPX, the most used methods in Europe. The SPB is based on measuring the noise produced by pass-by of vehicles in traffic at a specific section. The SPB device, placed on the side of the road, is an indicator for the noise experienced by individuals affected by the road noise. In contrast, the CPX is a direct measurement of the tire/road noise instead of a combination of factors, such as engine noise from vehicles. The project aimed to find a relationship between the two methods; nearly a one-to-one relationship was found between the two methods for passenger vehicles specifically when measured at the same reference speed (Kragh, 2015). Additionally, researchers tried to use parameters such as surface texture or sound absorption to harmonize pavement noise classifications with the data of CPX and/or SPB but no good results were reported. A summary table indicated that a road with low MPD showed higher noise levels from the two types of equipment, while another road with higher MPD had lower noise levels. The report stated that the effects relating to texture are too small or too random to characterize (Kragh, 2015).

1.2.2 Characterization of Texture

Several different devices were used to measure pavement texture. The contactless texture equipment used the capabilities of a laser-profilometer (TL5), fringe projection (T3Dk, T3Dg), and point-triangulation (ELA). The tests were performed on the IFSTTAR test track, with the devices measuring the same area. The intent was to describe the profile of the pavement that represented the tire/pavement contact rather than the raw profile. The ROSANNE project developed a modified profile of the pavement to describe the tire/pavement contact accurately in comparison to the raw profile, named the "indentation" method. The ROSANNE researchers believe that the indentation method better predicts the interaction between the two surfaces when describing noise, rolling, and skid resistance, as it excludes the profile where the tire does not contact the pavement. Resolution and measuring principles were found to have an effect on the texture characteristics; the new ISO/CD 13473-1 solves these issues. For correlations with MPD and skid resistance, it was noted that higher resolution of the collected profile showed higher correlations (Gottaut and Luc, 2016).

1.2.3 Characterization of Friction

Two test campaigns were performed in Nantes, France (IFSTTAR) on a test track and the surrounding roads. Two different operating methods for skid resistance were used: side-force friction and longitudinal friction, with a total of 15 devices commonly used in Europe, including the GripTester. The operating method was further split into three groups for the harmonization to achieve better precision.

1) Sideway-force (34% slip ratio)
2) Longitudinal low slip (15% to 20% slip ratio)
3) Longitudinal high slip (62.5%, 95%, and 100% slip)

Results showed the different devices could be compared by using a common scale with use of the Skid Resistance Index (SRI) principal (Cerezo, 2015). The draft of the modified SRI developed by ROSANNE was an improvement to the existing CEN/TC 13035-2 (Birkner, 2016), by considering the friction methods from the three groups listed above.

Chapter 2. Friction

Pavement friction is defined as the force that is generated because of vehicle tires rolling or sliding over the pavement surface. This force resists the relative motion between the tire and the pavement (Hall et al., 2009). Friction is typically characterized by the non-dimensional friction coefficient mu (μ), which is the quotient of the tangential friction force over the perpendicular force applied on the pavement, as per Equation 2-1.

$$\mu = \frac{F_t}{F_v} \tag{2-1}$$

Where,

$\mu =$ Friction coefficient

$F_t =$ Tangential (tractive) force applied at the tire/pavement interface (N or lbs.)

$F_v =$ Dynamic load on the tire perpendicular to the pavement (N or lbs.)

Skidding occurs when no sufficient friction force is developed at the interface between a tire and pavement to meet the required friction demand to stop the vehicle's motion along the pavement (Kennedy et al., 1990). When braking or change of direction occurs, the specific type of maneuver being attempted by the driver and certain characteristics of the vehicle determine the friction demand required to complete the maneuver (Viner et al., 2005). Skid resistance is defined as the ability of the traveled surface of the pavement to prevent loss of tire traction (AASHTO, 2008). Skid resistance of pavements plays a critical role in road safety, from a transportation infrastructure perspective. Several studies have proven that as the skid resistance in pavement decreases, the number of accidents on the road increases. Hence monitoring and management of skid resistance in the highway network is needed to control and reduce the number of road accidents (Serigos 2016).

2.1 Friction and Skid Resistance Characterization

This section will discuss the main fundamentals and parameters used to characterize both friction and skid resistance on pavement surfaces.

2.1.1 Friction Forces

Most of the frictional force generated on the pavement is due to acceleration, braking, or steering, all of which affect the movement of the vehicle's tires against the pavement (Flintsch et al., 2012). Two types of friction that are typically measured by transportation agencies are the longitudinal and side-forced friction. Longitudinal frictional develops along the driving direction and has two extreme modes of operations: free-rolling (no braking) and constant brake. For the free-rolling mode, the speed between the tire circumference and the pavement is equal to zero; this speed is also known as *slip speed*. In the constant break mode, the speed will increase from zero to the potential maximum of the speed of the vehicle (Flintsch et al., 2012). Any conditions in between are known as *variable slip* and are measured as a percentage of the maximum speed of the vehicle. Side-forced friction is the force generated because of the vehicle tires changing direction or compensating for pavement cross-slope and/or the effects of cross/winds (AASHTO, 2008).

2.1.2 Friction Mechanisms

Pavement friction is the result of a complex interaction between two major friction force components: hysteresis and adhesion (AASHTO, 2008; Hall et al., 2009; Choubane et al., 2004), as shown in Figure 2-1. It should be noted that other mechanisms can be used to explain the loss in kinetic energy in the vehicle, such as abrasion or shear of the rubber tire; however their contribution is negligible when compared to the hysteresis and adhesion mechanisms (Hall et al., 2009).

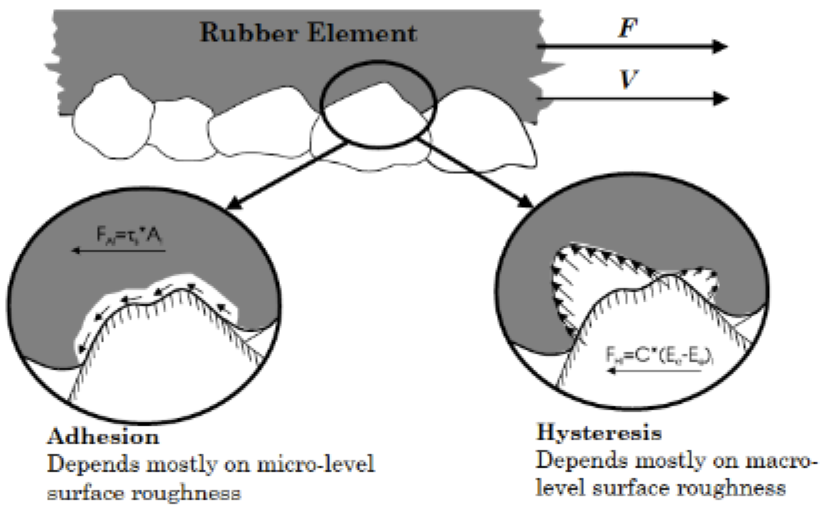

Figure 2-1 Main components of frictional forces between pavement and vehicle (Hall et al., 2009)

The adhesion component of the frictional force relates to the contact area between the rubber tire and the pavement surface. It is a result of Van der Waals forces developed at the tire-pavement interface. Van der Waals forces reflect the small-scale interlocking of microstructures as the micro-asperities of the two surfaces contact one another (Hall et al., 2009). Adhesion is a function of the interface shear strength and the contact area. It is very sensitive to changes in the microtexture of the aggregate particles. This mechanism will typically dominate on smooth-texture and dry pavements (AASHTO, 2008; Hall et al., 2009). The hysteresis mechanism results from the energy dissipation due to the bulk deformation of the rubber tire around bulges and depressions in the pavement's surface as it traverses along the road. This deformation is commonly referred to as enveloping of the tire around the texture. As a tire compresses against the pavement, the stress distribution causes the deformation energy to be stored within the rubber. When the tire relaxes, a fraction of the stored energy is recovered while the remaining portion is lost in the form of heat (hysteresis), which is irreversible. It is this loss that leaves a net-frictional force that aids in stopping the forward motion of vehicles (NASEM, 2009). Unlike adhesion, hysteresis is most responsive to the macrotexture at the pavement surface and will typically dominate under wet conditions and on rough-textured pavements (AASHTO, 2008; Hall et al., 2009, Henry, 2000).

The skid resistance of a pavement is represented by a parameter called the skid number (SN). The SN is determined by performing pavement friction testing using the locked-wheel method. As describe in ASTM E 274, 2015, the SN will equal to the force required to slide a locked test tire at a given speed, divided by the effective wheel load and multiplied by 100. SN can also be estimated by multiplying the coefficient of friction by 100. Nevertheless, this parameter is highly dependent on the texture of the pavement surface, and it can be very sensitive to wetness, distresses on the road, and temperature (Zuniga, 2017; Serigos 2016).

2.2 Factors Influencing Friction

According to Kummer (1966) and Sandberg (1998), three major factors affect the friction of pavements: roadway feature, vehicle tire characteristics, and the presence of fluids on the pavement surface. Out of the three, roadway feature is the factor that DOTs have the most control over. The roadway features encompass the texture levels on the road and the chemical and physical properties of the binder and aggregates used in the pavement mix. The vehicle tire characteristics are mostly controlled by the tire manufacturer, the tire's age, and the loading conditions under which the vehicle is driven. These characteristics include tread pattern design, rubber composition, inflation pressure, rubber hardness, load, thermal conductivity, specific heat, and sliding velocity. Finally, the influence of fluids on the pavement varies depending on the fluid's chemical structure, viscosity, density, temperature, thermal conductivity, specific heat, and film thickness. The most common fluid responsible for changes in the skid resistance is water.

2.2.1 Water

In the presence of water, the pavement surface and the vehicle tire become mildly lubricated and the overall skid of the roadway is significantly reduced. The effect of the water film thickness (WFT) on friction is minimal at speeds lower than 20 mph (32 km/h) and quite pronounced at speeds over 40 mph (64 km/h). Figure 2-2 plots the relationship between friction and WFT for three different types of tires (Hall et al., 2009). It is shown that the coefficient of friction between the vehicle tire and the wet pavement surface decreases as WFT increases. As WFT gets higher, friction does not reduce as drastically with each unit of WFT increase compared to when it is very thin. The friction on smooth tires is more responsive to WFT compared to both new and worn ribbed tires.

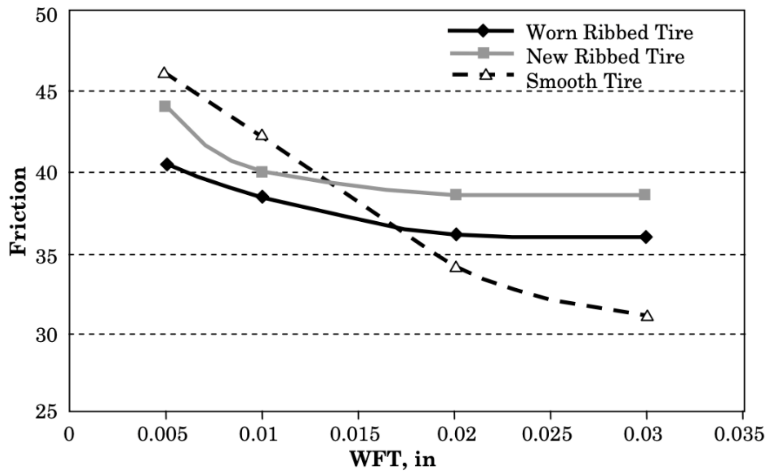

Figure 2-2 Friction varying with water film thickness (Hall et al., 2009)

The reduction in skid to due wet weather conditions can be mitigated by maintaining pavements with high levels of macro and microtexture. A high microtexture provides penetration through the thin water film that results in higher skid resistance; high macrotexture provides drainage channels for the water that allow for better contact between the pavement and the vehicle tire, which can ultimately prevent hydroplaning (Fontes et al., 2006). Hydroplaning is defined as the phenomenon that takes place when a relatively thick water layer or film is present and, as the vehicle is traveling at a higher speed, the water pressure accumulating along the pavement-tire interface separates the tire from the pavement surface (Horne and Buhlmann, 1983), resulting in a near-zero friction level. It can be affected by several factors, including WFT, vehicle speed, pavement macrotexture, tire tread depth, tire inflation pressure, and tire contact area. When rainfall is heavy, macrotexture cannot provide sufficient drainage, a thick layer of water film is formed, or puddles are created at pavement distresses, hydroplaning is more likely to happen, especially when the traveling speed of the vehicle is high. Hayes et al. (1983) identified that on puddles around 1 in. (25 mm) deep and 30 ft (9 m) long, direct pavement-tire contact can be lost at even lower speeds of 40 to 45 mph (64 to 72 km/h).

2.2.2 Slip Speed

The coefficient of friction is a function of the slip speed of the vehicle (Henry, 2000). As seen in Figure 2-3, the coefficient of friction rapidly increases with increasing tire slip until it reaches the peak friction value. This value is highly dependent on microtexture and will typically occur at the critical slip, which is a range from 10 to 30% slip (Hall et al., 2009). Any further increase in tire slip results in a decrease in the coefficient of friction until it reaches a value known as the *coefficient of sliding friction*. This occurs once the wheel is fully locked and the tire starts skidding over the pavement surface (Hall et al., 2009; Flintsch et al., 2012). Moreover, the macrotexture of the pavement will control the slope at which the coefficient of friction drops after reaching its peak. The higher the macrotexture of the pavement, the shallower the slope and the smaller the loss in the coefficient of friction (Hall et al., 2009).

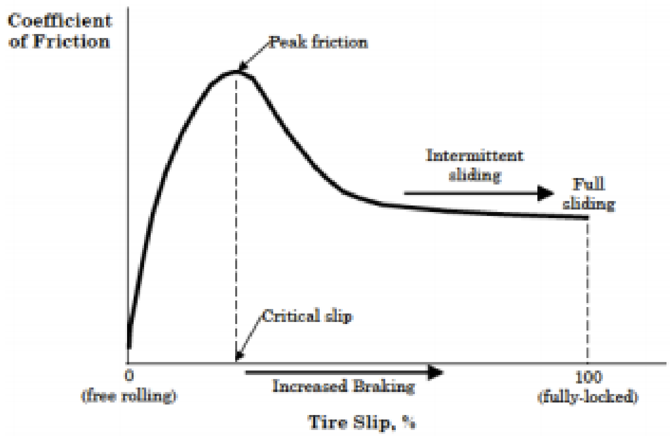

Figure 2-3 Friction coefficient and slip speed curve (Hall et al., 2009)

2.3 Skid Resistance Measurement

Friction measuring devices will always consider the main principle that a tire sliding over the road surface generates a measurable reaction force. The three major operating principles of frictional measurement equipment are slider, longitudinal friction coefficient (LFC), and side force coefficient. In this study, a slider was utilized and the LFC was observed.

2.3.1 Slider: British Pendulum Test (BPT)

Devices used for stationary testing employ the slider principle. A sliding component is attached either to the foot of a pendulum arm or to a rotating head, which slows down on contact with the pavement surface. The rate of deceleration is used to derive a value representing the skid resistance of the road (Flintsch et al., 2012). Typically, slider operational devices are relatively inexpensive and require traffic control to be used out in the field.

The BPT is a manually operated test that provides an on-spot measurement of the surface friction. It evaluates skid resistance at low speeds by measuring the friction coefficient at a skidding speed of approximately 6 mph (10 km/h) (Henry, 2000). The test uses a pendulum-type tester with a standard rubber slider and a drag pointer. After calibration, the pendulum is raised to a locked position and then released to allow the slider to skid over a pavement surface that has been manually wetted. A drag pointer will swing along with the pendulum and indicate the British Pendulum number (BPN) once the pendulum reaches its highest point on the first swing. The more friction the pavement has, the more it will retard the swing of the pendulum—hence, the higher the BPN reading (ASTM E 303, 1998). Typically, BPN measurements are used as a surrogate of microtexture characterization given that microtexture plays a very significant role at low-speed friction. Figure 2-4 illustrates the BPT equipment along with its field operation.

Figure 2-4 (left) BPT and (right) field operation

2.3.2 Longitudinal Friction Coefficient (LFC): GripTester and Micro-GripTester

The LFC is represented as the ratio of vertical forces to drag forces; testing based on the LFC principle consists of the application of a braking force to a test wheel so that it rotates more slowly than the forward speed of the vehicle. This makes the test wheel slip over the surface and allows for the development of frictional forces. LFC devices are divided into three modes: locked-wheel, fixed-slip, and variable slip. Each one has a different percentage of tire slip. All testing methods based on the LFC principle consist of a pulled device that utilizes one or two full-scale test tires to measure friction properties.

The GripTester and Micro-GripTester are continuous friction measuring devices capable of measuring continuously and dynamically the longitudinal skid resistance coefficient of the pavement in terms of Grip Number (GN), or the coefficient of friction. These devices used fixed slip mode for measuring friction experienced by vehicles with an anti-lock braking system. They are characterized by maintaining a constant slip that is typically between 10 and 20%, as a vertical load is applied to the test tire (Henry, 2000). They have a single measuring wheel, fitted with a special smooth threaded tire mounted on an axle designed to measure both the horizontal drag force and the vertical load force (Thomas, 2008). The difference between the GripTester and the Micro-GripTester is the scale of the device. The GripTester is towed behind a vehicle and uses measurement speeds ranging from 5 to 100 km/h (3 to 62 mph) (Kogbara et al., 2016). The micro-GripTester is pushed manually by a technician at an average speed of 0.7 m/s (2.3 ft/s). Figure 2-5 and Figure 2-6 display the GripTester and Micro-GripTester devices, respectively, and their operation on the field.

Figure 2-5 (left) GripTester device and (right) field operation

Figure 2-6 (left) Micro-GripTester device and (right) field operation

The GripTester was selected as the primary method for measuring friction in this study because it has been shown to have good repeatability and reproducibility, allows adjustable water usage, and is commercially available (Kouchaki, 2018). The device uses the braked-wheel fixed-slip principle with a ratio of 15%. The test tire is dragged over pavement wetted by an automated watering system that is controlled by the speed of the vehicle towing the GripTester. The axle of the GripTester outputs the dynamic friction from measurements of horizontal and vertical forces, resulting in the GN, or coefficient of friction, in real time (Thomas, 2008).

2.3.3 Locked-Wheel Skid Tester

Meyer et al. (1972) identified the usage of locked-wheel skid testers as the common practice by most highway departments in the United States. The standardized method is documented in ASTM E 274, with friction force measured as a locked test wheel equipped with a standard test tire, in accordance with ASTM E 249. The test tire is dragged over a pavement surface wetted by an automated watering system that generates a constant water thickness of 0.02 in (0.5 mm) above the pavement while being pulled at a constant speed, typically 40 mph (64 km/h), and a constant vertical wheel load. The tire may be either a ribbed tire (ASTM E 501) or a smooth tire (ASTM E 524), with the former more sensitive to the hysteresis component of friction, developed from macrotexture, and the latter more sensitive to the adhesion component of friction, derived from microtexture. The measurement system consists of a test vehicle with one or more test wheels incorporated or as part of a towed trailer, a standard tire used on the test wheel, a water container typically 200 to 500 gallons (750 to 1900 liters), an apparatus capable of distributing water in front of the test wheel at testing speeds to simulate wet weather conditions, a transducer connected to the test wheel that senses the friction force developed between the test wheel and the pavement, an electronic signal conditioning equipment that receives and modifies the output signal from the transducer, and suitable readout equipment to record either the magnitude of the developed force or the resulting SN (Equation 2-2). When taking measurements, the braking system is enforced, and the resistive drag force is measured and averaged for 1 to 3 seconds after the test wheel is fully locked (Hall et al., 2009).

$$SN = 100 \cdot \mu \tag{2-2}$$

Where μ = Friction coefficient as calculated in Equation 2-1.

Figure 2-7 (left) Locked-wheel skid tester and (right) trailer

Chapter 3. Texture

Pavement texture is defined by the irregularities on a pavement surface that deviate from a perfectly flat surface. The texture of a pavement has been deemed a crucial characteristic of a road surface, given that it determines most tire/pavement interactions, including noise, friction, and rolling resistance (Maguire and Carme, 2015). However, pavement textures are complex, and characterization typically requires specialized equipment and mathematical tools.

A linear profile is the simplest representation of pavement texture. The profile is a two-dimensional (2D) representation of the surface texture obtained using a sensor device that is described by its distance and height (Zuniga-Garcia, 2017). Profiles are considered stationary random functions of a given distance along the surface (Sanberg, 1987). However, advances in technology allow for the measurement and analysis of three-dimensional (3D) surface profiles too. Figure 3-1 illustrates the main parameters of a linear texture profile (2D).

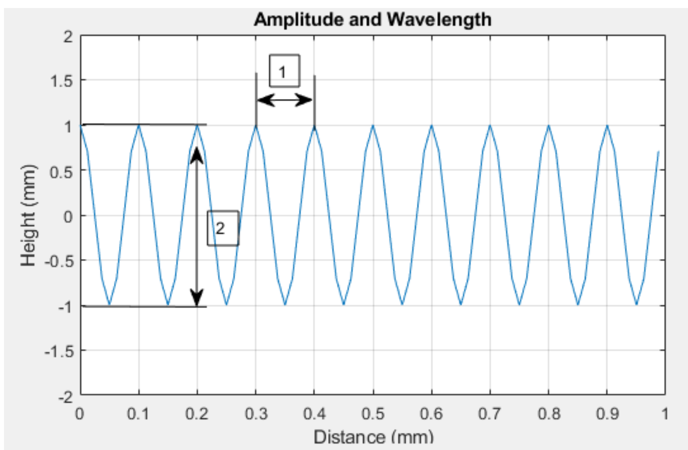

Figure 3-1 Basic terminology: 1. wavelength, 2. amplitude

3.1 Surface Texture Component Classification

To facilitate analysis, irregularities of the pavement surface are divided into four ranges: unevenness or roughness, megatexture, macrotexture, and microtexture. Each category is a function of the domains of texture wavelengths (λ) or spatial frequency (f_S), given that they are related by $f_S = 1/\lambda$ (Serigos et al., 2016). Figure 3-2 shows the surface texture spectrum, illustrating the four main texture components and their respective wavelength or spatial frequency domain.

Figure 3-2 Texture classes, as a function of the wavelengths or spatial frequency

Unevenness, also referred to as roughness, is the texture component that describes the irregularities in the pavement surface that affect the ride quality, smoothness, and serviceability. Its reference length is equivalent to a short stretch of road (AASHTO, 2008; Zuniga, 2017).

Megatexture is defined by the distresses, defects, and waviness of the road surface. Its reference wavelength is in the same order of size as the tire/road interface. This level of texture is easily observed with the naked eye. Some examples of megatexture include rutting, potholes, and major joints or cracks on the pavement (AASHTO, 2008).

Macrotexture refers to the large-scale texture of the pavement surface due to the aggregate particle arrangement. Macrotexture is controlled by mixture properties such as aggregate shape, size, and gradation, in flexible pavements, and by the method of finishing like dragging, tinning, grooving width and spacing, and direction of the texturing, in rigid pavements. State-of-the-art practice methodologies used for measuring pavement texture at highway speed typically account only for macrotexture (AASHTO, 2008, Zuniga, 2017, Serigos et al., 2016).

Microtexture alludes to the sub-visible or microscopic asperities of the aggregate surface, which controls the contact between the tire rubber and the pavement surface (Serigos et al., 2016). Microtexture is a function of the individual aggregate particle mineralogy and petrology, the aggregate source (natural or manufactured), and is affected by the environmental effects and the action of traffic (Zuniga, 2017).

Each of the four components influences tire/pavement to varying degrees. Smit reports that the unevenness of the pavement plays a significant role in the rolling resistance of the pavement, while the megatexture influences both rolling resistance and tire/pavement noise (Smit, 2008). However, the two components that seem to have a significant influence on a variety of pavement surface characteristics are microtexture and macrotexture. Based on previous research findings (Henry, 2000; and Sandburg and Ejsmont, 2002), Hall et al. (2009) summarized the pavement-tire interaction phenomena by mapping the most important pavement surface characteristics onto the texture wavelength ranges that each is most sensitive to, as shown in Figure 3-3.

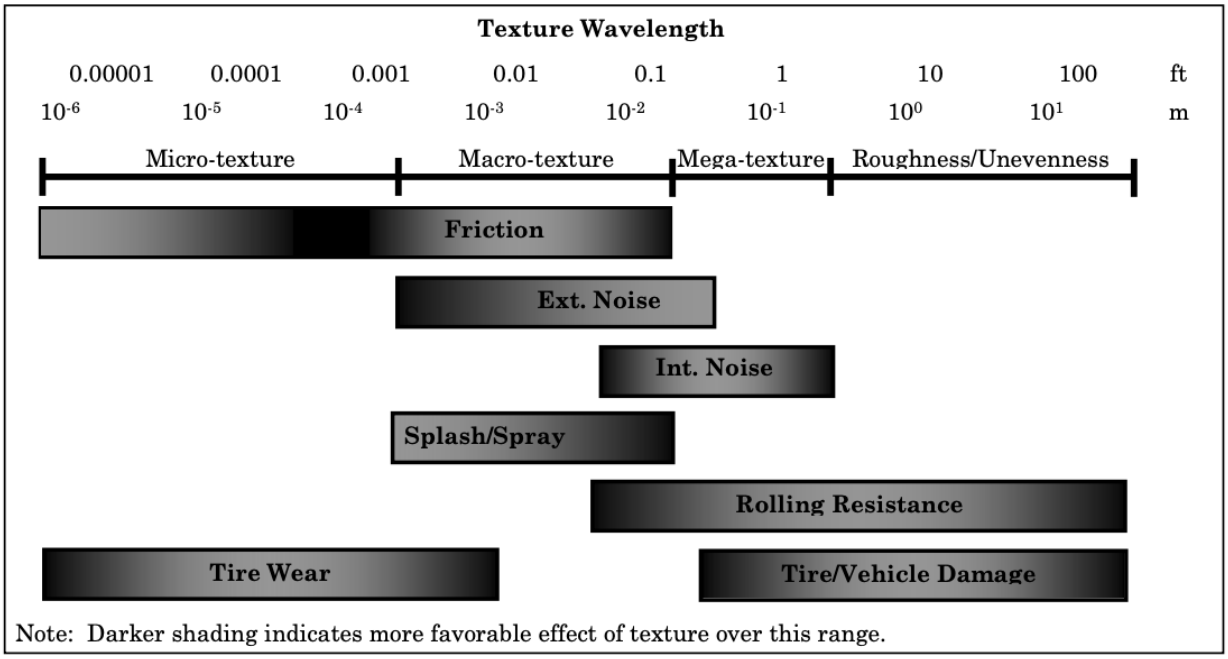

Figure 3-3 Texture wavelength influence on pavement–tire interactions (Hall et al., 2009)

Serigos and Zuniga agreed that when microtexture and macrotexture were taken into consideration on skid resistance correlation models, together they can account for at least 70% of the total variance in skid resistance on the road (Serigos et al., 2016; Zuniga, 2018). Furthermore, most traffic noise analysis research indicates that the peak of traffic noise occurs within the macrotexture wavelength spectrum, nevertheless, while there seems to be a correlation between texture (Smit et al., 2016.

3.1.1 Summary Statistics

Summary statistics are the base of pavement texture characterization. Each texture component is associated with specific parameters that provide a general description for the texture profile. At the unevenness and megatexture levels the most used and well-defined parameter is the International Roughness Index (IRI). Examples of statistics used to characterize pavement at the macrotexture level include the MPD and the mean texture depth (MTD). At the microtexture level, there are no standardized methods to characterize pavement texture; nonetheless, the same parameters used in macrotexture can be used to characterize the smallest wavelengths of texture using sophisticated signal processing techniques.

Texture summary statistics can be broken down into two main categories: spatial and spectral parameters. Spatial parameters are calculated in the spatial domain and are scale dependent. This means that these parameters can be defined separately at different levels of texture. For example, MPD can be defined at the macro or microtexture scale by using a band-pass or high-pass filter, respectively. These filters isolate the wavelengths for the texture level of interest before computing the MPD. In contrast, spectral parameters are calculated in the frequency domain and are scale independent. They are estimated along a wide range of texture wavelengths to avoid complexity of defining the same parameters at different scales (Serigos et al., 2016).

3.1.2 Spatial Parameters

Spatial texture parameters are divided into four categories: amplitude, spacing, hybrid, and functional parameters. Amplitude parameters, also known as height parameters, consist of the statistical distribution of height values along the vertical axis. Spacing parameters consider the periodicity of the data within the distribution. Hybrid parameters are a combination of spacing and amplitude. Lastly, the functional parameters give information about the surface structure based on the material bearing ratio curve. The bearing ratio curve is a cumulative probability distribution and the integral of the amplitude distribution function (ADF). The ADF is a function that gives the probability of a texture profile having a certain height, Z, at any position X.

Some examples of parameters used in the literature to characterize texture in the spatial domain include the MPD, MTD, average height (R_a), maximum height (R_z), root mean square (RMS), skewness (R_{sk}), kurtosis (R_{ku}), two-point slope variance (SV_2), and six-point slope variance (SV_6).

R_a is defined as the arithmetic mean of all the heights in the distribution. R_z is the maximum height value minus the minimum height value within the distribution. The RMS is a statistic that measures how much the measured profile deviates from the best fit of the data. One of its main applications is to provide a more accurate measurement of the surface roughness. It is typically used in conjunction with the MPD to identify whether if the surface has a negative or positive texture. For example, in Figure 3-4, both profiles have an identical variation hence they have the same RMS. But one can determine whether if the texture is negative or positive base on its MPD. The profile with the larger MPD will have a negative texture.

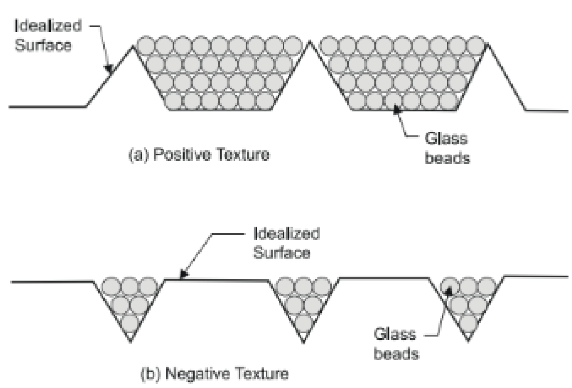

Figure 3-4 Positive and negative texture (McGhee and Flintsch, 2003)

R_{sk} and R_{ku} offer a more detailed description of the height distribution in the pavement surface. Skewness represents the degree of symmetry of the profile height about a mean plane. The sign of skewness indicates a predominance of peaks if it is positive and predominance of valleys if it is negative. Kurtosis indicates the presence of extremely high peaks or deep valleys ($R_{ku} > 0$), or the lack of them (R_{ku}< 0). Should the profiles follow a normal distribution, the value of kurtosis and skewness is zero for both statistics. Figure 3-5 shows different texture profile with varying values for skewness and kurtosis (ASME B46.1, 2009).

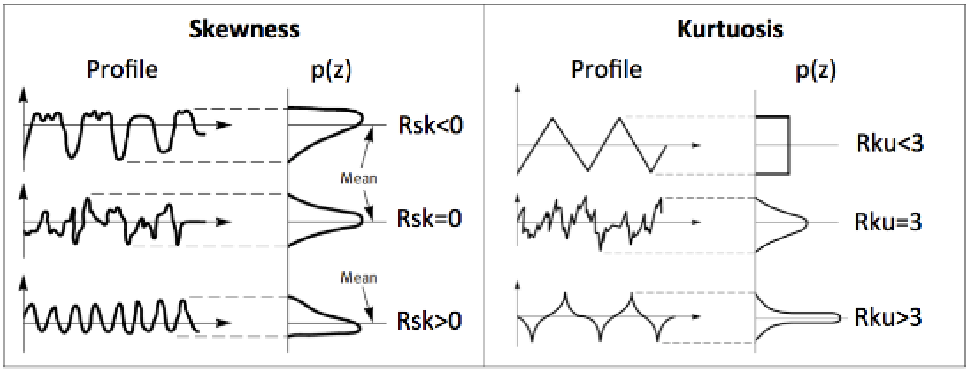

Figure 3-5 Texture profiles with different skewness values (left) and kurtosis values (right) (ASME B46.1, 2009)

The MPD is estimated by dividing the texture profile into segments of 100 mm in length. A slope and offset suppression are later applied to each segment by subtracting a linear regression to provide a zero-mean profile segment. The segment is then subdivided into two halves, and the height of the highest peak within each half is determined. The average of these two peaks is referred to as the *mean segment depth*, as shown in Figure 3-6. The average value of all segment depths along the profiles is the MPD (ASTM E 1845, 2009).

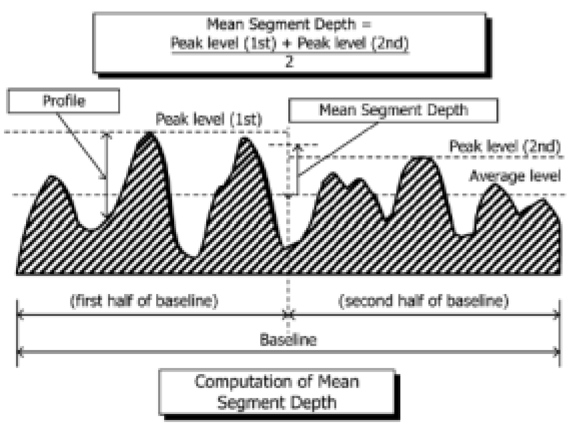

Figure 3-6 MPD procedure (ASTM E 1845, 2009)

Some hybrid parameters defined by Serigos et al. (2014) include the SV_2 and SV_6. The two-point slope variance measures the slope between two consecutive points as the difference in height between two consecutive coordinates, divided by the horizontal distance between them. The six-point slope variance calculates the slope using a weighted sum of the height values of six coordinates divided by the horizontal distance between them. A summary of all the spatial parameters mentioned in this section is shown in Table 3-1.

Table 3-1 Spatial texture parameters used for pavement texture characterization

Statistic	Equation
Maximum Height (R_z)	$R_z = \max(h_i) - \min(h_i)\,, \qquad i = 1, \dots, n$
Absolute Height Average (R_a)	$R_a = \frac{1}{n}\sum_{i=1}^{n} \lvert h_i \rvert$
Height Variance (R_v)	$R_v = \frac{1}{n-1}\sum_{i=1}^{n} \left(h_i - \bar{h}_i\right)^2$
Root Mean Square (RMS)	$RMS = \sqrt{R_v}$
Skewness (R_{sk})	$R_s = \frac{n}{(n-1)(n-2)} \sum_{i=1}^{n} \frac{\left(h_i - \bar{h}_i\right)^3}{RMS^3}$
Kurtosis (R_{ku})	$R_k = \frac{n(n+1)}{(n-1)(n-2)(n-3)} \sum_{i=1}^{n} \frac{\left(h_i - \bar{h}_i\right)^4}{RMS^4} - \frac{3(n-1)^2}{(n-2)(n-3)}$
Mean Profile Depth (MPD)	$MPD = 0.5\left[\max\left(h_1, \dots h_{m/2}\right) + \max\left(h_{m/2}, \dots h_m\right)\right]$
Two-Point Slope Variance (SV_2)	$SV_2 = \sqrt{\frac{1}{n}\sum_{i=1}^{n} \left(\frac{h_i - h_{i+1}}{\Delta x}\right)^2}$
Six-Point Slope Variance (SV_6)	$SV_6 = \sqrt{\frac{1}{n}\sum_{i=1}^{n} \left(\frac{h_{i+3} - 9h_{i+2} + 45h_{i+1} - 45h_{i-1} + 9h_{i-2} - h_{i-3}}{60\Delta x}\right)^2}$

Where,

h_i:	Elevation at point i	$\bar{h}$	Mean elevation
n :	Number of data points	h_{pj}:	The j^{th} highest peak in the profile
h_{vj}:	The j^{th} lowest valley in the profile	$h_{m/2}$:	Elevation value midway through segment
h_m:	Elevation value at the end of segment	Δx:	Spacing between adjacent transverse points

3.1.3 Spectral Parameters

Spectral parameters are parameters obtained in the frequency domain. Obtaining spectral parameters requires the use of Fourier analysis to examine the surface texture profile given that it can decompose a texture profile into a function of sinusoidal waves. A common approach is to determine the parameters from the texture spectrum. The technical specification ISO 1373-4 (ISO, 2008) describes the procedure to obtain the texture spectrum expressed in octave or one-third octave bands. The parameter used to characterize the texture spectrum is known as the *texture profile level* ($L_{tx,\lambda}$). A texture profile level is a logarithmic transformation of an amplitude representation of a texture profile having a center wavelength of lambda λ and reported in units of decibels (dB). This approach has been mainly used to find correlations between tire/pavement noise and the road texture; however, it has also been used in studies intended to correlate texture to friction (Sandber and Descornet, 1980; Millet et al., 2011).

Serigos et al. (2014) used a similar approach known as power spectral density (PSD), which is a description of how the energy of a pavement texture profile is distributed over the different frequencies. Serigos et al. used the slope and intercept of the linearized PSD curve to characterize the surface macro and microtexture. They observed a strong correlation between the log of the PSD and the log of the frequency in most of their sampled test surfaces.

3.2 Texture Measurement

Numerous techniques exist to measure the four different components of pavement texture. State DOTs collect unevenness, megatexture, and macrotexture data for road maintenance and research purposes. Currently, there is no standard method for measuring highway microtexture. Thus, much of the ongoing research in this field has been geared towards developing an affordable, efficient, and reliable way to measure the smallest texture component (Zuniga, 2017). This section gives a general summary on how unevenness and megatexture is measured while addressing macrotexture and microtexture in depth.

A topological survey can be used at the unevenness level to describe the pavement texture by obtaining the IRI. The IRI was developed in 1986 by the World Bank, as one of the first standardized primary indicators for highway network serviceability (Sayers et al., 1986). The index measures pavement roughness in terms of the number of inches per mile (in/mi.) or meters over kilometer (m/km) that a laser, mounted on a profiler van, "jumps" as the van is driven along the roadway. Figure 3-7 shows a schematic of a Road Surface Tester, which is one of the vehicles that can be used to measure IRI. These measurements of IRI are typically within a wavelength range of 1.3 to 30 meters (Sayers et al., 1986). Similarly, IRI measurements can also be used to characterize the pavement at the megatexture level using the highest resolution possible. Furthermore, other parameters, such as rut depth, can also be measured using the same equipment to characterize the pavement surface's megatexture.

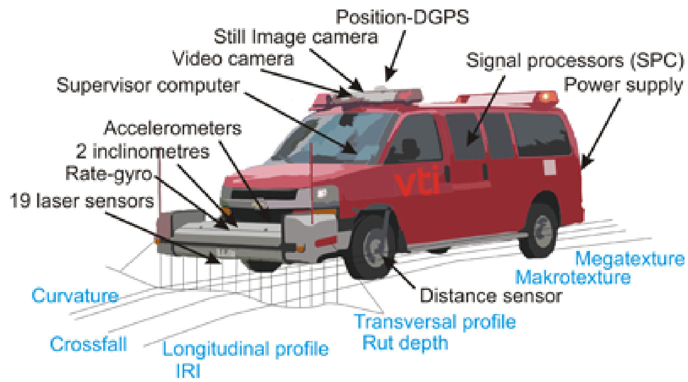

Figure 3-7 Schematic of a Road Surface Tester used to measure IRI and rut depth

Measurements at the macrotexture level can be taken in two different ways: with on-spot or in-motion measurements. On-spot measurements require traffic control for technicians to collect the data in a safely manner. Additionally, multiple measurements along the section are needed to get a representative sample of the pavement. Examples of on-spot measurements involve volumetric techniques such as the sand patch test (SPT) or non-contact measurements such as the circular track meter (CTM). In-motion testing typically involves taking continuous measurements while a vehicle or trailer equipped with proper instrumentation drives along the roadway. These procedures do not require traffic control; however, they are unable to collect microtexture data due to limitations of laser sensor technology. Examples of in-motion testing methods include the laser crack measurement system and the V-Texture; the latter is the method used by Texas Department of Transportation (TxDOT). This next subsection will cover in detail only on-spot measurements, given that those methods are the ones used in the analysis.

3.2.1 Sand Patch Test (SPT)

Some of the most common volumetric techniques used to measure macrotexture on pavement are the sand patch, the grease patch, and the outflow meter test. Out of the three, SPT is the simplest and most used by transportation agencies. The method involves applying a known volume, which is typically 25 mm^3, of either solid glass spheres of uniform size or Ottawa natural silica sand on a relatively uniform, not distressed section of the pavement surface. The sand is later spread in a circular motion with a spreading tool, as shown on the right side of Figure 3-8. Once the roughly circular patch of sand is made, four equally spaced diameters are measured and averaged to compute the area of the sand patch. The known volume of sand is then divided by the area of the circle using Equation 3-1 and reported as the MTD (ASTM E965, 2015). The grease patch method is a variation used by NASA in which grease is used instead of sand or glass spheres (Zuniga, 2017). The outflow meter is a transparent vertical cylinder placed on the pavement surface. The cylinder is filled with water and the time for the water level to fall by a fixed amount is measured and reported as the outflow time (ASTM E2380, 2015).

$$MTD = \frac{4V}{\pi D^2} \tag{3-1}$$

Where,

V = Material sample volume (mm^3)

D = Average diameter covered by material (mm)

Figure 3-8 (left) SPT equipment, and (right) field data collection

3.2.2 Circular Track Meter (CTM)

An alternative to indirect measurements of the texture profiles involves more modern techniques using non-contact lasers, such as the CTM or the Laser Texture Scanner model 9300 (LTS). The information collected from these devices can be used to compute various profile statistics such as the MPD.

The CTM is a device used to measure MPD and RMS. It consists of a laser displacement sensor that is mounted on an arm that rotates clockwise at a fixed elevation from the measured surface and a notebook computer that is used to control the device and save all the processed data as shown on the left side of Figure 3-9. The device measures a 2-D profile of a circle 284 mm in diameter and 892 mm in circumference. The profile is divided into eight segments with an arc length of 111.5 mm, as shown on the right side of Figure 3-9. The MPD is determined for each of the segments of the circle and the MPD reported as the average of the eight segments (ASTM 2157, 2015). The device then calculates the RMS for the profile using the equation provided in Table 3-1. A major drawback of the CTM arises when measuring textures of concrete pavement. Given that the system measures texture along a circumference, it makes it difficult to measure longitudinal or traverse texture separately. These two types of textures are very important for rigid pavements; hence, it is recommended that other techniques be used for that type of analysis.

Figure 3-9 (a) CTM, and (b) CTM segments

3.2.3 Laser Texture Scanner (LTS)

The LTS is a lightweight and portable piece of equipment designed to scan pavement surface coordinates to characterize its texture contents. It uses a laser sensor to scan the surface coordinate of parallel straight lines with a sampling rate of one point every 0.015 mm and a maximum scan area of 100 by 75 mm. The LTS computes the MPD, RMS, texture profile index, and estimated texture depth, which is an estimation of MTD based on MPD using an empirical equation, as shown in Equation 3-2. The resolution of the device allows it to measure and describe the two decades of macrotexture (wavelengths from 50 mm to 5 mm and from 5 mm to 0.5 mm) and the first decade of microtexture (wavelengths from 0.5 mm to 0.05 mm). However, scans performed at the highest resolution can take approximately two hours, making it impractical for field studies (Serigos et al., 2014). Zuniga (2017) also reports that the device is also not as reliable as the CTM, and the researchers have experienced many operational problems. Figure 3-10 illustrates the LTS device along with the scanned 3D surface profile plot.

$$ETD = 0.2 + 0.8 * MPD \tag{3-2}$$

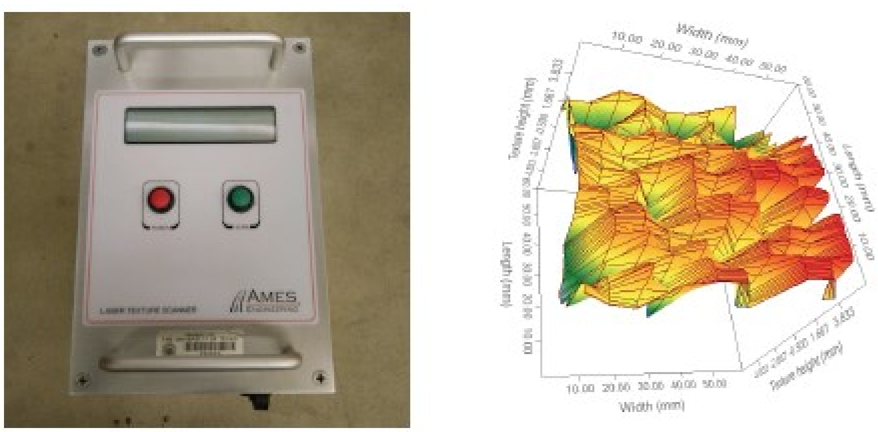

Figure 3-10 (left) LTS and (right) 3D plot of measured surface (Zuniga, 2017)

Due to the lack of standard methods to measure microtexture, some highway transportation agencies use low-speed-friction tests to characterize the pavement's microtexture due to the high correlation between the two. It should be noted though, that most of the research dealing with the measurement of microtexture is based on the use of laser scanners and image analysis techniques. Some of the methods used to quantify microtexture statically include the LTS, the Aggregate Imaging System (AIMS), and the LLS.

3.2.4 Aggregate Imaging System (AIMS)

The AIMS is a system that uses image analysis techniques to analyze the particle geometry of the coarse and fine aggregates through three independent properties: form, angularity, and surface texture. The equipment consists of a camera, two different lighting schemes, and microscope technology (Masad, 2005), as shown in Figure 3-11. AIMS analyzes the captured images of the aggregates using different techniques for each of the independent properties. The Wavelet method is used to analyze the aggregate texture; the gradient method and radius method are used to analyze the angularity of the aggregate, and the 3D form of the aggregate is analyzed using sphericity and shape factors (Masad, 2005).

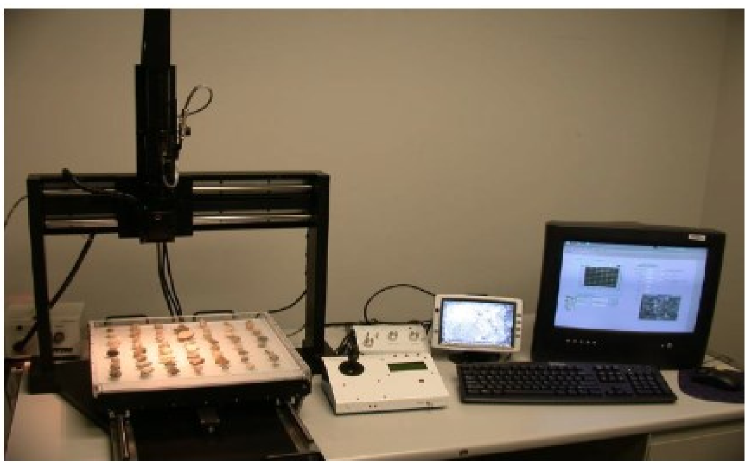

Figure 3-11 AIMS device (Mahamoud et al., 2010)

3.2.5 Line Laser Scanner (LLS)

The LLS is a surface profiling system developed to characterize macro and microtexture (Figure 3-12. The device consists of a high-resolution line-laser scanner and a translation stage. The LLS can collect a maximum of 800 points in the transversal direction and move up to 600 mm in the longitudinal direction. The equipment has an improved sampling rate, allowing for characterization of the two decades of macrotexture (wavelengths of 0.5 to 5 and 5 to 50 mm) and the first decade of microtexture (wavelengths of 500 to 50 microns) (Zuniga, 2017). The main advantage the LLS has over many other static laser profilers is its speed. The LLS can scan a wider area at a very high resolution in 15 seconds as opposed to the lengthy times of other devices such as the LTS. In her study, Zuniga claims that not only is the LLS more efficient and reliable than the CTM or the LTS, it also has a higher vertical resolution of 0.5 microns compared to the 3 microns in the CTM and 15 microns in the LTS (Zuniga, 2017).

Figure 3-12 (left) LLS and (right) field operation

The diagram shown in Figure 3-13 summarizes the most used texture measurement techniques to measure different texture components and their corresponding tests.

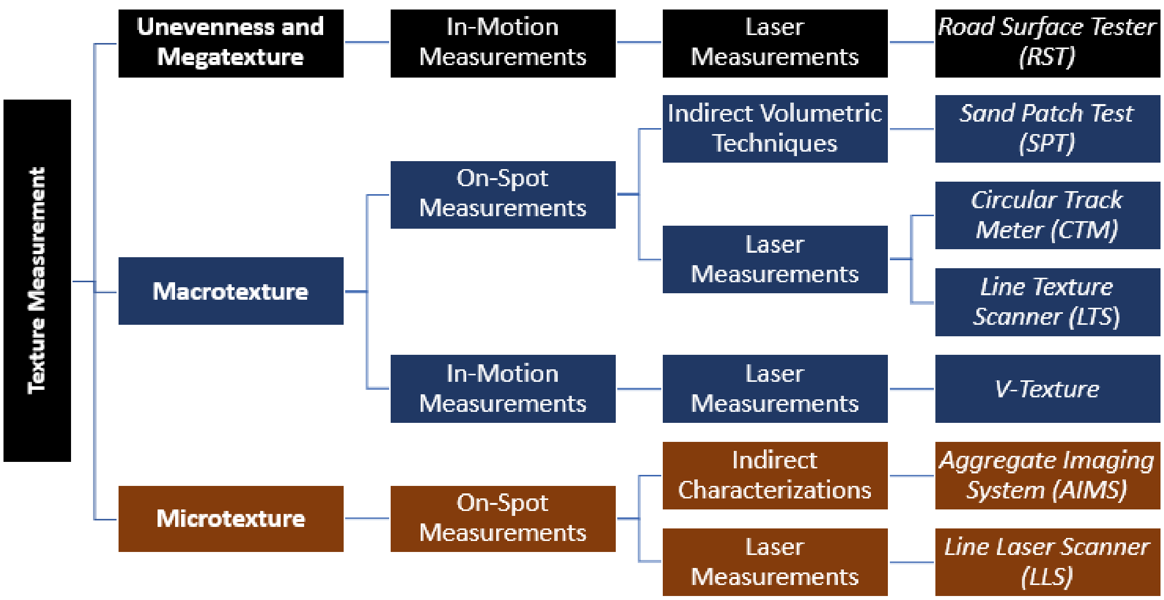

Figure 3-13 Summary of the most common texture measurements tests

Chapter 4. Noise

The term "noise" is colloquially used interchangeably with the word sound, but these words have different meanings. Sound is a vibration that typically propagates as an audible pressure wave, whereas noise is the generation of unwanted sounds. In terms of traffic, traffic noise is the generation of unwanted sound produced by any traffic component. Traffic noise can be broken down into two components: acoustic energy and frequency. The acoustic energy of noise can be represented either as sound pressure levels (SPL), sound intensity levels, or sound power levels. Typically, SPL and sound intensity level are the parameters of interest in traffic noise. The sound pressure is a scalar quantity, measured in units of Pascal (Pa) that indicate the amplitude level of a sound at a specific location in space. Sound pressure can be measured with a single microphone; nevertheless, noise pressures can vary from 2 kPa, the pain threshold, to 20 μPa, the hearing threshold. To make the range of values more manageable and convenient, sound pressure is converted to SPL, which uses dB units (Benhard and Wayson, 2005).

Sound intensity refers to the amount of energy a soundwave carries per unit area in a direction that is orthogonal to the given area. This parameter describes the flow of sound through a specific area and, due to its complexity, it requires at least two microphones set up in a specific arrangement. The unit used for sound intensity is the watt per square meter (W/m^2), but, like sound pressure, can also be represented using dB (Benhard and Wayson, 2005; Brüel & Kjær, 1993).

The frequency, often referred to as *pitch*, of a sound wave is the number of pressure oscillations per second, measured in units of Hertz (Hz). A noise spectrum of multiple audible frequencies must be studied when analyzing traffic noise (Benhard and Wayson, 2005). However, examining the acoustic energy generated at every frequency at the same time is impractical and creates enormous amounts of data. For this reason, the frequency range is divided into a set of broader ranges, each of which contains lesser of amount of detail (ATCO Noise Management, n.d.). The most common types of frequency analyses are narrowband, octave band, and one-third octave band, as Figure 4-1 illustrates. Typically, traffic noise analyses use octave and one-third octave bands as the frequency of preference.

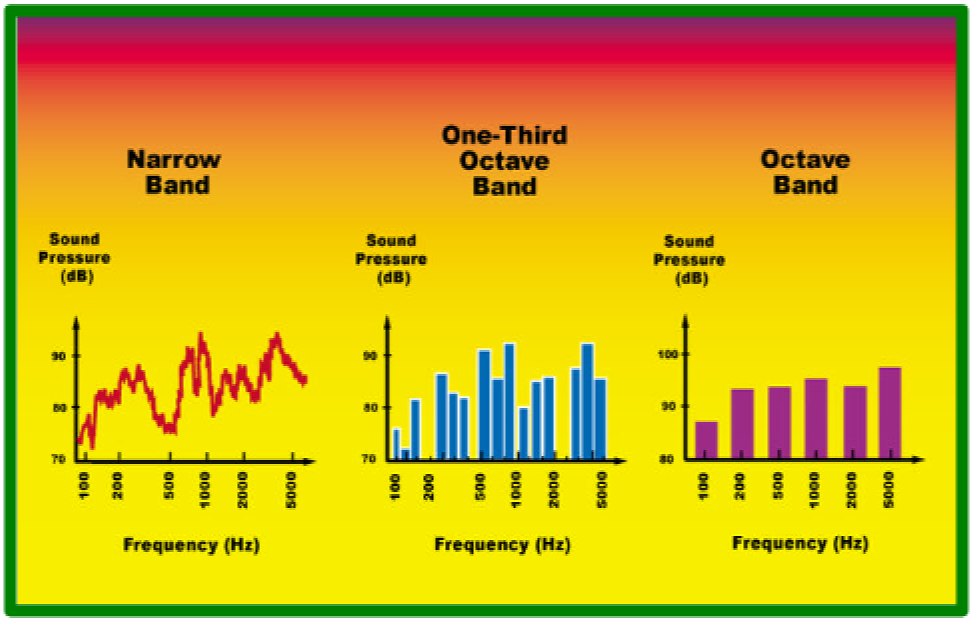

Figure 4-1 Narrowband, one-third octave band and octave band (ATCO Noise Management, n.d.)

An octave refers to the interval between one frequency and its double or its half. Octave bands are used as a filter method to split the audible spectrum into smaller segments, allowing the identification of different noise level across individual octaves. One-third octave bands provide a further in-depth look at noise levels across the frequency composition, given that each octave is further split into three, providing a more detailed view of the noise content. The center frequencies of these bands are shown in Table 4-1. Each octave or one-third octave band SPL represents the acoustic energy in that frequency band (Benhard and Wayson, 2005).

Table 4-1 Band center frequencies for octave bands and one-third octave band and attenuation factors for A-weighting network

Band	1/3 Octave Band Frequencies (Hz)	A-Weighting Attenuation Factor (dB)	Band	1/3 Octave Band Frequencies (Hz)	A-Weighting Attenuation Factor (dB)
Lower	25	-44.7	Lower	800	-0.8
Center	**31.5**	-39.4	**Center**	**1,000**	0
Upper	40	-34.6	Upper	1,250	0.6
Lower	50	-30.2	Lower	1,600	1.0
Center	**63**	-26.2	**Center**	**2,000**	1.2
Upper	80	-22.5	Upper	2,500	1.3
Lower	100	-19.1	Lower	3,150	1.2
Center	**125**	-16.1	**Center**	**4,000**	1.0
Upper	160	-13.4	Upper	5,000	0.5
Lower	200	-10.9	Lower	6,300	-0.1
Center	**250**	-8.6	**Center**	**8,000**	-1.1
Upper	315	-6.6	Upper	10,000	-2.5
Lower	400	-4.8	Lower	12,500	-4.3
Center	**500**	-3.2	**Center**	**16,000**	-6.6
Upper	630	-1.9	Upper	20,000	-9.3

However, the human ear does not treat sounds of different frequencies at the same level, because perception of loudness is not linear for the human auditory system. For this reason, traffic noise levels are quantified in dBA units. A-weighting uses the attenuation factors shown in Table 4-1 to quantify the intensity of pressure differentials created by sounds in a way that mimics how the human auditory systems perceives sounds of different frequencies at the same level (Benhard and Wayson, 2005). The A-weighting curve can be seen in Figure 4-2 alongside other sets of weighting values, like B, C, and D. The other weighting values are not used particularly for traffic noise analysis but have other purposes, such as assessment of high-level aircraft noise (Smit et al., 2016).

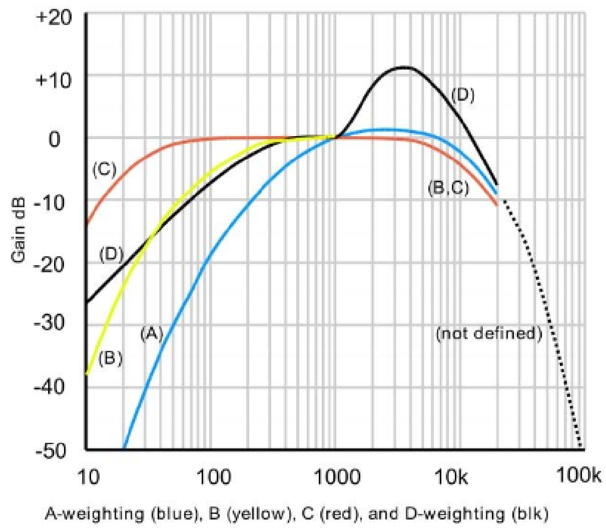

Figure 4-2 A-, B-, C- and D-weighting across the frequency range (Smit et al., 2016)

Human ears are particularly sensitive at frequencies of 1.0 kHz and various roadway noise research projects have confirmed this, as it has been pointed out that traffic noise tends to peak at frequencies of 1.0 kHz. Figure 4-3 shows a map of equal loudness contours derived from experiments on the subjective ratings of loudness as expressed by humans (Smit et al., 2016). These contour lines, also known as the Fletcher-Munson Curve, explain the non-linear response of the human ear to sound of different frequencies and show the SPL at which a certain frequency must be to be perceived by the human auditory system as having the same intensity (Maguire, 2015).

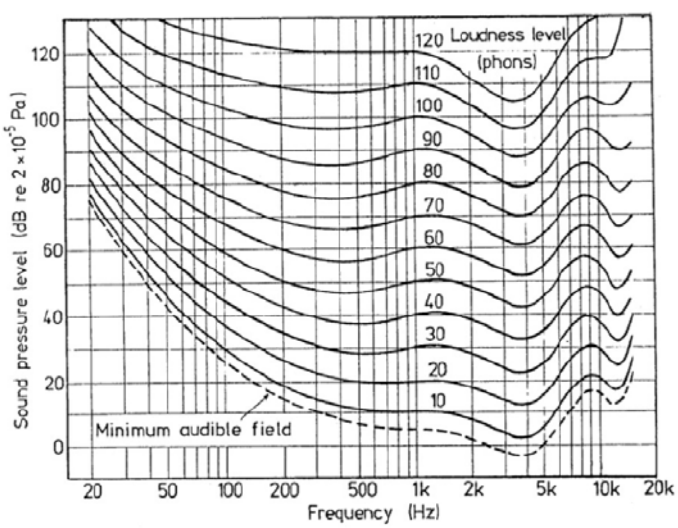

Figure 4-3 Equal loudness contours (Smit et al., 2016)

4.1 Noise Fundamentals

Numerous conditions can affect the noise levels perceived close to a roadway. One of these conditions is the distance between the receiver to the source of noise. It is known that noise levels will decrease as the distance from the noise source increases. This happens due to the inverse-square law, which states that sound is inversely proportional to the distance squared (Smit et al., 2016). Figure 4-4 will illustrate this phenomenon by using a blender as the point source of noise and a person as the receiver. At 1 m (3 ft.), the receiver perceives a noise of 85 dBA; when this distance is doubled the perceived sound drops to 79 dBA. When the distance is tripled to 3 m (9 ft.), the noise level drops to 75.5 dBA. This implies that doubling the distance from the noise source results in a reduction of 6 dBA, and tripling that distance reduces the perceived noise level by about 9.5 dBA. However, traffic noise does not originate from a point source, but rather a line source. The noise coming from roadways is transmitted along the length of the roadway as vehicles travel from one location to another. For a line source, the rate at which noise levels decrease with distance is much slower. Illustrated in Figure 4-5, a person standing 5 m (16 ft). away from the center of the lane in a road will perceive a noise level of 85 dBA. If this person were standing 10 m (32 ft). away from a line source of noise, the perceived noise level would be 82 dBA. Thus, doubling the distance on paved surfaces with line sources of noise results in a reduction of 3 dBA.

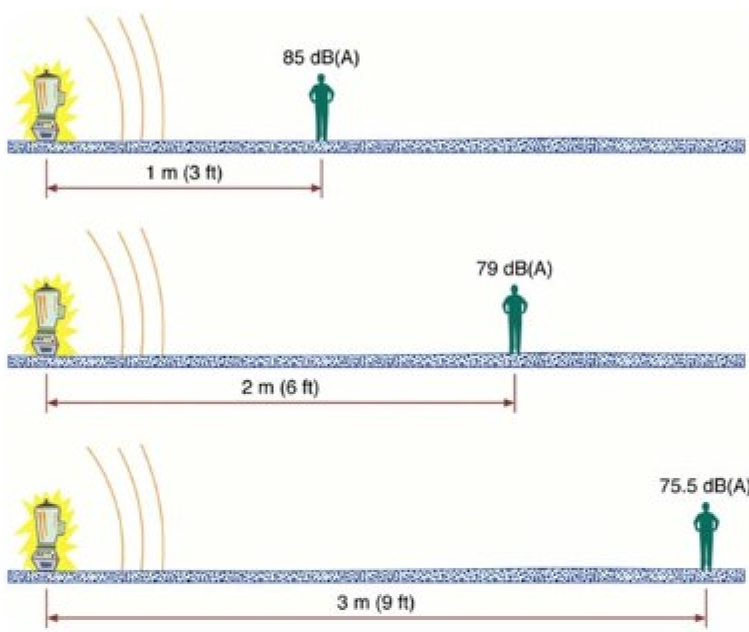

Figure 4-4 Effects of distance on noise levels emitted from a point source (Hanson et al., 2014)

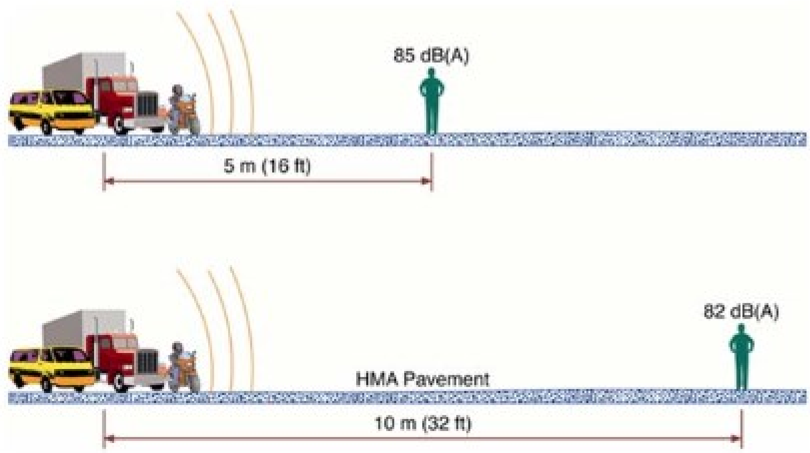

Figure 4-5 Effects of distance on noise levels emitted from a line source (Hanson et al., 2014)

Noise levels near the road are not only dependent on the noise generated by vehicular traffic, but also on the layer thickness of the road pavement and the characteristics of the ground adjacent to it (Smit et al., 2014). According to Smit (2008), layer thickness appears to have a significant influence on noise levels particularly for porous asphaltic mixtures. The greatest reduction in noise was observed when the layer thickness of porous European mixtures and, to a smaller degree, in permeable friction course (PFC) mixes was increased. It was noted that open-graded mixes will tend to have sound absorption properties, so long as the voids remain unclogged. The findings of this study suggest that the influence of layer thickness on noise reduction should be considered when designing porous mixtures as low-noise alternatives (Smit, 2008).

To account for the effects of different ground characteristics adjacent to the pavement, the FHWA (1980) uses a traffic noise model to predict noise levels along the roadway. Equation 4-1 illustrates the equation used by this model to approximate the drop off in noise levels:

$$P = 10\log_{10}\left[\left(\frac{d_1}{d_2}\right)^{1+\alpha}\right] \tag{4-1}$$

Where,

P = Sound pressure level (dBA)
α = Attenuation coefficient
= 0.0 for hard ground or pavement
= 0.5 for soft ground
d_1 = Distance from sound source to the first point of interest (ft.)
d_2 = Distance from sound source to the second point of interest (ft.)

Figure 4-6 illustrates a scenario in which a noise level of 85 dBA is perceived at the edge of the road that is 5 m (16 ft) (d_1) away from the noise source, and a noise receiver is standing 61 m (200) ft (d_2) away from the noise source with soft ground in between. The equation used in the traffic noise model would predict a perceived noise level of 68 dBA where the noise receiver is standing. Soft ground covered in vegetation is proven to mitigate noise levels in rural areas, given that the ground acts as an absorption media that heavily reduces the perceived noise levels in rural houses close to a roadway (Smit et al., 2014).

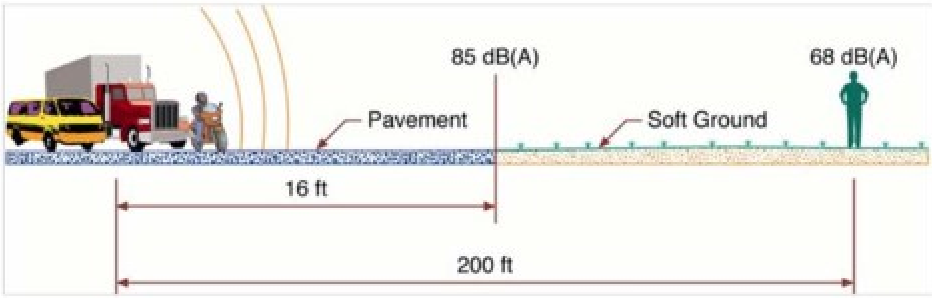

Figure 4-6 Effects of distance on a line source over soft ground (Hanson et al., 2014)

Moreover, noise on the roadways is not generated by a single vehicle. A road that is approaching its saturation flow will have multiple vehicles that contribute to the overall noise levels—hence the effects of doubling or tripling the noise sources must be considered. In Figure 4-7, a person standing at an arbitrary distance from a noise source (a blender) is perceiving a noise level of 85 dBA. However, as more blenders are added to this scenario, the perceived noise levels increase to 88 dBA and 89.8 dBA when one and two blenders are added, respectively. Hanson et al. stated that applying this analogy to the roadway implies that if the number of vehicles travelling on a road doubles or triples, then the perceived noise levels will increase by 3 and 4.8 dBA, respectively (Hanson et al., 2014).

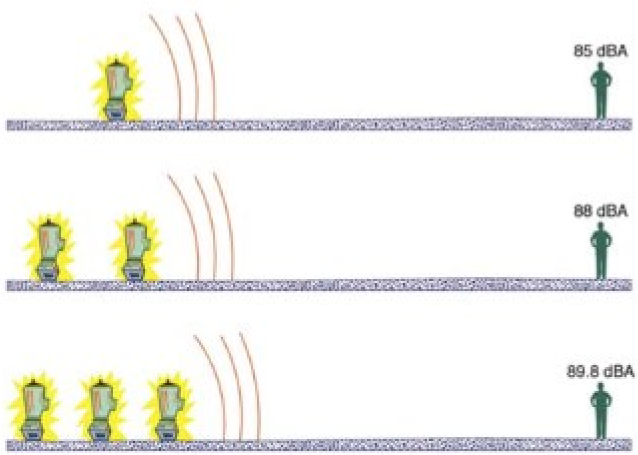

Figure 4-7 Effects of adding noise sources (Hanson et al., 2014)

4.2 Noise-Generating Mechanisms

Sound created by the interaction of the tires of a vehicle rolling on a pavement is by no means a simple phenomenon. The sound begins with various types of noise-generating mechanisms that occur simultaneously, numerous times, and to varying degrees depending on environmental conditions and the specific tire-pavement combination (Rasmussen et al., 2007). This section will discuss the most prominent noise-generating mechanisms in tire/pavement noise analysis and their frequencies of influence. Bernhard et al. (2005) classified noise-generation mechanisms into four sources: air pumping, tread impact, slip-stick, and adhesion.

4.2.1 Air Pumping

The air-pumping mechanism is a major source of tire-pavement noise (Ohiduzzaman et al., 2016). Air pumping occurs when air is forced between two surfaces, such as between tread blocks and pavement. The air that fills the gaps between the tread on a tire and the pavement is trapped and compressed. As the tire rolls and loses contact with the pavement, this trapped air is forced out into the environment (Rasmussen et al., 2007). The sound created by this mechanism is like clapping two hands together, where the air is compressed and forced out at the edges of the hands to create the clapping sound. This mechanism is generally highest around 1000 to 2500 Hz or higher frequencies (McDaniel, 2014). Nonetheless, researchers have found that increased pavement porosity or roughness can help mitigate air pumping noise by creating a path for the air to escape while being compressed between the tire tread and the pavement (McDaniel, 2014).

4.2.2 Impact-Induced Vibrations

Vibrations in the tire carcass are induced as the vehicle tires roll along the pavement and the tread blocks on the tire impact with the texture of the pavement. This is analogous to striking the surface of a pavement with several small rubber hammers every second (Rasmussen et al., 2007). Impact-induced vibrations can radiate sound and be a major source of tire-pavement noise. They are thought to affect noise below 1000 Hz. These vibrations can exist in the radial, tangential, or axial directions and depend primarily on surface macrotexture and the mechanical impedance of the pavement (McDaniel, 2014).

4.2.3 Slip-Stick Effect

Tire carcass vibrations can also be induced by very smooth pavements through friction (McDaniel, 2014). The rubber of the tire in contact with the pavement is continually deformed and distorted as the tire rolls along the road. This rubber will mostly stick to the pavement but will also periodically slip once a critical shear force is reached. These “slip and stick” motions happen thousands of times a second, creating high frequency sound, like the one produced by sneakers in a basketball court (Rasmussen et al., 2007). The slip-stick effect has been shown to cause noise in the 1000 to 2500 Hz range and above (McDaniel, 2014). Given that this mechanism is dependent on friction, it is likely to be affected by pavement texture at all wavelengths and by whether the texture is positive or negative. Moreover, temperature also has a great influence due to its effect on rubber friction. This implies that with temperature changes, frictional noise characteristics can vary even when using the same tire on the same pavement (Ohiduzzaman et al., 2016).

4.2.4 Adhesion-Induced Vibration

The adhesion mechanism occurs when the tire tread blocks stick to the pavement to later be stretched and released at the trailing edge of the contact patch, thus creating vibrations that radiate as sound energy in the radial and tangential directions of the tire carcass (McDaniel, 2014, Ohiduzzaman et al., 2016). The sound emitted by this mechanism is like the pop when a suction cup is released from a surface (Rasmussen et al., 2007). Adhesion is thought to be an important mechanism above frequencies of 1000 Hz, but its effects are reduced under wet pavement conditions and with increasing microtexture. Adhesion is also likely to be affected by temperature in similar ways to the slip-stick effects (McDaniel, 2014). Figure 4-8 shows a schematic illustrating the four major noise-generating mechanisms at the tire-pavement interface.

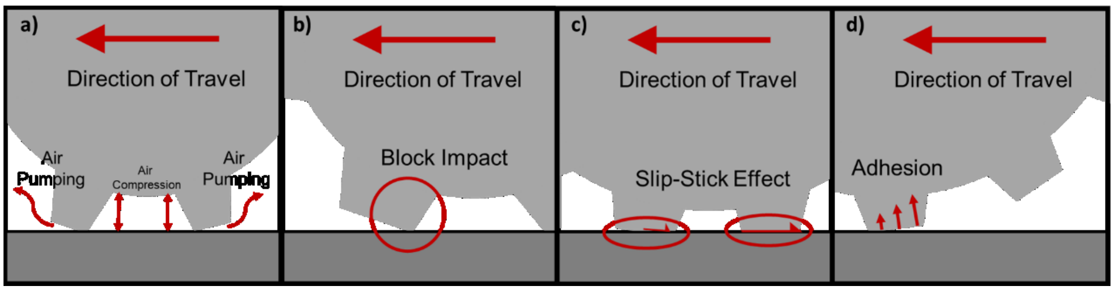

Figure 4-8 Schematic of noise-generating mechanisms: a) Air pumping, b) impact-induced vibrations, c) slip-stick effect, d) adhesion-induced vibrations.

The dominant noise frequency ranges related to each mechanism are as shown in Table 4-2. Vibration from tread impacts generate noise mostly in frequencies lower than 1000 Hz. These frequencies do not overlap with the primary range of the other three noise-generating mechanisms. Thus, they are easily separable from the rest when a spectral analysis is conducted. This is not case for any of the other three mechanisms. Their noise frequencies tend to overlap, which in turn complicates the process of separating their contribution to the overall noise level even when complex spectral analysis techniques are used.

Table 4-2 Frequency ranges for noise-generating mechanisms (Kuijpers and Van Blokland, 2001)

4.3 Factors Influencing Tire/Road Noise

Ongel and Harvey (2010) identified texture, roughness, air void content, thickness, stiffness, and age to be pavement surface characteristics that affect tire/road noise level. The researchers conducted regression analyses to explore the effects of pavement characteristics on the noise levels at different frequencies. They separated the noise levels into 11 one-third-octave bands from 500 Hz to 5000 Hz, with significant variables at a 5% significance level shown in Table 4-3. A plus sign indicates a positive correlation, while a negative sign indicates a negative correlation.

Table 4-3 Influence of pavement characteristics on tire/pavement noise

	500 Hz	630 Hz	800 Hz	1000 Hz	1250 Hz	1600 Hz	2000 Hz	2500 Hz	3150 Hz	4000 Hz	5000 Hz
MPD (micron)	+	+				-	-	-	-	-	-
Mix Type[1]	+	+	-	-	-	-	-	-	-	-	-
Air Void Content (%)	+	+	-	-	-	-	-	-	-	-	-
RMS	+	+				-	-	-	-	-	-
Fineness Modulus	+	+	-	-	-	-	-	-	-	-	-
Coeff. of Uniformity[2]	-	-	+	+	+	+	+	+	+	+	+
IRI (m/km)	+	+	+	+	+						
Age (years)					+					+	
Surface Thickness (mm)	-	-		+	+	+	+	+	+	+	+
Rubber Inclusion			-								
Nominal Maximum Aggregate Size (mm)				+	+	+	+	+			
Transverse Cracking[3]					+	+	+	+	+	+	+
Fatigue Cracking[4]					+	+	+				

4.3.1 Pavement Type

Van Keulen and Duskov (2005) have identified that the use of low-noise road surfacing is one of the most cost-effective and easy-to-implement approaches in terms of reducing traffic-induced noise. Two examples listed by the authors were porous asphalt and thin surfacing. Kandhal (2004) cited several European studies conducted in the 1990s, confirming that open-graded friction course was about 3 to 5 dB quieter compared to dense-graded hot-mix asphalt. While using dense-graded hot-mix asphalt as the reference, Kandhal claimed Portland cement concrete (PCC) to be 3 dB

[1] Mix type = Categorical Variable: Coded as 1 for open-graded mixes and 0 for gap and dense-graded mixes
[2] Coefficient of uniformity $C_u = D_{60} / D_{10}$; D_{60} is the sieve size associated with 60% passing and D_{10} is the sieve size associated with 10% passing
[3] Transverse Cracking = Categorical Variable Coded as 1 if the total length of transverse cracks ≥ 5 m in 150 m section, and 0 otherwise
[4] Fatigue Cracking = Categorical Variable Coded as 1 if the total fatigue cracking ≥ 5% of the wheel path area of the 150 m section, and 0 otherwise

louder (even more with transverse grooves or tinning), stone matrix asphalt 2 dB quieter, and open-graded friction course 4 dB quieter. Bernhard et al. (2005) identified surface texture with wavelengths greater than 20 mm to be a characteristic that correlates with noise positively, while surface texture with wavelengths less than 10 mm, porosity, elasticity, and negative texture tend to correlate with noise negatively. There can be as much as a 9-dBA difference in noise level for a single pavement type, and there can be as much as a 14-dBA difference between different types of pavements under similar conditions. Figure 4-9 shows the sound intensity level in dBA measured along different types of pavements.

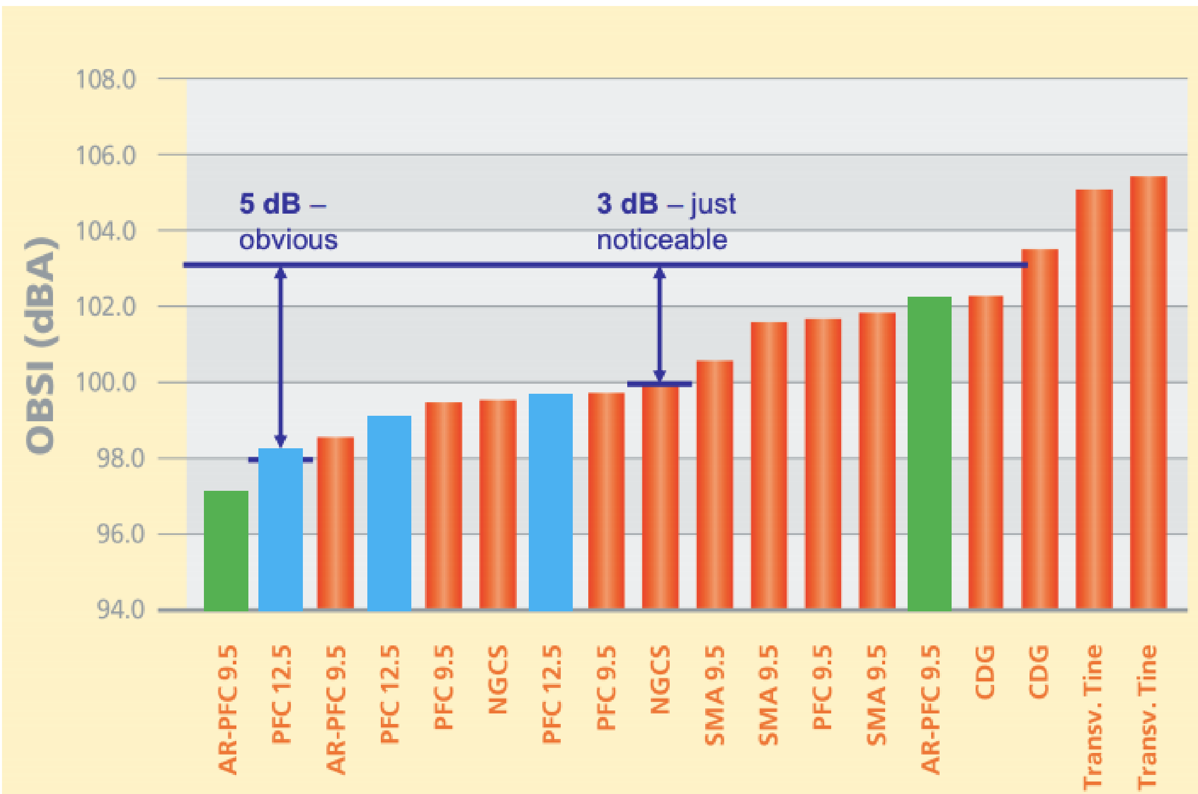

Figure 4-9 Noise level measured at different types of pavements (McGhee, 2012)

AR-PFC 9.5 is Asphalt Rubber Porous Friction Course produced with a 3/8 in. (9.5 mm) top size stone placed at 1 in. thickness. PFC 9.5 is polymer modified mix with 3/8 in. top size stone placed at 1 in. thickness. PFC 12.5 is polymer-modified mix with ½ in. (12.5 mm) top size stone placed at 2 in. thickness. NGCS is Next Generation Concrete Surface. SMA is finer-gradation stone-matrix asphalt placed at 1.5 in. thickness. CDG is conventional diamond grinding.

4.3.2 Air Void Content

Porous asphalt, which was originally developed for the purpose of water drainage, consists primarily of gap-graded aggregates held together by a polymer-modified binder to form a structure in which water can pass through the interconnected voids (Keulen and Duskov, 2005). They normally contain at least 20% voids in comparison with stone mastic asphalt's 3 to 6%. Researchers have ascribed the noise reduction effect of porous asphalt to acoustical absorption, elimination of horn effect, and reduction of air-pumping. The authors claimed a 4 dBA reduction in noise at high speeds.

4.3.3 Thickness

Many researchers have agreed that when combined with air void content or porosity, a sufficiently thick layer of surface tends to provide better acoustic absorption for noise reduction (Van Keulen and Duškov, 2005, Haider et al., 2007). Haider et al. (2007) proposed a combination of air void content of 20% and surface thickness of 40 mm to be favorable for sound absorption.

4.3.4 Age

As Ongel and Harvey (2010) pointed out, pavement surface characteristics are time dependent. For example, asphalt pavement becomes stiffer, the air paths in the open-graded pavement surface can become clogged, and various types of distresses may develop over the pavement's service life. How these time-dependent characteristics impact noise generation may be complicated.

4.4 Pavement-Noise Measurement

Highway transportation agencies have two methods to measure noise: wayside and on-source measurements.

4.4.1 Wayside Measurements

Wayside measurements, also known as roadside measurements, are the most basic and common method of measuring traffic noise. They consist of SPL measurements normally conducted by setting a sound meter mounted on a tripod either at a fixed distance from the road (typically 7.5 m (25 ft) or 15.2 m (50 ft)), or at a location where human receivers would usually be, such as residential backyards or playgrounds (Smit et. al., 2014, Rasmussen et al., 2007). These measurements capture all the noise from all sources: tire-pavement, aerodynamic, powertrain, reflections, and even other sources of noise not related to traffic. It is important to consider the influence of the environment surrounding the road when analyzing noise levels and not only the noise created by vehicles since roadway features may increase road noise levels through reflection and propagation. Moreover, embankments and slopes on the road may serve to absorb and mitigate noise levels (Smit et. al., 2014).

Wayside measurements can be categorized into two main methods of testing: pass-by and time-averaged methods. Pass-by noise methods for noise testing refer to the procedures of measuring vehicle noise emission levels from the side of road. These types of noise testing methods are commonly used in Europe by department of transportation agencies. The most common pass-by testing method is the statistical pass-by method (SPB). SPB involves measuring the maximum noise levels at the roadside from a statistically significant number of vehicles. As described in ISO 11819 (2001), SPB is a technique designed to evaluate the total traffic noise generated on a given section of road surface under specific traffic and weather conditions. The standard specifies that a microphone is mounted on a tripod and placed 7.5 m (25 ft.) from the center of the lane of traffic to be tested and 1.2 m (4 ft.) above the plane of the roadway. Once the microphone is set up, technicians will proceed to measure vehicle speeds and SPLs for at least 100 passenger cars and 80 dual-axle or multi-axle heavy vehicle pass-bys. Each individual pass-by is recorded with its corresponding vehicle speed and a regression line of the maximum A-weighted SPL versus the logarithm of speed is calculated for each vehicle category. Then, the average maximum A-weighted SPL is determined at the reference speed using the regression lines. This level is also known as the vehicle sound level.

The other two most common pass-by measurements are controlled pass and coast by method. Controlled pass-by method makes use of a similar microphone set up as the SPB method but instead of measuring noise from the existing traffic stream, this method employs a single test vehicle while no other vehicles are on the road (Smit et al., 2014). In this method, several passes of the test vehicle are made and from those passes the maximum pass-by SPL is recorded. Coast-by method can be considered a variation of the controlled pass-by method that is oriented towards isolating and recording mostly noise created due to tire pavement interaction. In the coast-by method, the driver of the test vehicle will shut off the engine as the vehicle approaches the testing location to drastically reduce the contribution of noise from the powertrain of the vehicle.

The second type of wayside measurement is time-averaged methods. On occasion, the conditions required to conduct a pass-by test are too difficult to be satisfied. Whenever this occurs, transportation agencies resort to time-averaged methods. The most used time-average test is the continuous flow traffic time-integrated model. This model, based on AASHTO TP 99 (2012), is a procedure for measuring the influence of road surfaces on highway traffic noise at a specific site. In this method, a sound pressure meter measures all traffic noise over a specified period, which is typically 5 to 30 minutes (Rasmussen et al., 2017). In addition, traffic volumes, speeds, vehicle categories, and meteorological data are measured continuously for a long enough period to properly represent these conditions on a typical day on the site (Smit et al., 2014). An equivalent continuous sound level (L_{eq}) over the specified time is later calculated and reported as the arithmetic mean of repeated measurements. The parameter L_{eq} is used for all traffic noise analyses for TxDOT highway projects, and it is defined as the equivalent steady-state sound level at a given time that contains the same acoustic energy as a time-varying sound level during the same period (Smit et al., 2014).

4.4.2 On-Source Measurements

Alternatively, state DOTs may prefer to run on-source measurements, as opposed to wayside measurements. On-source testing provides isolated noise measurements from a specific source, such as at the tire-pavement interface. However, a limitation shared by these methods is that they cannot provide an indication of the influence of roadway features such as geometry and cross section on noise generation, mitigation, or propagation. The two more typically used on-source test methods in the US and Europe are OBSI and CPX, respectively. The OBSI method is a measurement procedure used to evaluate the tire/pavement noise component resulting from the interaction of an ASTM F2493, Standard Reference Test Tire (SRTT) on a pavement surface by installing a dual or single configuration of microphone probes at the trailing and leading edges of the tire, as shown in Figure 4-10. The vehicle is later driven at a reference speed 96.6 km/h (60 mph) for 134 m (440 ft) on 3 selected sites within a section of road, with minimum elevation grades or curves, to measure the sound intensity created as the vehicle moves along the pavement (AASHTO TP 76-15). The main advantage of this method is that it is relatively fast compared to wayside measurements, and it isolates the tire-pavement noise from all other traffic noise making it simpler to analyze sound intensity levels on different frequencies by means of correlation. The main drawback to this method is that it requires a vehicle with a specific reference tire to rule out variations in tire geometry, it must be conducted under specific environmental conditions (such as dry pavement and low wind speeds), and it does not consider other road features that might influence the sound propagation at the tire-pavement interface.

Figure 4-10 OBSI dual probe configuration setup

The CPX method, developed in Europe and defined by ISO 11819 (2002), measures the tire-pavement noise at the source. In this method, a test tire is mounted along with an array of microphones within a specially designed trailer that is towed behind a test vehicle at highway speeds (Ohiduzzaman et al., 2016). The tire is enclosed in a box of sound-absorbing material to minimize the change in noise levels due to environmental variations and only measure tire-pavement noise (Smit et al., 2014). The primary disadvantage of CPX testing is that a larger investment must be made to purchase microphones, data processing equipment, and the trailer. The CPX shares some of limitations to the OBSI method, but it is not affected by high wind speed because the microphones are isolated inside the trailer. A diagram summarizing the major noise testing methods used by transportation agencies can be seen in Figure 4-11.

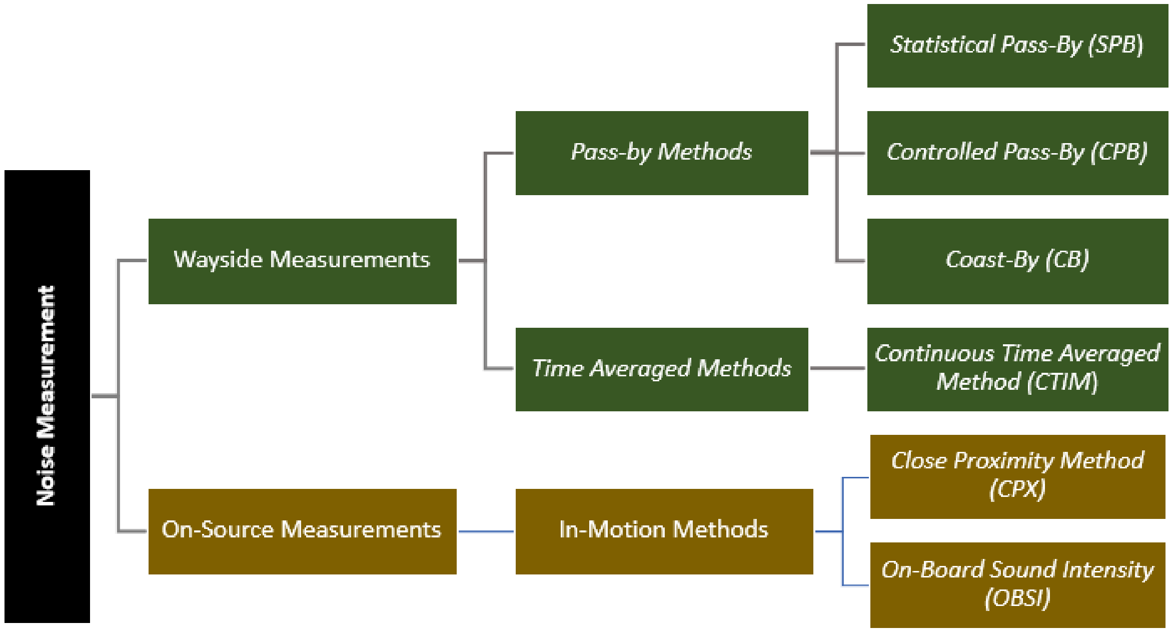

Figure 4-11 Summary of the most common noise measurements tests

4.5 Correlations Identified by Past Studies

Anfosso-Lédée and Do (2002) proposed the concept of a profile indenter, composed of a profile peak and its neighboring valleys to the left and to the right, to characterize the profile by its shape and relief. The indenter shape is defined by the cotangent of its summit semi-angle calculated by Equation 4-1. Its relief, defined by the angle between the horizontal line and the segment connecting the summits of two consecutive indenters, is calculated by Equation 4-2. Another parameter that can be used to characterize indenters is density, defined as the number of indenters per unit length (Equation 4-3).

$$\alpha = \frac{1}{2}\left[\tan^{-1}\left|\frac{x_e - x_{e-1}}{z_e - z_{e-1}}\right| + \tan^{-1}\left|\frac{x_{e+1} - x_e}{z_{e+1} - z_e}\right|\right] \tag{4-2}$$

Where,

α = Profile indenter

z_e = Height of the e^th^ extremum

x_e = Abscissa of the e^th^ extremum

$$\theta = \tan^{-1}\left|\frac{z_{p+1} - z_p}{x_{p+1} - x_p}\right| \tag{4-3}$$

Where,

θ = Profile relief

z_p = Height of the p^th^ extremum

x_p = Abscissa of the p^th^ extremum

It was found that rolling noise increases when cotangent (α) or (θ) increases, or when the density decreases, and the three geometric parameters are strongly intercorrelated. The authors pointed out that when cotangent (α) increases, both the drainage capacity and vibration excitation decrease. As drainage capacity is reduced, more high-frequency noise is generated through air pumping, as the number of asperities enveloped by the tire rubber increases, while as vibration excitation decreases, low-frequency noise is reduced due to decreased rubber deformation. As these two effects counteract each other's impact on total noise, the extent to which an increased cotangent (α) or (θ) affects the overall noise level varies depending on the specific tire and pavement. Meanwhile, when the indenter density increases, smaller spacing is found in between two consecutive ones, causing lower vibration excitation as well as higher drainage capacity for air. As discussed earlier, lower vibration excitation reduces low-frequency noise from tread impact, and higher drainage capacity reduces high-frequency noise from air pumping.

Domenichini et al. (1999) agreed with the pattern that texture wavelength ranging from 10 to 500 mm increases the noise in the low frequency range (<1000 Hz for light vehicles and <500 Hz for heavy vehicles), originating from tire vibration, and the texture wavelength ranging from 0.5 to 10 mm decreases the noise at high frequencies (>1000 Hz), originating from air pumping, consistent with what Sandberg and Descornet (1980) identified. The researchers identified three pavement surface characteristics relevant to tire/pavement noise: texture, wearing course porosity, and thickness of the porous surface layer. The study evaluated MPD based on pavement profiles using the TINO 3D profilometer according to ISO 13473-1 and MTD based on the SPT according to ASTM E965. The texture level of the pavement profiles was analyzed using the PSD. The classification of the texture wavelengths with respect to traffic-induced vibrations was performed following ISO 8608, and conformed to the World Bank Index IRI (WB TP 46). The skid resistance properties at various speeds were evaluated as a function of MTD and BPN.

Noise measurements were made with a slick tire and a standard tire at 50 and 80 km/h. The correlation between texture and noise was analyzed at each spatial frequency of texture level with a noise level at a certain temporal frequency, called "texture-noise gradient."

Friction properties were estimated from the results of the BPT and MTD measurements based on the relationships (Table 4-4) from Leu and Henry (1978).

Table 4-4 Summary of equations used by Leu and Henry to relate noise and texture

Statistic	Equation
Zero Speed Skid Number (SN_0)	$SN_0 = -31 + 1.38 \cdot BPN$
Percentage Skid Number-Speed Gradient ($PSNG$)	$PSNG = 4.1 \cdot \left(\frac{MTD}{0.0254}\right)^{-0.47}$
Skid Number at Velocity, V (SN_V)	$SN_V = SN_0 \cdot \exp(\frac{-PSNG \cdot V}{100})$
Peak Slope Parameter (PSP)	$PSP = \frac{L_{PEAK} \cdot i}{100}$
Unevenness Level (L_{UNE})	$L_{UNE} = \frac{L_{1.26} + L_{1.58} + L_{2.00}}{3}$
Texture Index (TI)	$TI = 2.5 \cdot PSP + L_{UNE}$
First Maximum Relative Texture Level (L_{PEAK})	$L_{PEAK} = \frac{L_{fPEAK^-} + L_{fPEAK} + L_{fPEAK^+}}{3}$
Slope of Descending Portion (i)	$i = \frac{L_{PEAK} - SL_{500}}{\log(\lambda_{PEAK}) - \log(2)}$
Smoothed Texture Level at 2mm (SL_{500})	$SL_{500} = \frac{L_{500^-} + L_{500} + L_{500^+}}{3}$

Where,

f_{PEAK}: spatial frequency corresponding to λ_{PEAK}

λ_{PEAK}: wavelength at which relative maximum occurs

f_{PEAK^-}: previous spatial frequency

f_{PEAK^+}: following spatial frequency

Once all the parameters in Table 4-4 were computed, the SPL was calculated. There are two equations that can be applied; the choice of equation to use is based on the speed of the vehicle.

When V = 50 km/h,

SPL = 0.47 TI + 49.39

When V = 80 km/h,

SPL = 0.47 TI + 42.94

Liu and Shalaby (2015) state that pavement texture is a factor that influences tire-pavement interactions such as noise and friction. The authors cite Flinsch et al. (2003) as the argument to use 3D texture descriptors instead of MPD, which is a 2D approximation of the 3D MTD. Vehicle-mounted laser devices can measure macrotexture of pavement without disrupting traffic flow. However, studies show that 2D texture measurement and indicators are insufficient, especially when analyzing friction and noise (Liu and Shalaby, 2015, El Gendy and Shalaby, 2007, El Gendy et al., 2011). Texture size, spacing, and distribution are factors to be considered as well.

The authors' goal was to come up with several 3D texture parameters to describe texture and to correlate with friction and noise. They used a section of the South Extension of the I-355 North-South Tollway between I-55 and I-80 near Joliet, Illinois, as the test site, selected for testing the

PCC surface texture. The test section was divided into 13 segments, each about 160 m long, representing different types of PCC pavement texture. Texture was measured using a photometric stereo device and high-speed texture profiler. Friction was measured using a dynamic friction tester (ASTM E1911 2009), and sound intensity was measured in accordance with AASHTO Provisional Standard TP076 (AASHTO, 2008).

The first 3D macrotexture indicator was simulated mean texture depth (SMTD), calculated using Equation 4-4. The RMS roughness (S_q), skewness (S_{sk}), and kurtosis (S_{ku}) are calculated by Equations 4-5, 4-6, and 4-7, respectively.

$$SMTD = h_{max} - \frac{1}{A}\sum_{i=1}^{M}\sum_{j=1}^{N}\frac{1}{3}ah_{ij} \tag{4-4}$$

$$S_q = \sqrt{\frac{1}{A}\sum_{i=1}^{M}\sum_{j=1}^{N}ah_{ij}^2} \tag{4-5}$$

$$S_{sk} = \frac{1}{A(S_q)^3}\sum_{i=1}^{M}\sum_{j=1}^{N}ah_{ij}^3 \tag{4-6}$$

$$S_{ku} = \frac{1}{A(S_q)^4}\sum_{i=1}^{M}\sum_{j=1}^{N}ah_{ij}^4 \tag{4-7}$$

Where,

h_{max}: Highest elevation of surface texture — A: Area of the surface

h_{ij}: Elevation of the (i^{th}, j^{th}) pixel — a: area of pixels

N, M: Number of pixels in each direction

It was found that skewness and kurtosis, which are based on third and fourth moment of surface texture heights, respectively, are highly correlated. Therefore, only one of them would be sufficient to describe the shape and distribution of the surface texture. The regression conducted among sound-intensity noise, SMTD, and skewness was found to be:

$$Noise = 105.87 + 2.06\,SMTD + 3.88\,S_{sk}$$

$$R^2 = 0.71 \qquad SEE = 0.559$$

The friction number F (60) was found to be:

$$F(60) = 14.64 + 11.54SMTD - 0.45\,Ssk$$

$$R^2 = 0.53 \qquad\qquad SEE = 2.45$$

where, *F (60)* indicates the friction measured at 60 km/h

The authors concluded that both texture heights and texture distribution (skewness and kurtosis) are important factors in pavement noise/friction. Negatively skewed surface texture tends to provide better friction and generate less noise (Liu and Shalaby, 2015). They also cited Do et al. (2000) and Flintsch et al. (2003) to support the argument that information on macrotexture alone is not sufficient to predict pavement friction, and that both microtexture and macrotexture are needed to obtain higher accuracy in friction prediction.

Chapter 5. Analysis on Friction, Texture, and Noise

This chapter presents the data collection process and describes most of the processing algorithms involved in the research project.

5.1 Data Collection Procedure

The dataset for the initial analysis comprises a total of eight in-service flexible pavements in Texas. The eight sites were chosen from four different TxDOT districts and include the following asphalt mixes: thin overlay mix (TOM), open-graded PFC, NovaChip, and dense-graded type-C. The sites were chosen to evaluate variation of surface texture across different mix designs. A summary of all tested sites can be found in Table 5-1.

Table 5-1 Sites and mix design distribution

Section Number	District	Highway	Surface Type
1	Austin	SH 195	PFC
2	San Antonio	US 181	NovaChip
3	Brownwood	IH 20	Seal Coat
4	Brownwood	SH 36	Type C
5	Bryan	US 84	Seal Coat
6	Austin	FM 1431	PFC
7	Austin	RM12	TOM
8	Austin	FM 1626	TOM

For each site, spot measurements of texture were taken in three different locations over a span of 30 meters (98.5 ft) with a 15-m (49.2 ft) spacing between each location in the longitudinal direction. The sections selected were homogeneous areas, representative of the specific highway pavement. The right wheel path of the outside lane was measured for all three sections, in a single direction of traffic. The safety of the researchers and motorists was assured with the assistance of TxDOT, who provided traffic control for all the sites. Figure 5-1 illustrates the sampling method used to collect data for on-spot measurements. For the dynamic measurements, the micro-GripTester, OBSI, and GripTester surveyed the whole right wheel path along the section. The OBSI was the only equipment where it was necessary to measure both directions of traffic, on the rightmost lane, to adhere to the AASHTO standard.

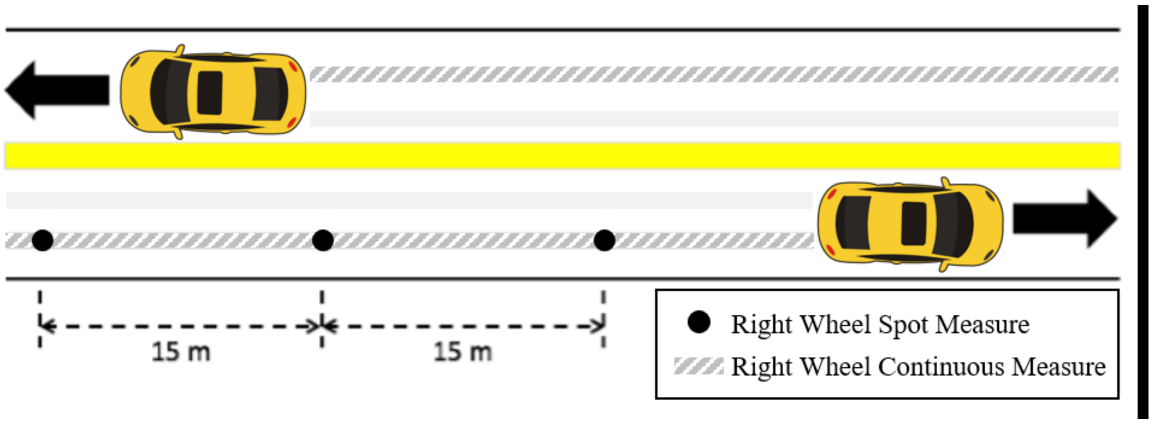

Figure 5-1 Field test sampling method

5.1.1 Noise Data Collection

The tire/pavement noise of the road was evaluated using the OBSI method. All measurements were taken alongside the leading and trailing edge of the SRTT on the passenger side of the vehicle opposite of the driver using a dual probe configuration of microphones (Figure 5-2) at a constant speed of 96.5 km/h (60 mph), as per AASHTO standard TP 76-15. To ensure consistency, the vehicle was driven by a single driver who used the same testing vehicle and SRTT on all eight sites. Additionally, the vehicle only had necessary equipment on board, to avoid variations in total vehicle weight.

Figure 5-2 OBSI setup on passenger side rear wheel

5.1.2 Texture Data Collection

The LLS was used to collect 3D data of the pavement texture, utilizing a laser that moved along the direction of traffic. The LLS covered a longitudinal distance of 600 mm with a laser line width of 200 mm. The CTM measurements were made in the same area covered by the LLS. The SPT was also performed adjacent to the area where the LLS and CTM were performed to avoid contamination from the SPT's sand. Figure 5-3 shows all the static texture measurement equipment in operation.

Figure 5-3 (Left) LLS in operation, (middle) CTM placement, (right) SPT

5.1.3 Friction Data Collection

The friction characterization consisted of three different friction tests (Figure 5-4). The BPT was applied in each of the sampling sites following the traffic direction. The micro-GripTester collected a continuous measure of friction at a walking speed of 0.7 m/s (2.3 ft/s). The result consists of an averaged value of friction measures, expressed as GN, for the three sections. For the Grip-Tester, the output is given as GN at a target speed of 70 km/h (43.5 mph). Previous studies indicated Grip-Tester measurements taken at higher speeds correlate better with texture (Kouchaki, 2018). The vehicle towing the GripTester was driven at a speed within 5% of 70 km/h. The pavement was wetted with a constant water thickness of 0.5 mm with an automatic water tank system. The GN for each section was obtained as the average of the GN measures along the total evaluated distance (approximately 30 m).

Figure 5-4 (left) BPT in operation, (middle) micro-GripTester, (right) GripTester attached to vehicle

5.1.4 Data Processing

The noise data collected using the OBSI system was processed as per AASHTO TP-76. The intensity levels collected from the trailing and leading-edge probes were energy-averaged to yield an average intensity level, using Equation 5-1. The individual test run average levels were then arithmetically averaged to calculate the average noise intensity levels for the three test runs at each one-third octave band frequency between 400 and 5,000 Hz.

$$L_{E-avg} = 10\log_{10}\left(\frac{1}{N}\sum_{i=1}^{N}\left(10^{\left(\frac{L_i}{10}\right)}\right)\right) \tag{5-1}$$

Where:

L_{E-avg}:	Average energy level (dBA)
L_i:	Levels (dBA)
N:	Number of sets of data

The result of this processing yields 12 data points for noise intensity levels ranging from one-third octave band frequencies of 400 to 5,000 Hz as shown in Figure 5-5.

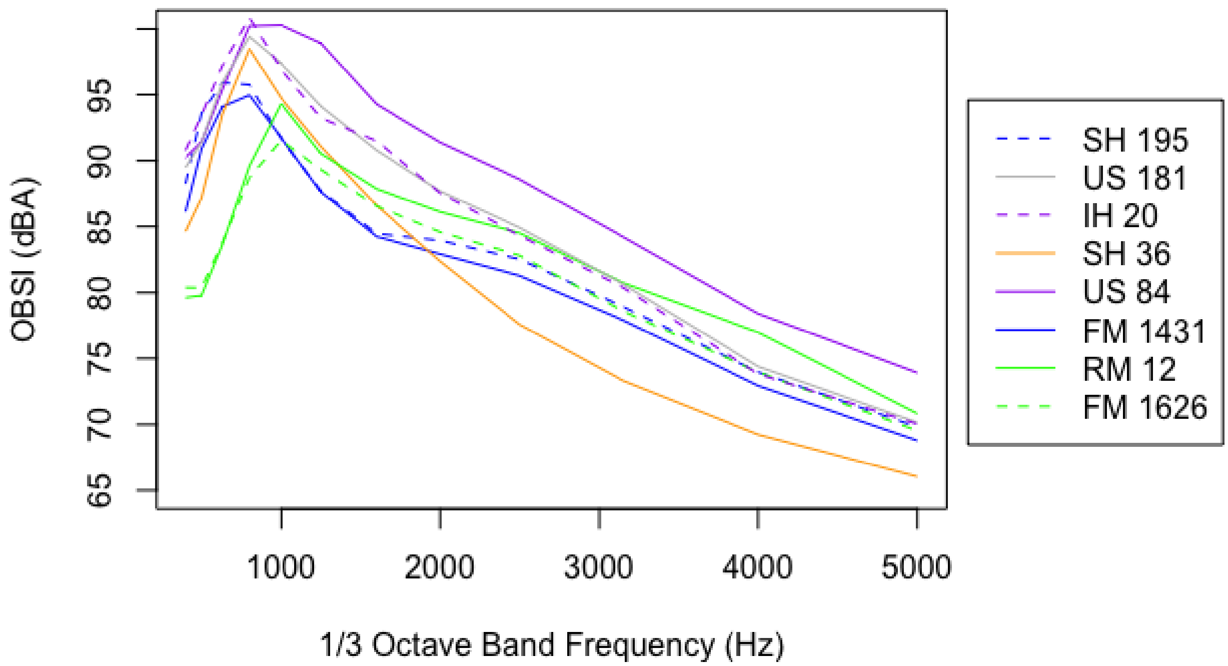

Figure 5-5 Distribution of A-weighted OBSI over one-third octave band frequencies

Texture data collected using the LLS setup was processed as per ISO/TS 13473, which involves applying multiple transformation algorithms. First, invalid points were located within the dataset by using numerical thresholds and computed as a percentage of all points. This percentage is known as the drop-out rate, and it must never exceed 10%. Once all sections were confirmed to have a drop-out rate below 10%, all invalid points were replaced by using one-dimensional linear interpolation as per Equation 5-2.

$$z_i = \frac{z_n - z_m}{n - m}(i - m) + z_m \tag{5-2}$$

Where:

i: Sample number where the value is invalid.
m_i: Sample number of the nearest valid value before i
n: Sample number of the nearest valid value after i
z_i: Interpolated value for sample i
z_{m_i}: Value for sample m
z_n: Value for sample n

A least-square fitting algorithm is then used to achieve a slope of zero in the profile in a process called slope suppression. The mean amplitude of the profile is later set to zero in a process referred to as offset suppression. This yields a profile with a base height of 0.0 mm, where peaks and valleys can be easily distinguished (as Figure 3-1 illustrated). Next, the profile is subjected to a windowing algorithm to reduce the signal amplitude to zero at the edges of the profile and avoid leakage. Given that the length of the measured profile is less than one meter, a split cosine bell window is applied as per Equation 5-3.

$$(3)\ w_{i,C} \coloneqq \begin{cases} cos^2\left(\frac{5\pi i}{N} - \frac{\pi}{2}\right) & for \quad 0 \le i < \frac{N}{10} \\ 1 & for \quad \frac{N}{10} \le i < \frac{9N}{10} \\ cos^2\left(\frac{5\pi i}{N} - \frac{9\pi}{2}\right) & for \quad \frac{9N}{10} \le i < N \end{cases} \tag{5-3}$$

Where:

$w_{i,C}$: Window coefficient
i: Sample number
N: Number of data points

The window coefficient was multiplied by the signal and later normalized by the integral of the window to prevent attenuation of the signal as per Equation 5-4.

$$(4)\ Z_{i,win} \coloneqq \frac{w_{i,C} * z_i}{0.9354} \quad for\ i = 0, \dots, N-1 \tag{5-4}$$

Where:

$Z_{i,win}$: Windowed profile height at point i (mm)

To transform the texture data from the spatial time domain into the spatial frequency domain, a discrete Fourier transform (DFT) is applied to the windowed profile, as defined by Equation 5-5.

$$(5)\ Z_k := \frac{1}{N}\sum_{i=0}^{N-1} Z_{i,win} * e^{-j\left(\frac{2\pi k}{N}\right)i} \quad for\ k = 0, \dots, N-1 \tag{5-5}$$

Where:

Z_k:	DFT of the windowed profile
j:	The imaginary unit ($j^2 = -1$)

The result of the DFT is a constant bandwidth narrow band spectrum with complex values. The bandwidth is a function of the evaluation length defined by Equation 5-6.

$$(6)\ \Delta f_{sp} = \frac{1}{l} \tag{5-6}$$

Where:

Δf_{sp}:	Bandwidth intervals (cycle/meter)
l:	Evaluation length (m)

An important property of the DFT is that it obeys the Nyquist Sampling Theorem, which states that the sampling frequency should be at least twice the highest frequency contained in the original signal. An alternate way to interpret this statement is that the shortest wavelength that can be obtained from a discrete signal is twice the sample spacing. Given that the LLS is capable of sampling two points with a spacing of 0.008 mm in the longitudinal direction, the shortest wavelength that can be analyzed using the LLS is 0.016 mm. This implies the DFT can capture all the information up to the shortest wavelength of the first decade of microtexture (0.05 mm).

The results of the DFT are later converted into a PSD by means of Equation 5-7.

$$Z_{PSD} = \frac{2|Z_k|^2}{\Delta f_{sp}} \quad for\ k = 0, \dots, \left(\frac{N}{2} - 1\right) \tag{5-7}$$

Where:

Z_{PSD}:	Power Spectral Density

Given that the result of a PSD is a form of constant bandwidth spectral data, it was later transformed into constant-percentage bandwidth spectral data such that it can be represented in the form of fractional octave bands. The power within the fractional octave band, *m,* can be calculated from the narrow band PSD according to Equation 5-8.

$$Z_{P,m} = Z_{PSD,low} * \left(f_{sp,low} + \frac{1}{2}\Delta f_{sp} - \left(10^{\left(-\frac{1.5}{10n}\right)}\right) * f_{sp,m}\right) + \sum_{k=low+1}^{up-1} Z_{PSD,k} * \Delta f_{sp} + Z_{PSD,up} * \left(f_{sp,m} * \left(10^{\left(-\frac{1.5}{10n}\right)}\right) - f_{sp,up} + \frac{1}{2}\Delta f_{sp}\right) \quad (5\text{-}8)$$

Where:

$Z_{PSD,low}$:	PSD of the narrow band that coincides with the lower boundary of the fractional octave band.
$f_{sp,low}$:	Center frequency of the narrow band that coincides with the lower boundary of the fractional-octave band
$f_{sp,m}$:	Center frequency of the fractional-octave band *m*
$Z_{PSD,up}$:	PSD of the narrow band that coincides with the upper boundary of the fractional-octave band
$f_{sp,up}$:	Center frequency of the narrow band that coincides with the lower boundary of the fractional octave band.
n:	Integer whose value can be freely chosen to obtain a desired speed; for this study it was chosen to be 1

Finally, a texture level distribution (TLD) was computed. The TLD provides a more detailed metric by which to evaluate texture and can be related to mixture properties. The TLD estimates the proportion of wavelengths in the profile that can be attributed to aggregate and mixture properties (Miller et al., 2011). These wavelengths are captured in the form of fractional one-third octave bands. The texture profile level (L_{tx}) is measured in dBs and computed using Equation 5-9.

$$L_{tx,m} = 10\, log_{10}\left(\frac{Z_{P,m}}{a_{ref}^2}\right) \quad (5\text{-}9)$$

Where:

a_{ref}:	Reference value of the surface profile, equal to 10^{-6} m
$L_{tx,m}$:	Texture level within fractional-octave band *m* (dB)

Once the texture data is converted to a TLD at different one-third octave band wavelengths, it is further trimmed to wavelengths for which there was enough texture data to compute a texture level. The final distribution of wavelengths covered 36 different one-third octave band wavelengths ranging from 80 mm down to 0.025 mm. Figure 5-6 illustrates the TLD for one of the test sites. Next, the texture data was further subdivided into 26 texture wavelength sets of 12 consecutive wavelengths, to create a one-for-one match with the noise data and facilitate statistical analysis. For example, the texture set A includes the texture wavelengths from 80 mm down to 6.3 mm. Table 5-2 shows the different texture wavelength sets that were created in terms of their spatial frequency; Table 5-3 shows those sets in terms of wavelength.

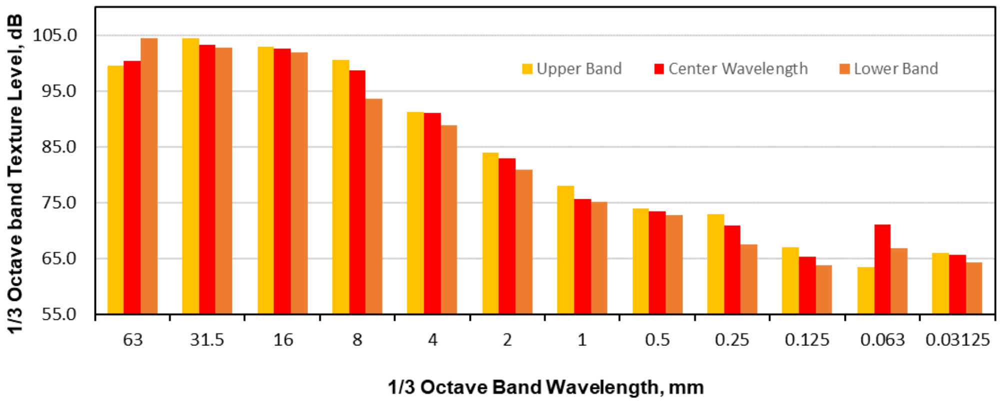

Figure 5-6 TLD for one of the test sites, values in the x-axis show the center wavelength (red bar) of the one-third octave band wavelength.

Table 5-2 Texture sets in terms of spatial frequency

Set	Frequency (cycle per meter)		Set	Frequency (cycle per meter)	
	Start	*End*		*Start*	*End*
A	12.5	160	O	250	3,150
B	16	200	P	315	4,000
C	20	250	Q	400	5,000
D	25	315	R	500	6,250
E	31.5	400	S	625	8,000
F	40	500	T	800	10,000
G	50	625	U	1,000	12,500
H	62.5	800	V	1,250	16,000
I	80	1,000	W	1,600	20,000
J	100	1,250	X	2,000	25,000
K	125	1,600	Y	2,500	31,500
L	160	2,000	Z	3,150	40,000
M	200	2,500	~	~	~

Table 5-3 Texture sets in terms of wavelength

Set	Wavelength (mm)		Set	Wavelength (mm)	
	Start	*End*		*Start*	*End*
A	80.0	6.30	O	4.00	0.315
B	63.0	5.00	P	3.15	0.250
C	50.0	4.00	Q	2.50	0.200
D	40.0	3.15	R	2.00	0.160
E	31.5	2.50	S	1.60	0.130
F	25.0	2.00	T	1.30	0.100
G	20.0	1.60	U	1.00	0.080
H	16.0	1.25	V	0.800	0.063
I	12.5	1.00	W	0.630	0.050
J	10.0	0.80	X	0.500	0.040
K	8.00	0.63	Y	0.400	0.031
L	6.30	0.50	Z	.315	0.025
M	5.00	0.40	~	~	~

5.2 Noise: Statistical Analysis

Three statistical methods were used to analyze the data set: simple and multiple linear regression, panel data analysis, and hypothesis testing.

5.2.1 Hypothesis Testing

Hypothesis testing was conducted before the two other methods for the purposes of grouping the data set adequately, given that for certain mix designs there are two different sites that have been reported to have the same mix. Such sites should not be grouped together, unless they are statistically identical to one another, in terms of their texture and noise data. Disregarding this step would result in lower accuracy of statistical models when the entire data is analyzed based on the different mixes. Therefore, hypothesis testing was conducted to evaluate whether the assumption that two roads with the same mix design are statistically similar is true. It was assumed that distribution of texture and noise data was a student distribution and hence the hypothesis was tested using Equation 5-10 and Equation 5-11:

$$H_o: \beta_1 - \beta_2 = 0 \tag{5-10}$$

$$H_A: \beta_1 - \beta_2 \neq 0 \tag{5-11}$$

Where:

H_o: The null hypothesis (two roads with the same mix are statistically identical)
H_A: The alternative hypothesis (two same mix roads are not statistically identical)

β_1: Parameter for road 1
β_2: Parameter for road 2

The p-value obtained from hypothesis testing is an indicator of whether two roads are statistically identical. For two roads to be considered identical, the p-value obtained from the difference in their texture and noise data must both be greater than 0.05; otherwise the null hypothesis is rejected. The p-values obtained from the hypothesis testing analysis are reported in Table 5-4. The hypothesis test showed that there is sufficient evidence in the data to suggest that the pairs of roads that shared the same mix design are not statistically identical in terms of their noise and texture, since all P-values are less than 0.05. Hence, they should not be grouped together when the data is analyzed using panel data based on their mix design. A possible reason for these differences in noise could be differences in the aggregate size and type, layer thickness of the pavements, differences in pavement temperature at time of testing, or the age of the asphalt binder.

Table 5-4 P-values obtained from hypothesis testing two roads

	Texture		Noise	
	Number of Std Dev from 0	*P-value*	*Number of Std Dev from 0*	*P-value*
PFC	2.499	0.0173	4.584	0.0008
TOM	7.807	0.0000	3.428	0.0056
Seal Coat	9.674	0.0000	2.888	0.0148

5.2.2 Linear Regression Analysis

Simple and multiple linear regressions were used to determine whether a correlation existed between noise and texture. Regression analysis was used to quantify the relationship between measured friction and texture statistics related in a nondeterministic fashion. The most straightforward deterministic mathematical relationship between two variables x and y is a linear relationship. This relationship is also known as the simple linear regression (SLR) equation (Equation 5-12).

$$Y = \beta_0 + \beta_1 x \tag{5-12}$$

The first regression model tested was an SLR model where wavelength sets of texture levels from Table 5-2 were used to the predict the noise intensity levels across all the noise frequencies (Equation 5-13).

$$IL_{noise} = \beta_0 + \beta_1 * L_{tx} \tag{5-13}$$

The main parameters of interest obtained from the linear regression were the R^2, to determine how well the data collected fits the model; the standard error of the model; and the p-value, to determine the significance of the texture parameter. For this analysis, a p-value smaller than 0.05 is an indicator that the texture wavelength set selected is significant when predicting noise levels. The results from this analysis are summarized in Table 5-5 and Figure 5-7.

Table 5-5 Example of SLR results for highway FM 1431, section 1

Texture Wavelength Set	R^2	Standard Error	P-value	Texture Wavelength Set	R^2	Standard Error	p-value
A	0.44	7.12	0.018	O	0.40	7.38	0.028
B	0.49	6.81	0.012	P	0.33	7.85	0.061
C	0.66	5.51	0.001	Q	0.25	8.21	0.095
D	0.80	4.28	0.000	R	0.38	7.48	0.033
E	0.77	4.50	0.000	S	0.61	5.92	0.003
F	0.74	4.83	0.000	T	0.69	5.33	0.001
G	0.70	5.17	0.001	U	0.65	5.62	0.002
H	0.76	4.63	0.000	V	0.14	8.84	0.240
I	0.80	4.24	0.000	W	0.15	8.76	0.212
J	0.70	5.19	0.001	X	0.02	9.43	0.684
K	0.55	6.37	0.006	Y	0.16	8.74	0.206
L	0.48	6.88	0.013	Z	0.01	9.47	0.783
M	0.46	7.01	0.016				

Starting from wavelength set A to U, all the p-values are smaller than 0.05, implying that the full spectrum of macrotexture and the wavelengths corresponding to the first decade of microtexture have a significant influence on noise levels. The R^2 peaked at the macrotexture wavelength sets of C, D, and E, and peaks again, but to a smaller degree, at the microtexture wavelength sets of S, T, and U. Furthermore, the influence of these texture wavelengths was also positive. This indicates that, regardless of mix type, as the texture level of the pavement increases the noise intensity levels will also increase. The set of texture wavelengths that showed the strongest correlation were sets C, D, and E, which include texture wavelengths within the first decade of macrotexture. A graph of the fitted regression line on the data points for one of the highways is shown in Figure 5-7. This result agrees with results obtained by Hall et al., 2009, where the macrotexture component has the greatest influence in determining noise intensity levels in a highway.

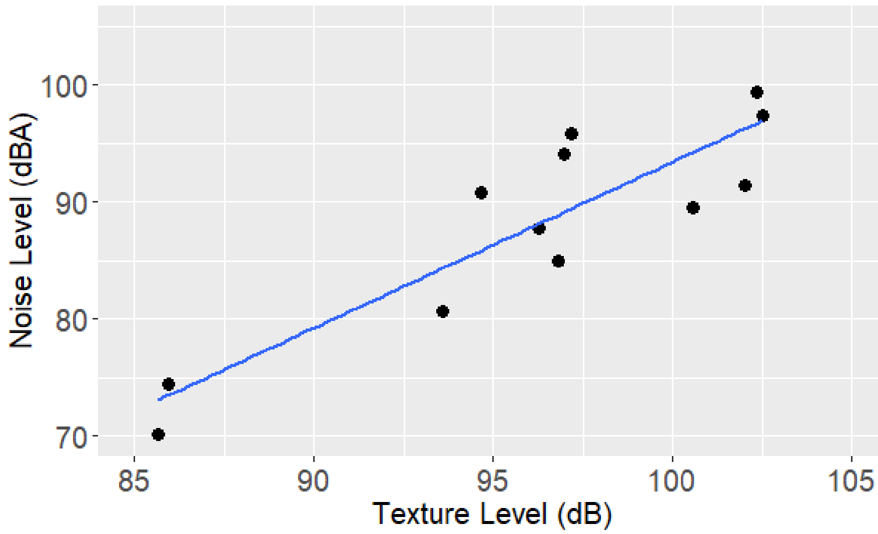

Figure 5-7 Linear regression line for texture wavelength set D on FM 1431, section 1

The second model was a multiple linear regression (MLR). The general equation for MLR is given by Equation 5-14. In SLR only one texture wavelength was used to correlate texture with noise. Multiple regression analysis allows the incorporation of more components of the texture spectrum, by including more texture wavelength sets as predictors. The first MLR model (Equation 5-15) uses macrotexture wavelength sets for the first predictor and subsequent texture wavelengths sets for the second predictor. For example, if the first predictor is set A ($80.0\ mm \leq \lambda \leq 6.30\ mm$), then the second predictor would be set M ($5.00\ mm \leq \lambda \leq 0.40\ mm$). For simplicity, the first predictor is referred to as the profile's macrotexture and the second, as the profile's microtexture. The second MLR model (Equation 5-16) used the entire TLD. It consisted of texture sets A, M, and Z, which correspond to long, medium, and short wavelengths, respectively.

$$Y = \beta_0 + \sum_{i=1}^{n} \beta_i x_i \tag{5-14}$$

$$IL_{noise} = \beta_0 + \beta_1 * L_{tx_{macro}} + \beta_2 * L_{tx_{micro}} \tag{5-15}$$

$$IL_{noise} = \beta_0 + \beta_1 * L_{tx_{Long}} + \beta_2 * L_{tx_{Medium}} + \beta_3 * L_{tx_{Short}} \tag{5-16}$$

It was observed that, across all sites, the adjusted R^2 values were higher than the simple regression analysis counterpart; however, the microtexture predictors are not significant enough in any of the cases. All possible combinations of macro and microtexture sets were tested, but in none of those attempts were both texture parameters significant. The only trend found was that noise tended to be more strongly correlated to macrotexture than microtexture. When three texture sets were used, the significance of all three parameters was marginally higher than when only two texture sets where used. Thus, it appears that even when all possible texture wavelengths are used in the regression, only those within the macrotexture component appear to have significant influence on tire/pavement noise. Moreover, this correlation is positive: as macrotexture increases, the noise also increases. Sample results for US-181, Section 1, using MLR are summarized in Table 5-6.

Table 5-6 Summary of multiple regression analysis results from US 181 section 1

Texture Wavelength Set	R^2	Standard Error	P-value		
			Long Wavelength	*Middle Wavelength*	*Short Wavelength*
AM	0.48	6.55	0.153	~	0.128
BO	0.42	6.91	0.155	~	0.417
CP	0.59	5.81	0.011	~	0.960
DQ	0.77	4.32	0.000	~	0.382
ER	0.75	4.51	0.002	~	0.363
FS	0.69	5.07	0.060	~	0.784
GT	0.65	5.35	0.360	~	0.569
HU	0.71	4.87	0.067	~	0.888
IV	0.81	3.92	0.000	~	0.138
JW	0.67	5.18	0.002	~	0.335
KX	0.51	6.33	0.001	~	0.313
LY	0.36	7.22	0.042	~	0.835
MZ	0.43	7.00	0.014	~	0.341
AMZ	0.57	5.97	0.070	0.058	0.131

5.2.3 Panel Data Analysis

Across different mixes the effect of texture levels over noise intensity levels was very similar, based on the SLR and MLR plots. This implies the slopes of the regression lines, β_1, were very similar for all the tested highways. A regression model can capture this relationship by using a fixed effect panel data analysis. Fixed effect panel data analysis was used to determine the significance of texture levels accounting for the difference in variance across different mixes. Highways that did not have a statistically identical response in terms of noise and texture in the hypothesis testing were not grouped together. Furthermore, only the texture wavelength sets that were statistically significant and had a $R^2 > 0.50$ were used in the panel data analysis. Results obtained from regressing the texture wavelength set C with tire/pavement noise across all one-third octave bands can be found in Figure 5-8 and Table 5-7.

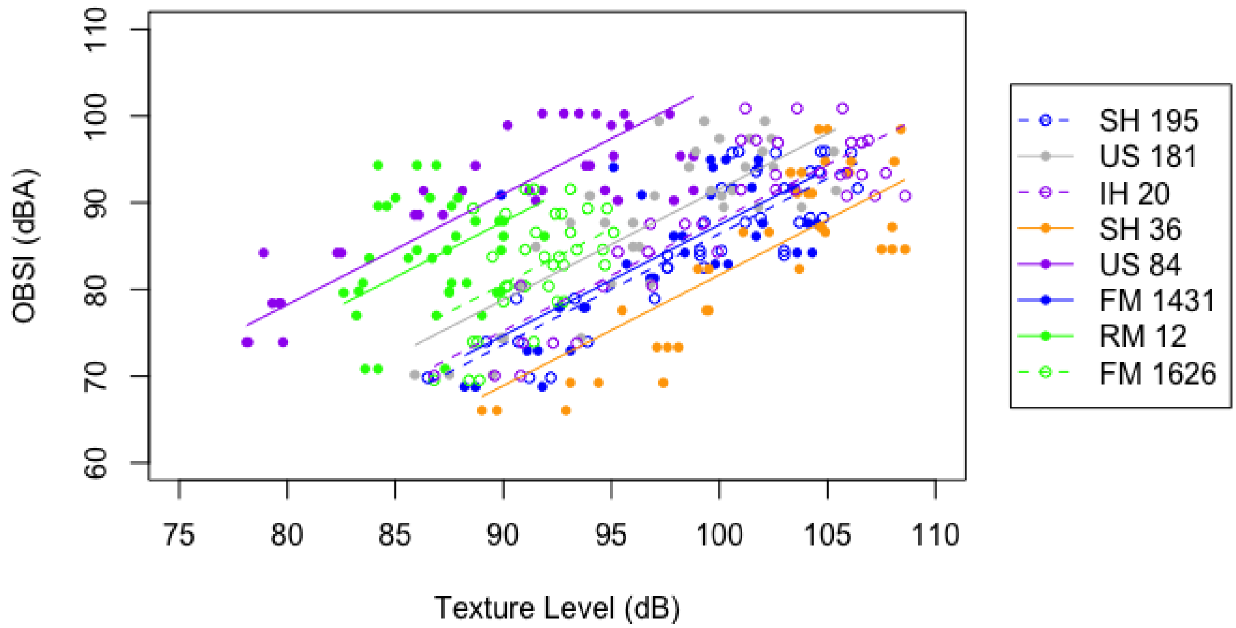

Figure 5-8 Results of panel data with respective noise level

Table 5-7 Panel data results for texture set C

Parameter	Mix Type	Estimate	Standard Error	P-Value
Slope	~	1.28	0.063	0.000
Intercept US181	Novachip	-36.1	6.21	0.000
Intercept SH195	PFC	-41.3	1.24	0.000
Intercept IH20	Seal Coat	-39.7	1.25	0.004
Intercept SH36	Type C	-46.0	1.27	0.000
Intercept US84	Seal Coat	-23.9	1.32	0.000
Intercept FM1431	PFC	-40.2	1.24	0.001
Intercept RM12	TOM	-27.1	1.4	0.000
Intercept FM1626	TOM	-34.3	1.29	0.162
Model's Adjusted R^2		0.6222	Residual Standard Error	5.243

5.2.4 Correlation Mapping

In 1980, Sandberg and Descornet conducted a study on pavement friction, noise, and texture using four types of tires on pavements of asphaltic concrete, rubber bitumen (3–6% rubber), open-graded asphalt concrete, resinous slurry, surface dressing, cement concrete (grooved and non-grooved), and paving blocks surfaces, with SPT-measured texture depth varying over a range of 0.4 to 4.6 mm. They measured macrotexture profile curve with profilometers, taking samples at intervals of 1.0 mm in the longitudinal direction and 2.0 mm in the transverse direction. Skid resistance measurements were taken either as side force coefficient at 20, 50, and 80 km/h or friction coefficient at 15% slip at 50 and 70 km/h. The researchers explored noise/texture correlations between every couple of noise and texture one-third octave band levels. The correlation coefficient was a function of sound frequency and profile wavelength. It was found that highly significant correlations appear in two separate frequency/wavelength domains: noise with low frequency ($f \leq 1500$ Hz) is positively correlated with profile components with large wavelength ($\lambda \geq 10$ mm), while high frequency noise is negatively correlated with profile components with shorter wavelengths. Critical frequencies and wavelengths are defined as where the correlation coefficients have been found—respectively, maximum and minimum. Sandberg (1987) later concluded from this analysis that the general pattern is similar across all four tires, with both positive and negative correlations between noise and texture. The point where the correlation changes from positive to negative is called the crossover frequency and is approximately 1000 to 1250 Hz for passenger car tires. The maximally positive correlation exists between noise 400–500 Hz and texture 63–80 mm, while the maximally negative correlation exists between noise 2500–8000 Hz and texture 2–3.2 mm. The authors inferred from these findings that tire/road noise is a superposition of two independent spectra, with uncorrelated mechanisms separately generating the low frequency and high frequency noise. One mechanism is such that the noise level increases with surface texture, which is identified with lower frequency noise and larger texture profile wavelength, while the other produces less noise on increasing texture levels, which is identified with higher frequency noise and shorter texture profile wavelength, and that tire/road noise is the superposition of two independently generated spectra.

A similar study was carried out by Anfosso-Lédée and Do (2002) across 12 pavements:

- two were dense asphalt concrete with maximum aggregate size of 10 mm,
- four were surface dressing with maximum aggregate size of 1.5 mm, 4 mm, 10 mm, and 14 mm,
- two were porous asphalt concrete with maximum aggregate size of 10 mm,
- one was porous cement concrete with maximum aggregate size of 10 mm,
- one was very thin asphalt concrete with maximum aggregate size of 10 mm,
- one was cement concrete, and
- one was smooth epoxy surface.

Texture was expressed in texture level, with center wavelength ranging from 250 mm to 2.5 mm, divided into 21 one-third octave bands, and noise measured at 90 km/h was expressed in SPL, with frequency ranging from 100 Hz to 5000 Hz, divided into 18 one-third octave bands. Correlation coefficients between 18 sets of noise level and 21 sets of texture level were calculated across 12 pavements. While similar patterns were discovered, the authors also noticed that correlation was stronger when porous pavements were excluded. They ascribed this finding to two reasons:

overestimation of texture when negative texture is evaluated as a positive one, and sound attenuation along the propagating path due to acoustic absorption by the pores.

Correlation mapping following the procedure described by Sandberg and Descornet (1980) and Anfosso-Lédée and Do (2002) was conducted with the collected data, with texture level over the range of 80 mm to 0.025 mm and noise level over the range of 400 Hz to 5000 Hz for eight pavements, with correlation coefficients mapped in Figure 5-9.

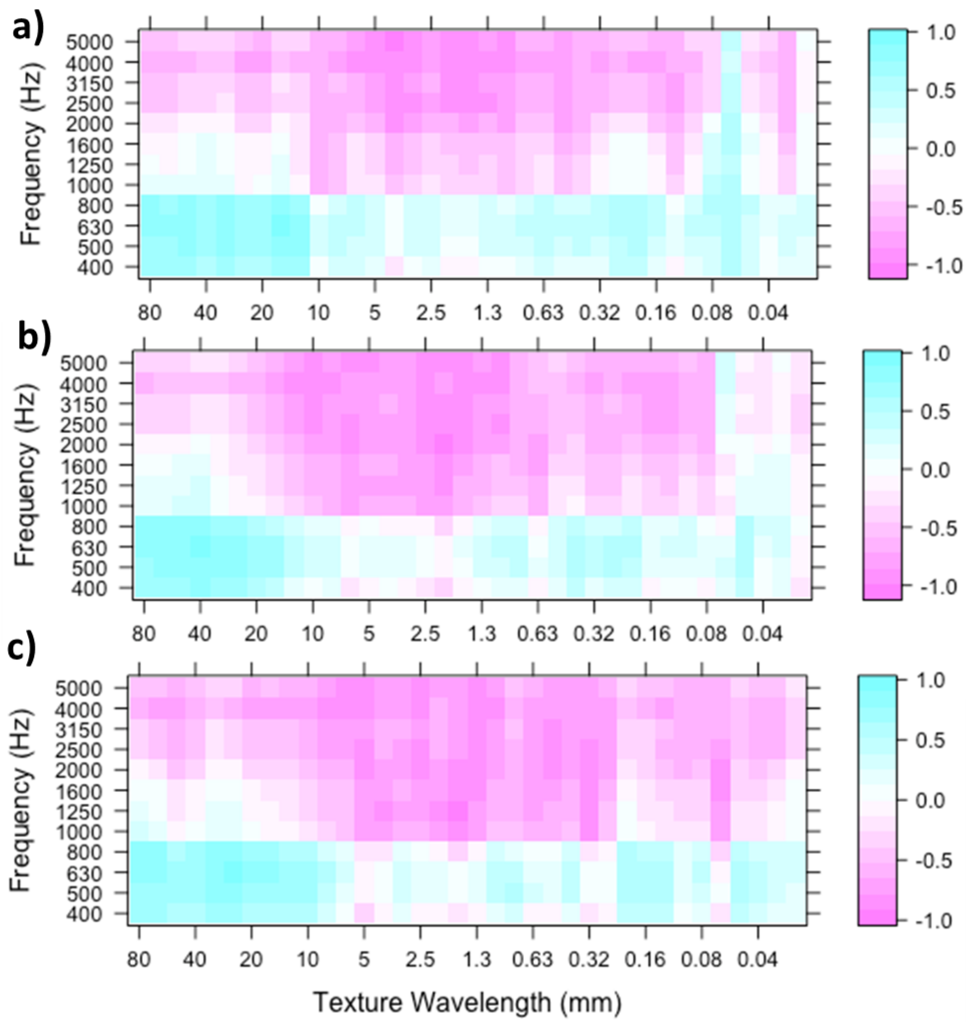

Figure 5-9 Correlation coefficient between sound pressure level and texture level for sections 1 (a), 2 (b), and 3 (c)

The overall pattern is consistent with what previous researchers have found, that low frequency noise (frequency < 1000 Hz) correlates positively with large-scale texture (λ > 10 mm), and high frequency noise correlates negatively with small-scale texture. However, from the plots, it can be observed that a very high level of randomness is found between noise and microtexture around the wavelength of 0.05 mm. One reason is that, as shown in Figure 5-10, the pavements have a high variability in the microtexture spectrum.

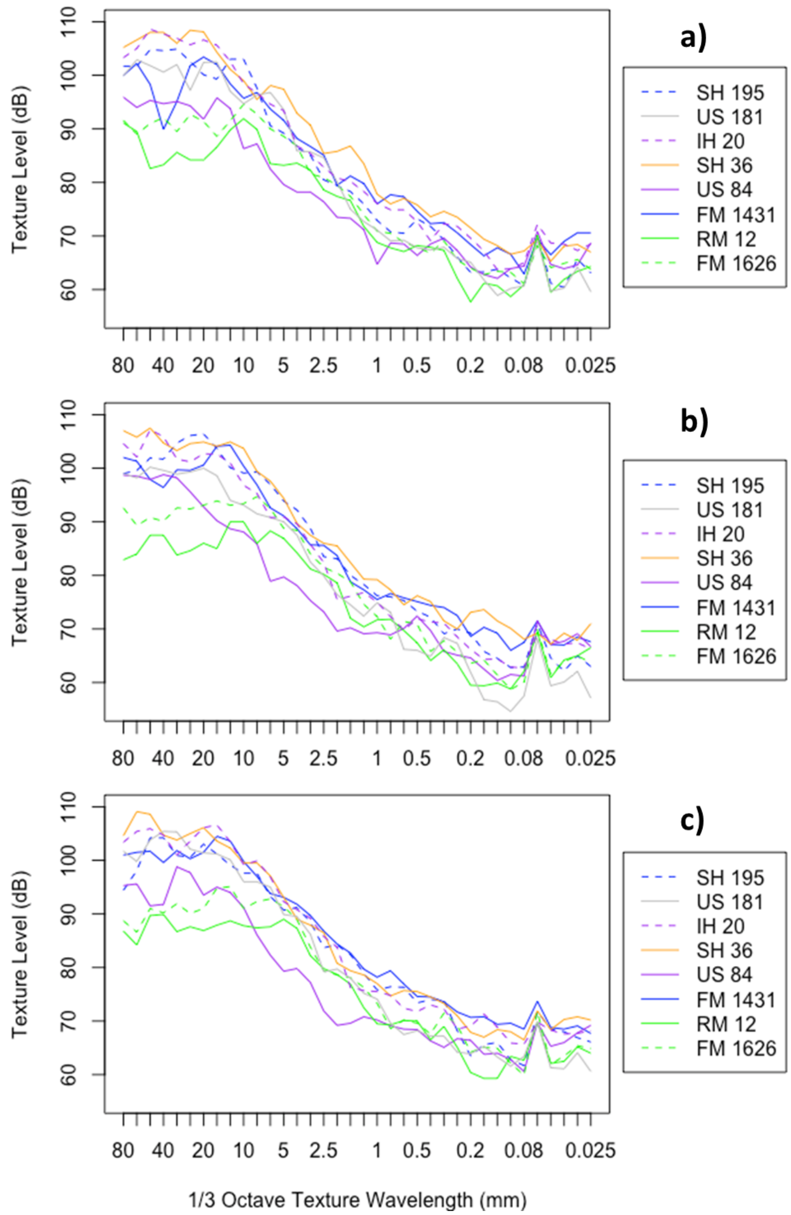

Figure 5-10 Texture level distribution sections 1 (a), 2 (b), and 3 (c)

5.2.5 Linear Regression at Maximal Correlation, No Grouping

Across all three samples, the maximum positive correlation occurs around noise level of 630 Hz and texture level of 50 mm, while the maximum negative correlation is not concentrated at a single location: local minima in correlation coefficients are spread all around over the domain from 8 mm to 0.25 mm and the range from 1000 Hz to 5000 Hz across three samples. As a result, for the purpose of a detailed analysis of the positive correlation between low frequency noise and long wavelength texture, the frequency of 630 Hz and the wavelength of 50 mm were selected. The most common critical values identified by Sandberg and Descornet (1980) were chosen to explore the negative correlation between high frequency noise (3,150 Hz) and short wavelength texture (3.2 mm).

An SLR was first conducted with the noise level at 630 Hz as the dependent variable and the texture level with a 50-mm wavelength as the independent variable. The regression results with coefficients and goodness-of-fit measure are shown in Table 5-8. The plots with noise level versus texture level are shown in Figure 5-11. From both the regression results and the plots, it was observed that noise level at frequency of 630 Hz correlates positively with texture level at 50 mm, though the overall goodness-of-fit is not high.

Table 5-8 Regression results for low frequency noise vs. long wavelength texture, no grouping

	Sample 1	Sample 2	Sample 3
Intercept	41.9	27.8	40.0
Coefficient	0.511	0.654	0.526
Adjusted R^2	0.640	0.660	0.445

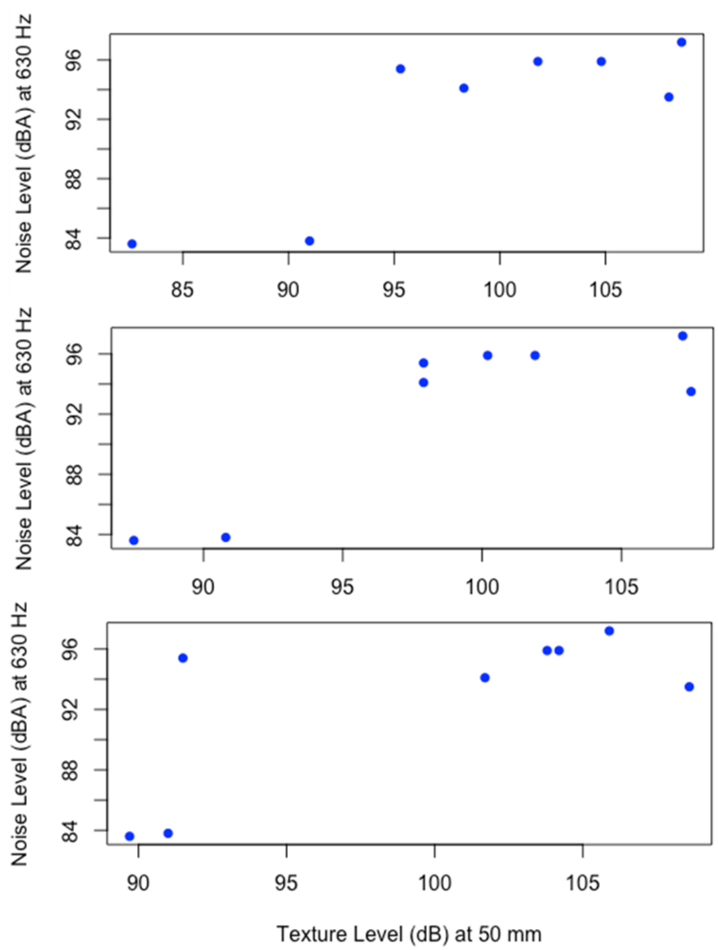

Figure 5-11 Low frequency noise vs. long wavelength texture, no grouping

A similar procedure was repeated for high frequency noise at 3150 Hz and texture with a 3.2-mm wavelength, without grouping the pavements. The regression results are as shown in Table 5-9. The plots are as shown in Figure 5-12. From both the regression results and the plots, the ungrouped goodness-of-fit for the negative correlation was not high either.

Table 5-9 Regression results for high frequency noise vs. short wavelength texture, no grouping

	Sample 1	Sample 2	Sample 3
Intercept	139	127	119
Coefficient	-0.706	-0.566	-0.469
Adjusted R^2	0.682	0.535	0.322

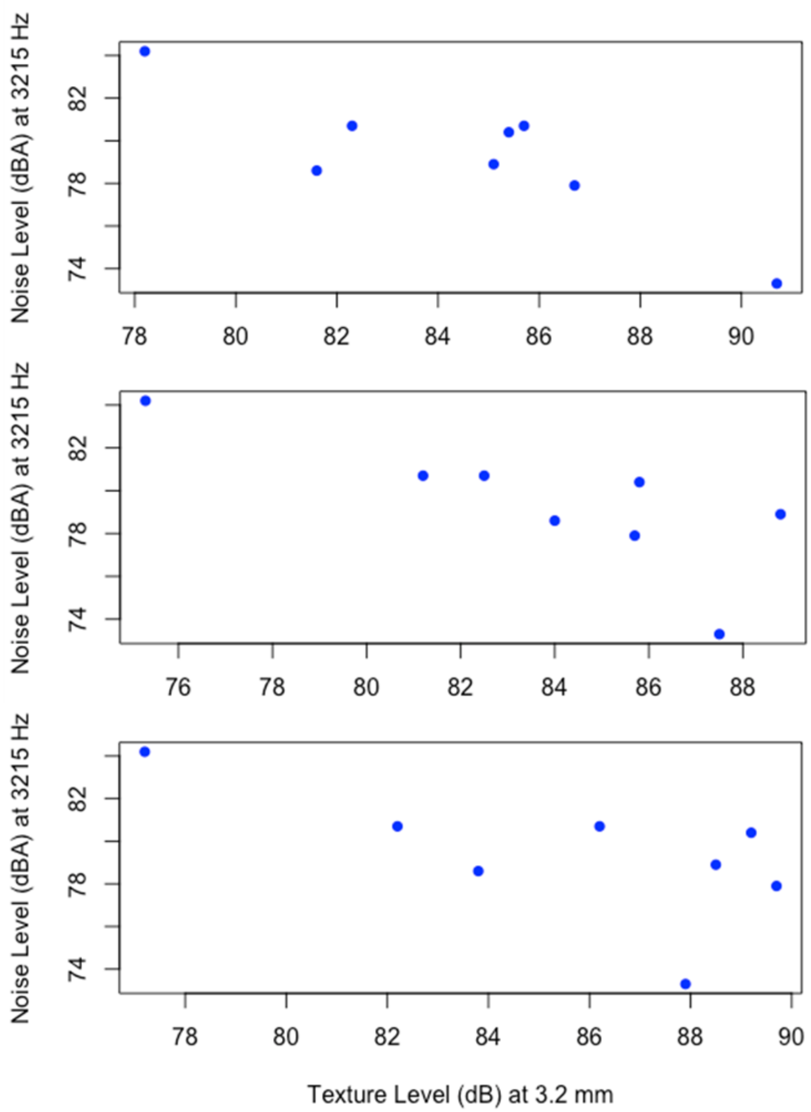

Figure 5-12 High frequency noise vs. short wavelength texture, no grouping

5.2.6 Linear Regression at Maximal Correlation, with Grouping

As has been discussed, texture alone is not sufficient to determine the tire/pavement noise. For example, Anfosso-Lédée and Do (2002) noticed that porous pavements tend to behave differently within noise-generating patterns. It is then helpful to separate the pavements into different groups. From the plots in Figure 5-11, the pavements were separated into three groups: SH 36 (Type C), RM 12 (TOM), and FM 1626 (TOM) as Group 1; SH 195 (PFC), FM 1431 (PFC), IH 20 (Seal Coat), and US 181 (NovaChip) as Group 2; and US 84 (Seal Coat) as Group 3.

When the data points were separated, the regression results and plots are as shown in Table 5-10 and Figure 5-13. The three groups are assumed to have the same slope but different intercepts. Intercept 1 is for the three pavements in Group 1, represented by the blue dots in Figure 5-13. Intercept 2 is for Group 2, represented by the red dots. Intercept 3 is for Group 3, represented by the green dot. When the pavements were separated into three groups, the model's overall goodness-of-fit improved for all three samples. With the same level of texture, pavements in Group 1 tend to generate the lowest level of noise, with Group 2 being louder than Group 1, and Group 3 even louder.

Table 5-10 Regression results for low frequency noise vs. long wavelength texture, three groups

	Sample 1	Sample 2	Sample 3
Intercept 1	49.8	40.7	34.6
Intercept 2	54.9	46.4	39.3
Intercept 3	57.7	47.9	45.7
Coefficient	0.396	0.485	0.543
Adjusted R^2	0.938	0.969	0.996

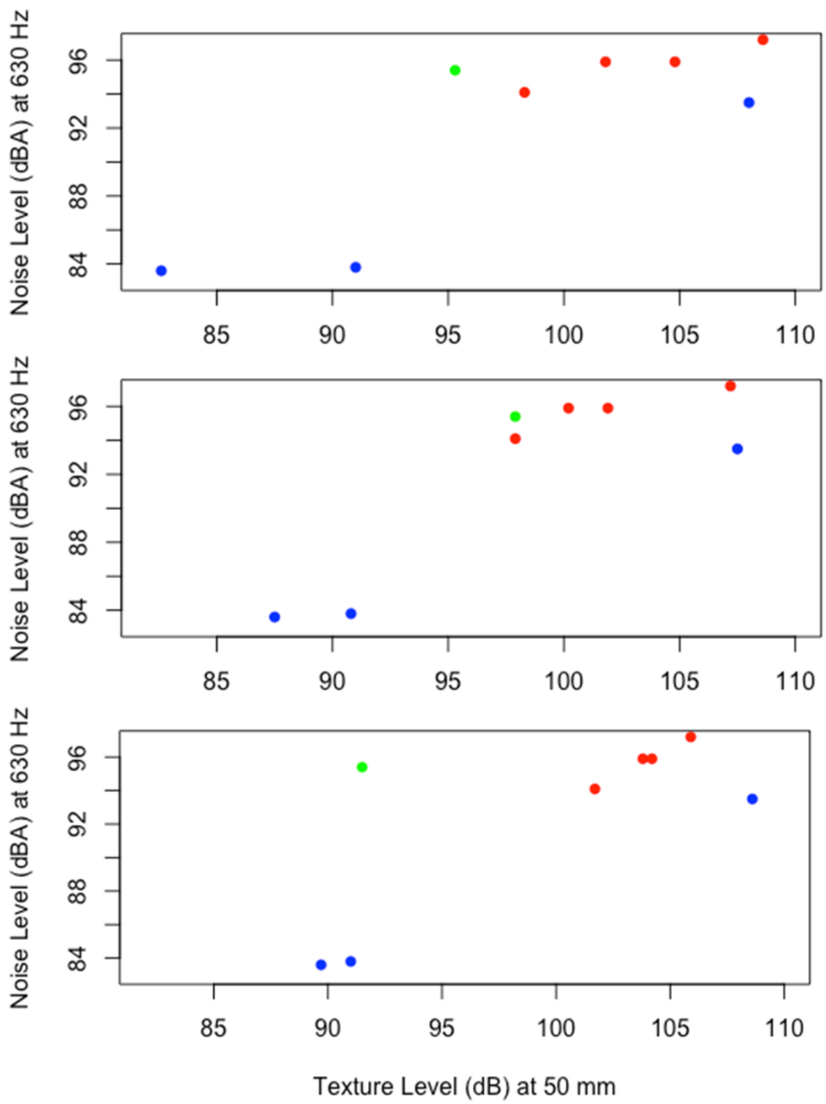

Figure 5-13 Low frequency noise vs. long wavelength texture, with grouping

Analysis with grouping was the next step for the negative correlation between high-frequency noise and short wavelength texture (Table 5-11, Figure 5-14). Interestingly, US 84, which was showing a different pattern from all the rest of the pavements in the low frequency range, appears to behave similarly to the pavements in Group 1, and thus is placed into Group 1 for this analysis. Grouping the pavements by mix type while enforcing the same slope improves the linear fit between noise and texture level at the critical frequencies/wavelengths. This indicates that with unit increase in texture level, the unit increase/decrease in noise is consistent across all sampled pavements, but at a given texture, different pavements might generate a different level of noise.

Table 5-11 Regression results for high frequency noise vs. short wavelength texture, two groups

	Sample 1	Sample 2	Sample 3
Intercept 1	147.98	140.07	159.14
Intercept 2	150.34	143.09	164.85
Coefficient	-0.8266	-0.7423	-0.9657
Adjusted R^2	0.8187	0.7377	0.8736

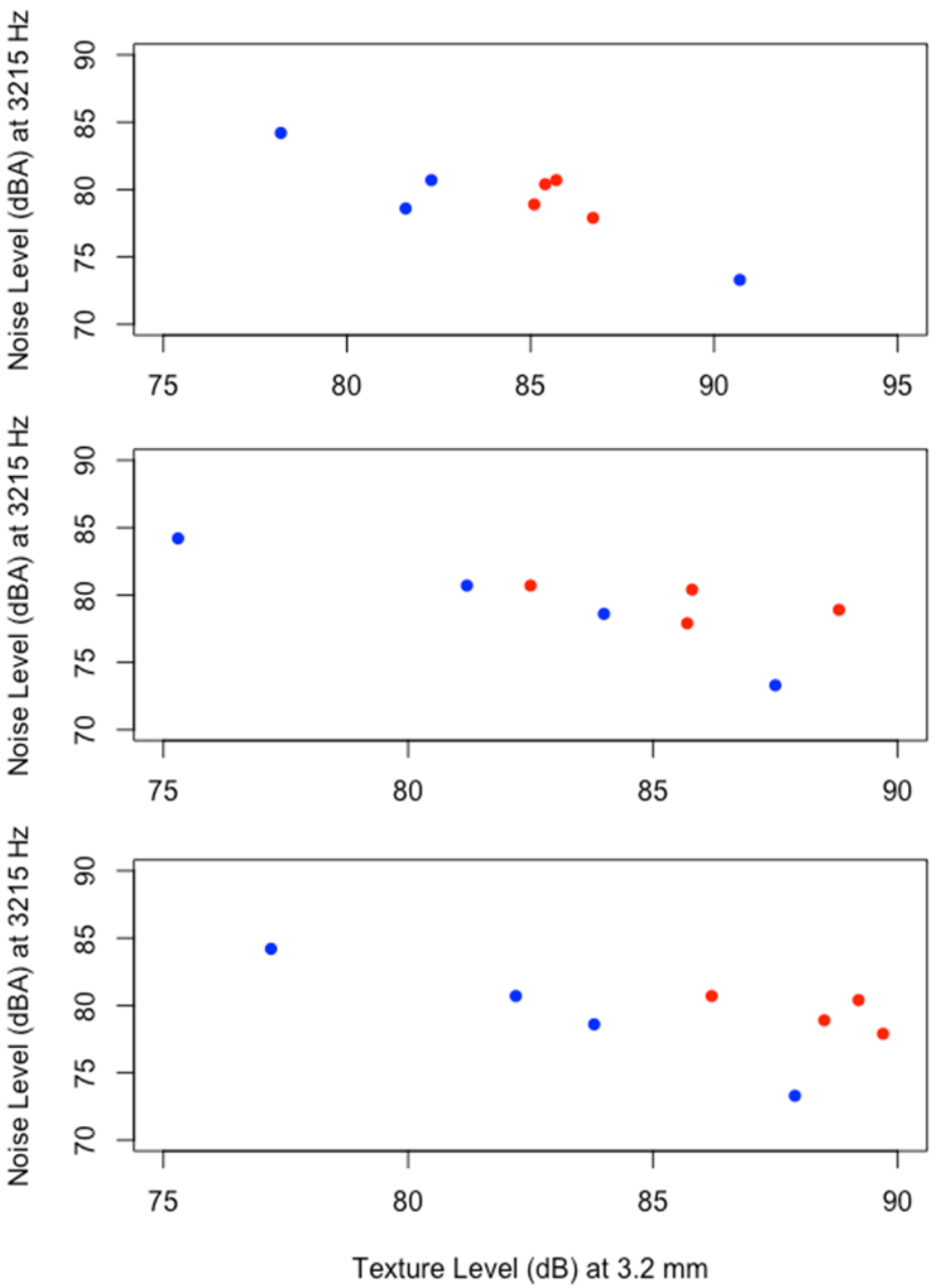

Figure 5-14 High frequency noise vs. short wavelength texture, with grouping

5.3 Friction: Statistical Analysis

Past researchers have also attempted to correlate friction with texture and noise. Baran and Henry (1983) measured friction with the BPT and a full-scale locked-wheel tester using both smooth and ribbed tires, near-field tire/pavement noise with an on-board microphone mounted near the tire, and far-field tire/pavement noise while the vehicle was traveling through the testing sites with a microphone 15 m from the edge of the pavement along six pavements covering a wide range of textures. Though spectral characteristics of near-field noise data obtained from the study correlates well with friction for PCC, and far-field noise data at 64 and 80 km/h correlate well with friction for all pavements, no strong relationship was obtained between near-field noise and friction for asphalt concrete surfaces. Caltrans conducted a study in 2008 on pavements with longitudinally tined PCC, burlap drag PCC, dense-graded asphalt concrete, and open-graded asphalt concrete surfaces (Rymer et al., 2010). OBSI was measured in accordance with the AASHTO standard, dividing the measured pavement into three 440-ft sections, while measuring the A-weighted noise at 60 mph. Friction was measured with a dynamic locked-wheel friction trailer and a dynamic friction tester. Pavement macrotexture was measured in MPD with the CTM. Compared to the dense-graded pavements, the open-graded pavements tested exhibited a much higher texture level, generally comparable friction, higher noise level at lower frequencies (f < 1000 Hz), and lower noise level at higher frequencies. McDaniel et al. (2014) developed a one-parameter model using MPD as the input parameter. Skewness was also attempted as an independent variable, but the effect was not found to be significant. The single parameter model using friction, however, does not have as strong a predicting power compared to the model based on texture. Thus, it is expected that noise does not correlate as well with friction as it does with texture.

The friction results were compared with those from the OBSI, to investigate the relationship between friction and noise. In the previous analysis, both texture and noise were split into one-third octave bands to provide a further in-depth outlook on levels across the frequency composition. To compare noise with friction, the overall OBSI level for each of the eight locations were used. The overall OBSI level was calculated from Equation 5-1, resulting in a single value representative of the noise for each location.

Similarly, three friction measurements were collected per location. A single value of friction was obtained by averaging the three respective samples. This was done for all three types of friction-measuring equipment to compare to the overall OBSI level. The coefficient of determination (R^2) was used to determine the relationship; the results showed weak relationships between the three different equipment types and the overall OBSI level (Figure 5-15).

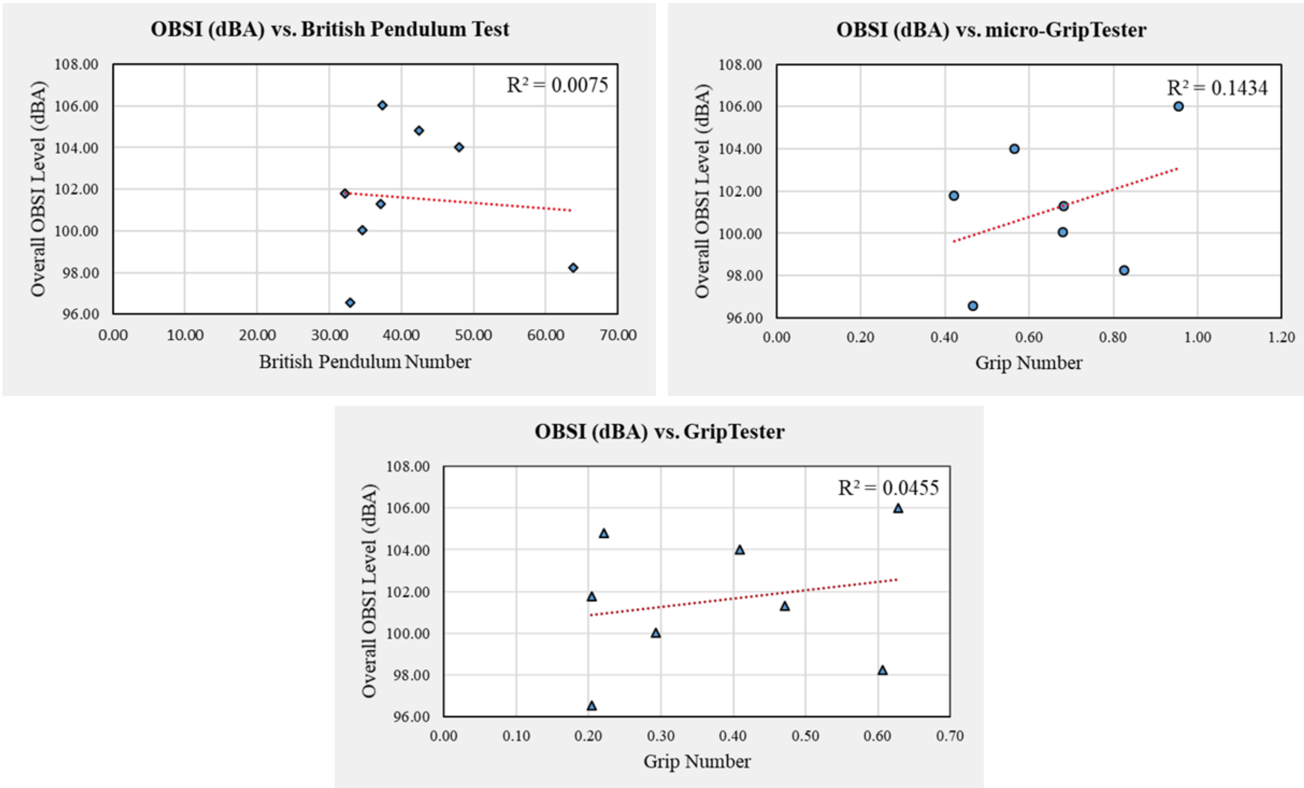

Figure 5-15 Plotted noise – friction data points including dBA, BPN, and GN values

To observe the relationship between friction and noise, the asphalt mix types were separated into groups (Figure 5-16). For noise, the overall OBSI (dBA) was used, representing a single value of the location tested and compared to the GripTester's averaged result per location. The locations were separated by the mix designs, with some mix designs represented by one location.

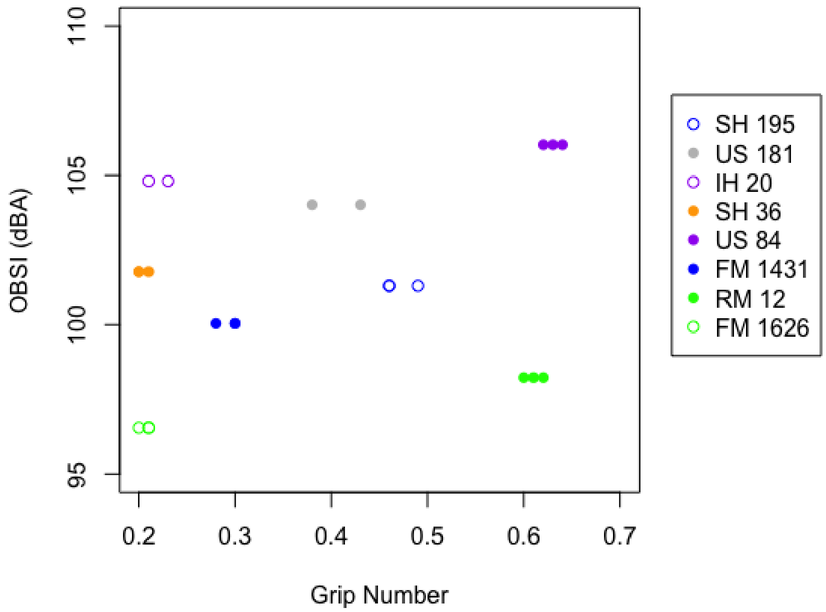

Figure 5-16 Noise against friction – represented by the GN from the GripTester

The surface characteristics of the asphalt pavements were described by the MPD given by the CTM and the LLS. The MPD values obtained by the LLS, denoted as MPD-by-LLS, were found to be very close to the MPD obtained by the CTM with a relationship of $R^2 = 0.998$. Therefore, the succeeding analysis for texture uses the MPD-by-LLS as it contains a larger sample size.

The various friction-measuring equipment types were compared to the MPD. For each of the locations, the values of texture and friction from the three spots sampled were utilized. Therefore, more information was compared to define a trend. The linear regression showed the relationship between GN from the GripTester and the MPD to have $R^2 = 0.4$ (Figure 5-17). One of the TOM mixes was found to behave differently from a second TOM mix and influenced greatly the relationship in the overall linear regression.

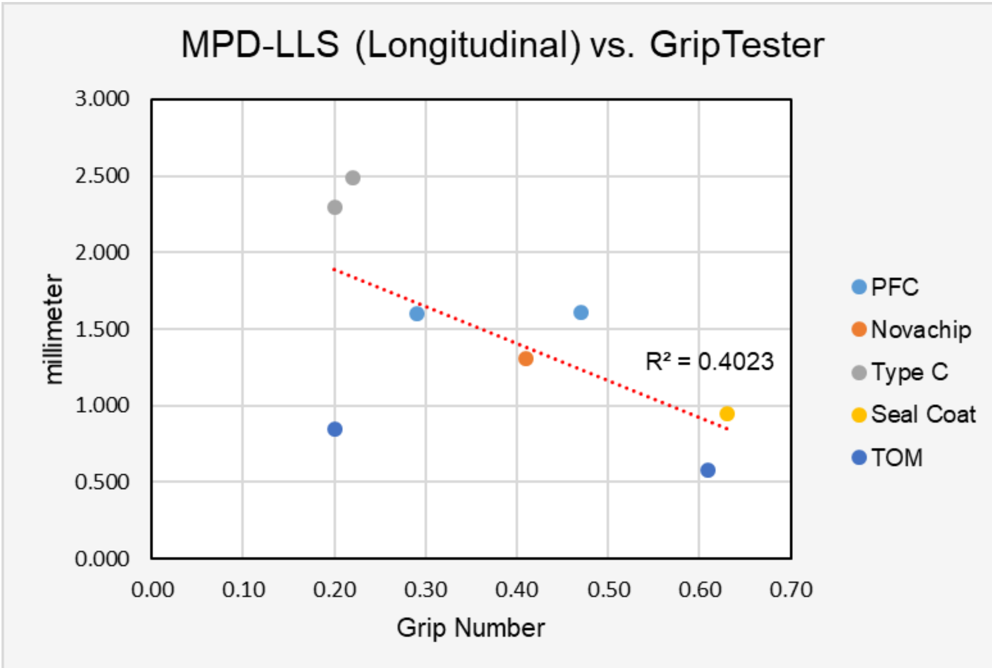

Figure 5-17 Relationship of friction against texture represented by the GripTester

In 1992, PIARC sponsored a study to allow conversion among friction measures used worldwide with representatives from 16 countries participating. After conducting measurements at 54 sites across the United States and Europe with 51 different testing systems, including ones measuring friction such as locked-wheel, fixed-slip, ABS, variable-slip, side-force, pendulum, and some prototype devices, and those measuring texture such as the sand patch, laser profilometers, an optical system, and outflow meters, the International Friction Index (IFI) was developed (Hall et al., 2009). From an MPD measurement, the speed number and friction number upon which the IFI depends can be calculated by Equations 5-17 and 5-18.

$$S_P = 14.2 + 89.7\,MPD \qquad \text{5-17}$$

$$FS = F60 \times EXP\left[\frac{60-S}{S_P}\right] \qquad \text{5-18}$$

Where:

S_P: Speed constant

MPD: Mean profile depth, km/h

FS: Adjusted value of friction for a slip speed of *S*

S: Measured speed, km/h

The result is provided in Figure 5-18 and Figure 5-19: no significant difference was observed between IFI and the GN from the GripTester. The R^2 value did reduce slightly from 0.8 to 0.7385 after applying the IFI equations. The ROSANNE project used the modified SRI for correcting the friction values but the proposed SRI from ROSANNE was a draft at the time of their published paper. No information could be accessed at the time of this study to evaluate the modified SRI for the GripTester.

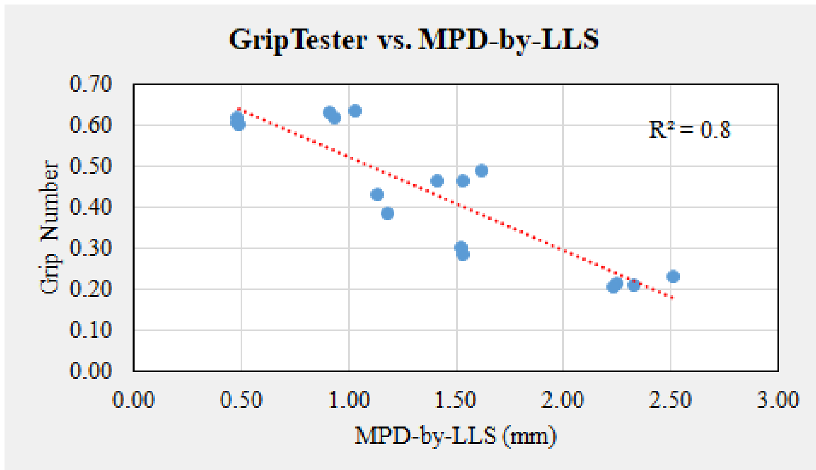

Figure 5-18 GN against MPD-by-LLS

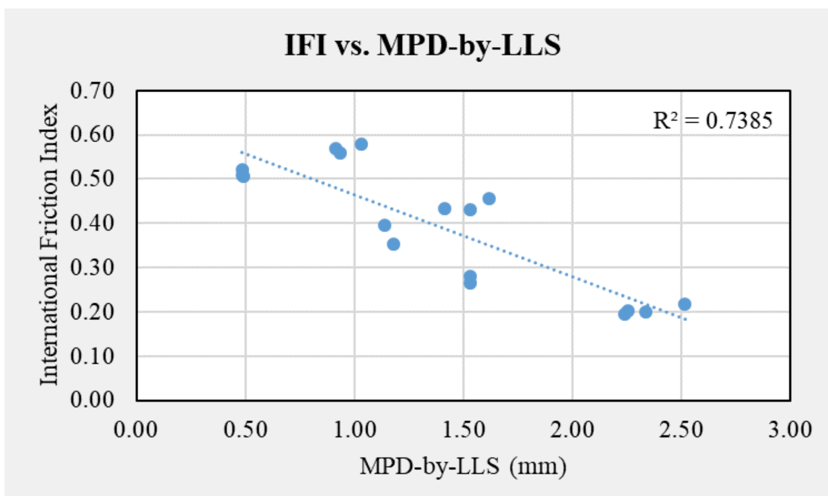

Figure 5-19 International Friction Index against MPD-by-LLS

Analyzing the various mix types together was inconclusive as they each have different characteristics in terms of friction, texture, and noise. Therefore, to model the three parameters it is necessary to separate the sections by mix type. Figure 5-20 demonstrates that the PFC and Type C tend to follow the same high/lows as the BPN, MPD, GN, and noise. One of the TOM sections did not follow the same pavement characteristic as the other.

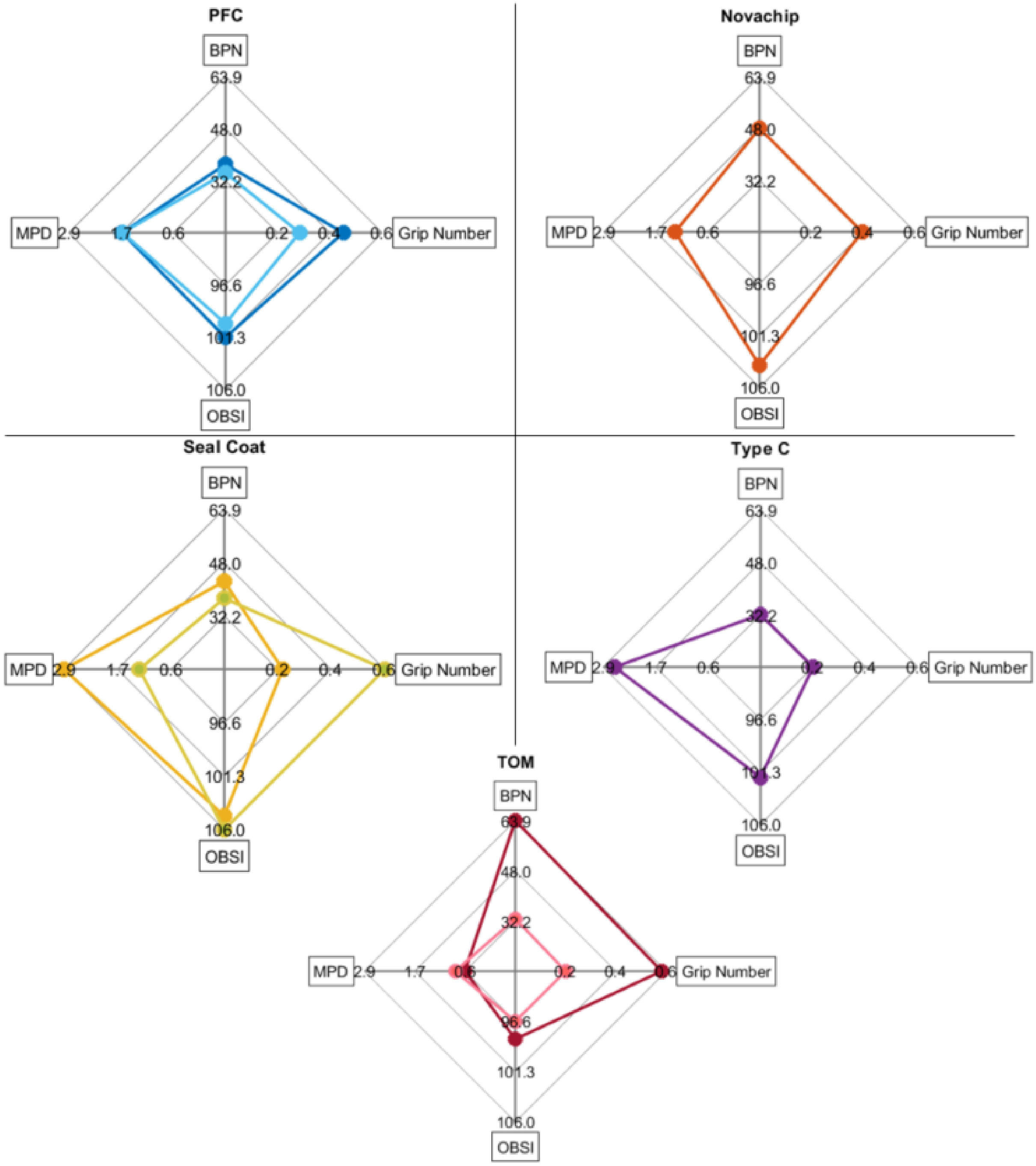

Figure 5-20 Spider plot of separated mix types

Chapter 6. Enhanced Friction Prediction Model based on Field Texture Data

One potential reason for the low correlation between friction and texture from the data collected could be the inconsistency of measurement location in the data collection process. As friction and texture are measured separately, it is very difficult to ensure that both measurements are taken at exactly the same point. As early as 1978, when Leu and Henry developed a model to characterize skid resistance using micro and macrotexture, they suggested a simultaneous measurement of texture and skid from a single test without interrupting traffic, while acknowledging that obtaining microtexture using non-contacting, high-speed methods was not possible with the technology at that time. In 1983, Arnberg developed the laser road surface tester, addressing the need for developing a reliable, integrated measuring device operating at highway speed, and capable of obtaining data for several characteristics simultaneously, and thus maximizing the efficiency of the roadway surface evaluating process. As technology advances, not only has measuring both macrotexture and skid resistance together become possible, but attempts have been made to incorporate microtexture as well. In 2004, the Florida Department of Transportation (FDOT) conducted a study to assess the feasibility of collecting data on both surface texture and friction characteristics of pavement sections while operating at highway speed (Jackson et al., 2007).

To enhance the efficiency and safety of pavement surface characteristics data collection, researchers at the University of Texas at Austin have developed a prototype measuring device capable of collecting texture and friction data simultaneously, at high speeds, and on the same wheel path, as shown in Figure 6-1. Texture and skid resistance data were collected on 15 highway sections with varying surface types within 60 miles from the city of Austin using the prototype. Stringent quality control was established to ensure that the best quality texture and skid data were used to develop the prediction models. Based on the most recent literature in the subject, 14 different texture summary statistics were used to find the best prediction model for pavement skid resistance. The results from this study are robust and indicate that texture summary statistics have a statistically significant influence on the skid resistance of roads and, when used in the right combination, one can develop a model with predictive power on the order of 55% in terms of the coefficient of determination (R^2).

Figure 6-1 Texture-friction measuring device

6.1 Methodology

In terms of data collection, the research team selected six distinct pavement surfaces that cover some of the most common asphalt pavements used in Texas with the intention of sampling pavement surfaces that cover a wide range of textures and skid numbers. Table 6-1 shows a breakdown and summary for all pavement selection surveyed in this study.

Table 6-1 Pavement surfaces selection

Surface Type	Number of Samples
Dense Coarse Mix	2
Dense Fine Mix	2
Gap Graded Mix	4
Chip Seal	4
Distressed Chip Seal	2

Within these sections, texture and skid resistance data were collected at highway speeds. The skid resistance and pavement texture data used for this analysis were collected using an innovative equipment prototype developed in-house that combines a GripTester and an accurate line laser sensor. This prototype can measure the full spectrum of pavement macrotexture (50 to 0.5 mm) and a portion of the first decade microtexture (the sensor can reliably measure up to a wavelength of 0.322 mm) at highway speeds while simultaneously collecting skid on the same spot where the laser is scanning the pavement profile.

6.1.1 Prototype Specifications

The GripTester was selected for measuring skid resistance due to its wide range of testing speeds, good repeatability and reproducibility, and the fact that it gives the operator full control of the water flow used to achieve a given water thickness between the test tire and the pavement surface.

The device follows ASTM E2340 (14) and uses a smooth tire of 25 cm (10 in.) diameter that, when in motion, simulates a fixed wheel with 15% continuous slippage. The system is completed with an automatic watering system that provides enough flow to create precise water thickness set by the operator. The amount of water flowing to the wheel self-adjusts depending on the traveling speed. The device was retrofitted with a laser-sensor to capture texture profiles in-sync with the GripTester's built-in encoder. The specifications of the laser-sensor are shown in Table 6-2.

Table 6-2 Datasheet for laser sensor

Characteristics		
Resolution height		5.0 µm
Field of view		330 mm
Light source	Wavelength	660 nm
	Laser class	Class 3B
	Output	130 mW
Resolution lateral		0.161 mm
Sampling cycle (max)		25000 profiles/s
Repeatability		2.6 µm
Linearity (% of Z-Range)		±0.01

In the transverse direction the laser has a resolution of 0.161 mm, meaning the spacing in between each point within the laser line is on average 0.161 mm with a total distance of 330 mm for a single profile. In the longitudinal direction, or the direction of traffic, a profile is obtained every 40 mm. Lastly, the resolution in the vertical direction of the sensor is 5.0 µm. Figure 6-2 portrays the axis/direction convention for the line laser sensor being used.

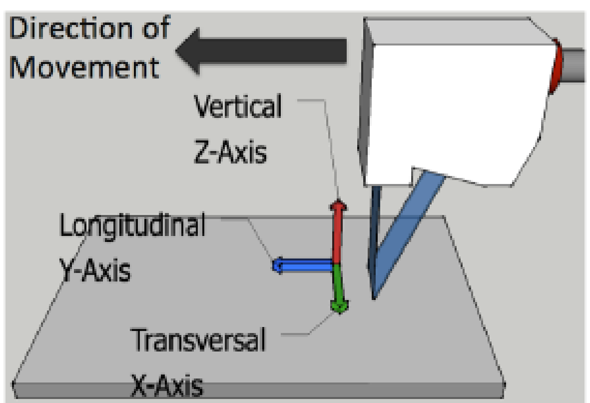

Figure 6-2 Axis convention and direction of movement (18)

The GripTester is used for measuring skid resistance at a wide range of testing speeds. The laser-sensor is synchronized with the GripTester and centered in front of the measuring tire and the water outlet (Figure 6-3). The laser-sensor can measure 330 mm in width in the transverse direction, enabling the researchers to capture the tire's contact area with the pavement (50 mm [2 in.] wide).

The two systems work together as they are both simultaneously triggered to collect data. For the GripTester, the trigger is converted to distance and, for every meter of travel, the drag and load force are averaged and saved. For the laser-sensor, the trigger is used to capture a single profile of height values. When the tires are inflated to 20 psi, the diameter is 254 mm, resulting in profile spacing of approximately 40 mm, which is subject to vary as the tire expands and contracts. More importantly, the trigger sends a signal to both systems to initiate data collection to keep both data streams synchronized.

Figure 6-3 Data collection prototype

6.2 Data Collection Protocol Using the Prototype

The test starts when the survey vehicle reaches the test section that has been previously marked and pre-programmed in a GPS. Near the test site, the system is connected to the test vehicle. The system has only two cables for data communication with the computer and is operated from inside the vehicle. A minimum of two individuals are needed: one for driving the vehicle and one for operating the software. While collecting data, two software packages are used: SkidTexture, an in-house software, and Roads, a proprietary software for the GripTester. With the vehicle is stationary, each software awaits the trigger to initiate data collection. When the vehicle starts to move and reaches testing speed, the user can monitor real-time data from the laser-sensor (profiles, MPD, exposure of camera, and threshold of laser brightness) and real-time data from the GripTester (GN, target water flow, actual water flow, and vehicle speed). Furthermore, as data are collected, the operator can make notes that are saved with the data and stamped with the corresponding location. This is important when there is a specific start and stop in the test section or for the operator to denote changes in pavement. As data are collected, the operator checks the real-time data and views the system in a rearview camera for proper operation of the system. After completion of the test, the system is stored inside the vehicle to reduce wear.

6.3 Data Processing

Before performing the statistical analysis, meticulous inspections and quality control measures were set in place to ensure the data was of the best possible quality. In terms of skid number, the GripTester provides a file of the survey performed, summarizing the distance travelled, GN measurements every meter, load on the device, measuring speed, and water flow. Based on all the preliminary testing done on the prototype, the research team agreed upon certain filtering criteria to isolate valid GNs from invalid ones. A GN is considered valid under these conditions:

- The load on the GripTester device is between 100 and 400 Newtons,
- The water flow to the wheel is in between ± 5 liters per meter from the target, and
- The speed of the surveying vehicle is higher than or equal to the tenth percentile target speed.

The first filter exists to avoid measurements taken when the GripTester goes over a pothole, debris, or some other pavement distress that might make the device bounce and the wheel load fluctuate excessively. The second filter avoids measurements where the water flow to the wheel is not correct to provide a water thickness of about 0.5 mm. Finally, the last criterion filters out measurements taken before the survey vehicle reaches highway speeds. Typically, during preliminary testing, this speed would be to 65 km/h (40 mph).

The texture data collected using the laser-sensor mounted on the GripTester is first filtered to keep only those profiles for which there is valid GN information. In other words, if the friction data for a given portion of the pavement section were invalid and filtered out, then all texture profiles corresponding to that interval of length were also filtered out. This filtering process enables a one-to-one relationship when doing a correlation analysis between the friction and texture parameters.

The next step consists of trimming the texture profiles to include the texture that is within and adjacent to the measurement wheel's path. In terms of profile width, 100 mm of the profile centered around the tire/pavement contact area are kept for further analysis. The width is kept larger than the actual contact area to enable estimation of MPD.

The software outputs a value of -97.4 mm whenever the laser goes out of range or there is extreme light interference such that the camera is unable to tell what the true elevation of the pavement is. Therefore, every time a -97.4 mm data point is seen within the profile, that point can be classified as an invalid point and converted to a "NULL" data point. This step prevents extreme negative invalid values from skewing summary statistics.

The next step consists of applying a filter to the data to identify and remove spikes or flat signals. A spike is defined as any data point that experiences a fast, short duration; drastic increase or decrease in elevation; and is simply not consistent with the surface being analyzed. Some spikes are extreme outliers and can easily be identified but others are mild outliers and not as easy to identify. These data points break the trend of the pavement profile at close inspection and must be removed. A flat signal is the result of the combination of a low exposure time for the camera and a very dark pavement surface. In this situation the sensor blurs the measured information and outputs a flat line where the elevation at multiple locations is the same as the last "good" point it measured. Figure 6-4 shows examples of the different types of spikes and flat-line signals.

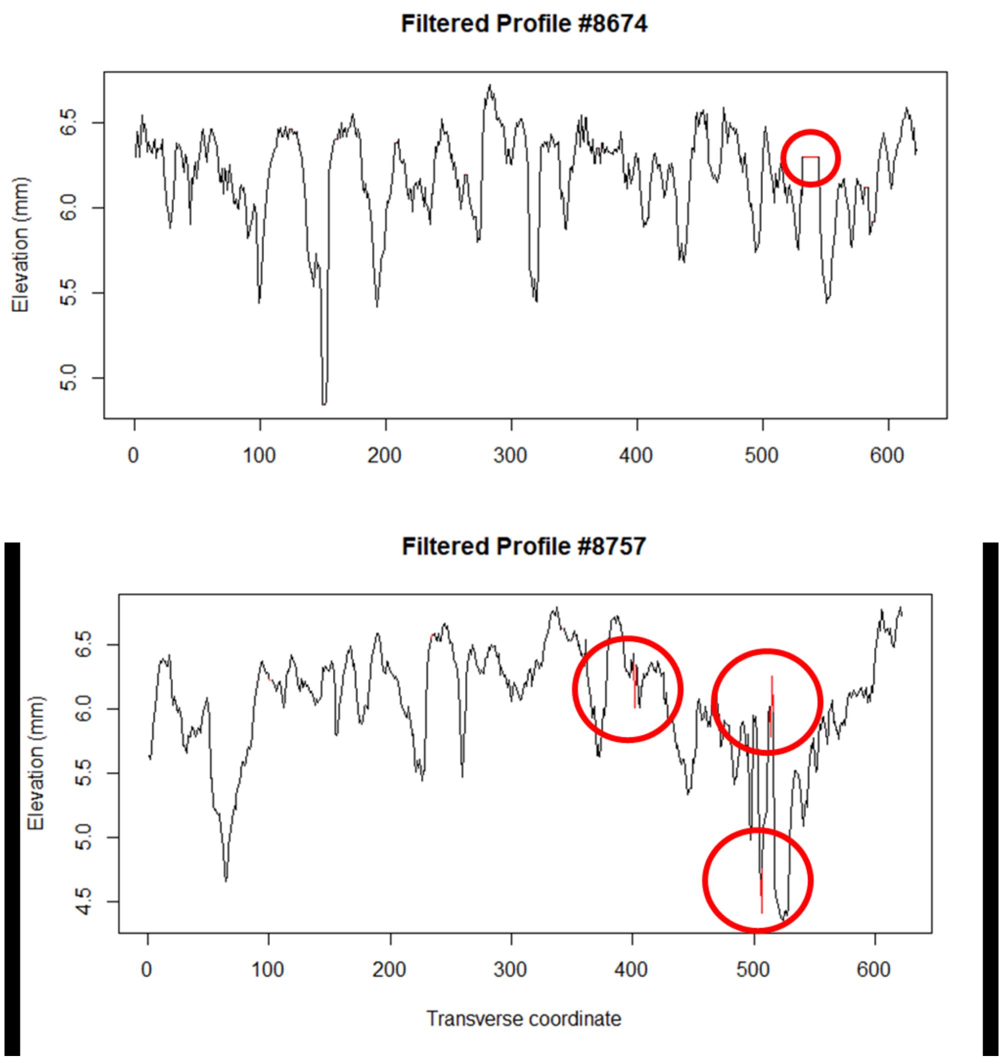

Figure 6-4 (Top) Example of a profile with a flatline signal due to low exposure time and a very dark pavement surface, (Bottom) example of single point spikes within the profile.

6.3.1 Rolling Variance Filtering Algorithm

The filtering algorithm employed is based on the variance of three consecutive points. If the algorithm encounters a flat signal at any point in the profile, the section contains only repeating values, yielding a variance of zero, whereas sections containing spikes yield large variance values. The algorithm flags points with either of these characteristics and removes them from the profile.

The section variance is computed in a rolling form. For example, for a data point P_i being considered, a section variance for three consecutive points (P_i, P_{i+1}, P_{i+2}) is calculated. If the variance is equal to zero or above the 98th percentile of all possible three-point sections in the dataset, the point being considered (P_i) is removed. Then, the algorithm moves to the next point to its right and the next three data points (P_{i+1}, P_{i+2}, P_{i+3}) are used to compute variance and to determine whether P_{i+1} needs to be removed. If there are n data points within a profile, the algorithm continues to move on to the next data point until P_{n-2}. Once all profiles have been filtered for flat signals and spikes, summary texture statistics can be computed.

At this point in the process, the points removed from the profile are kept as NULL values given that there is no consensus as to what the best imputation method would be, such that the imputed data follows the trend of the profile regardless of whether the NULL values occur at single instances across the profile or on a continuous string, as is the case for flat signals.

6.4 Statistical Analysis

Regression analysis was used to quantify the relationship between measured friction and texture statistics related in a nondeterministic fashion. The most straightforward deterministic mathematical relationship between two variables x and y is a linear relationship. This relationship is also known as the SLR equation. However, an SLR may not be good enough to obtain a consistent and accurate prediction of the dependent variable. This is likely because the variance of the parameter of interest cannot be fully explained with a single independent variable, but rather by the combination of multiple parameters. Hence, a multiple regression analysis is proposed. In this type of analysis, the objective is to build a probabilistic model that relates a dependent variable to more than one explanatory variable. The general additive multiple regression model is defined by Equation 6-1:

$$Y = \beta_0 + \beta_1 x_1 + \beta_2 x_2 + \cdots + \beta_k x_k + \epsilon \qquad \mathbf{(6-1)}$$

Where, Y is the dependent variable, β_k are correlation parameters, x_k are the explanatory/independent variables and ϵ is the random deviation term.

6.4.1 Friction Prediction Models

Multiple models were evaluated during the statistical analysis; however, only those that were deemed the two most relevant are presented. Model 1 used the best combination of profile summary statistics to predict skid. These are the standard deviation (RMS), six-point slope variance, and the intercept of the linearized PSD curve. Model 2 used the skewness and kurtosis of the profile and introduces the surface type information as dummy variables (S_i) to explain the friction within each different surface material. This experiment evaluated five common surface types as presented in Table 6-1; nevertheless, those groups were further subdivided into eight clusters based on the aggregate material (see Appendix A) and type of pavement mixture used. S_1 is a high-quality chip seal (CS_{HQ}); S_2, a raveled and flushed chip seal (CS_{RF}); S_3, a chip seal with limestone (CS_{LM}); S_4, a chip seal with rough hard aggregates (CS_{RJ}); S_5, fine mixes with crushed sands (FM); S_6, an open-graded mix measured on the center lane (GG_{CL}); and S_7, an open-graded mix measured on the wheel path (GG_{WP}). The base case for this model is a dense-graded coarse mix whose influence is captured by the parameter β_0.

$$Model\ 1: \quad .GN = \beta_0 + \beta_1(RMS) + \beta_2(SV6) + \beta_3(PSD_{int})$$

$$Model\ 2: \quad .GN = \beta_0 + \beta_{M3}(R_{sk}) + \beta_{M4}(R_{ku}) + \sum_{i=1}^{7} \beta_i(S_i)$$

In addition to the MLR, a variety of machine learning models were also tested on the dataset. However, those models were unfavorable for two main reasons. First, the current dataset contains a limited amount of texture and friction information, which leads to overfitting for complex models such as XGBoost (18). Second, simple linear models are easier to interpret and quantify, and interpretability is crucial for future decision making and applicability. The summary of the regression analyses performed on all models is presented in Table 6-3.

Table 6-3 Statistical summary of each model

Model 1				
Adjusted R^2			0.559	
Residual Standard Error			10.0	
Parameter	**Coefficient**	**Influence**	**Standard Error**	**P-value**
~	β_0	-87.4	16.1	*0.000
RMS	β_1	-26.0	6.01	*0.000
$SV6$	β_2	257	32.6	*0.000
PSD_{int}	β_3	-0.28	0.05	*0.000
Model 2				
Adjusted R^2			0.976	
Residual Standard Error			2.4	
Parameter	**Coefficient**	**Influence**	**Standard Error**	**P-value**
~	β_0	37.5	1.42	*0.000
R_{sk}	β_1	6.16	2.99	0.052
R_{ku}	β_2	1.91	1.01	0.061
$S_1\ (CS_{HQ})$	β_3	42.4	1.40	*0.000
$S_2\ (CS_{RF})$	β_3	-11.1	1.90	*0.000
$S_3\ (CS_{LM})$	β_3	7.49	1.64	*0.000
$S_4\ (CS_{RJ})$	β_3	13.6	1.89	*0.000
$S_5\ (FM)$	β_3	13.4	1.23	*0.000
$S_6\ (GG_{CL})$	β_3	17.3	1.70	*0.000
$S_7\ (GG_{WP})$	β_3	6.66	1.90	*0.000

* The p-value is less than 1 e -04

Model 1 had an R_{adj}^2 = 0.559 and a standard error of 10 GN and every parameter within the model was found to be highly significant based on its p-value. Before interpreting the summary of Model 1, note that Figure 6-5 displays the range of values for each explanatory variable.

The RMS has a negative influence on skid where every tenth of an increment reduces the GN by 2.6. This implies that profiles with low amplitudes will have better friction, but this could also be indicative of the presence of cracks. $SV6$ has the greatest influence on GN, where every tenth of a unit increment increases the GN by 25.7. Recall, SV_6 is a weighted sum of the slopes across six points. At this scale, a high SV_6 is indicative of aggregate angularity that can be related to high macro and microtexture. Lastly, PSD_{int} has a positive influence on skid where every unit increment increases the grip by about 0.3. The physical implications of this metric are hard to interpret as it is a property of the profile in the frequency domain and not in the spatial domain.

Nevertheless, empirically it can be observed that profiles with high microtexture or high second decade macrotexture tend to have high PSD_{int}.

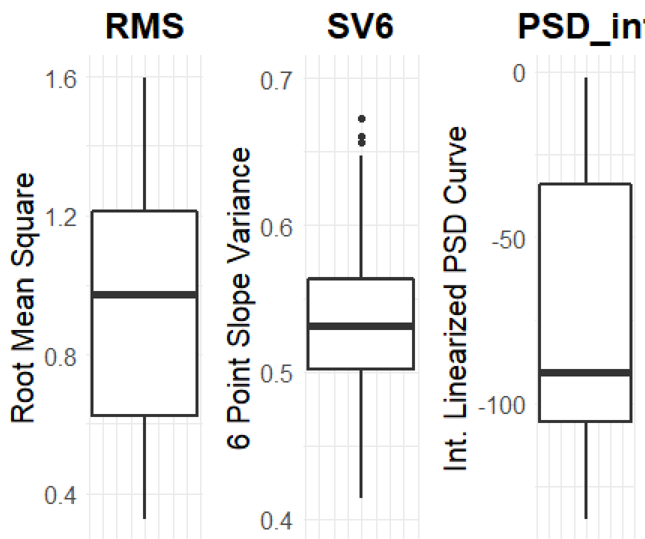

Figure 6-5 Boxplots of distributions for RMS, $SV6$ and PSD_{int}

Model 2 was developed to capture the fact that the relationship between texture and friction is not constant but varies across mixture types. Figure 6-6 shows a few of these graphs with the eight new surface groups that were based on the surface type, aggregate quality, and type (see Appendix B), and the part of the travel lane that was measured. In addition, Figure 6-7 shows the distribution of skewness and kurtosis values, which will aid in explaining their influence within Model 2.

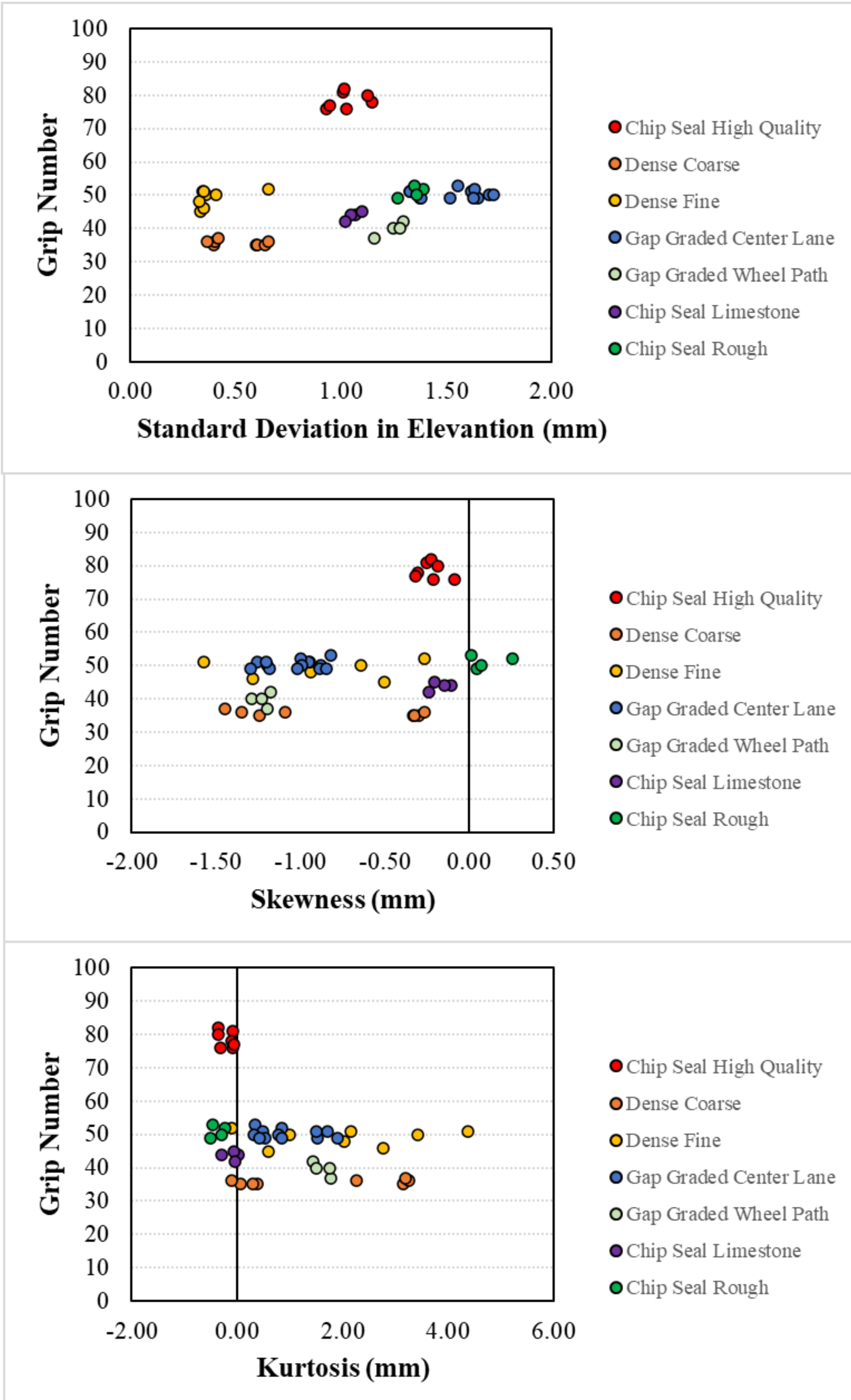

Figure 6-6 Scatterplot of GN versus standard deviation (Top), versus skewness (Middle) and versus kurtosis (Bottom)

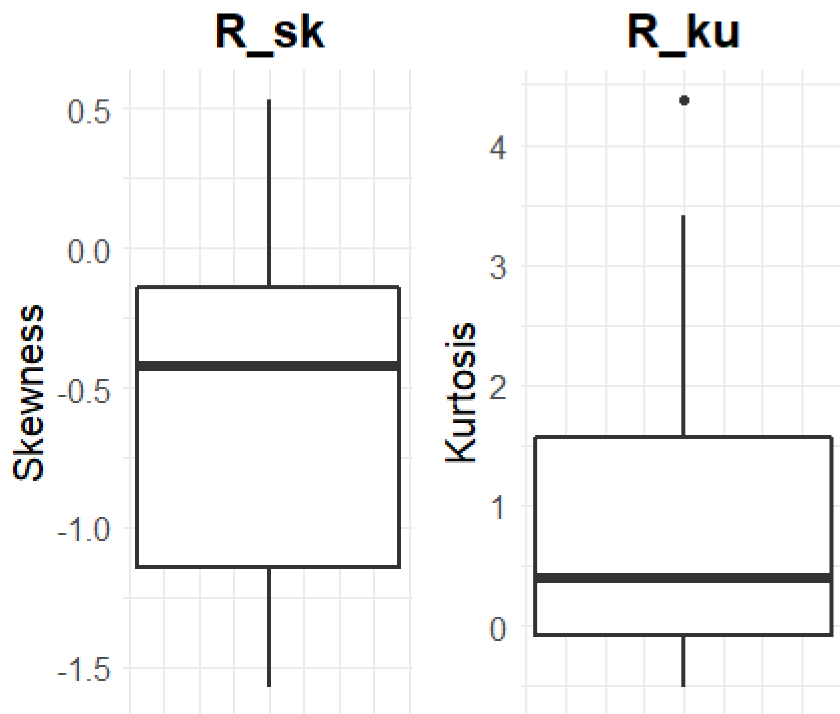

Figure 6-7 Boxplots of distributions for R_{sk}, and R_{ku}

Model 2 had a R_{adj}^2 = 0.976 and a standard error of 2.4 GN. This drastic increase in R^2 supports the conclusion reached by Zuniga (2017), where she stated that accounting for surface type information in the model can significantly increase its predictive power. Recall, this model uses dense coarse mix as its base case and its influence can be seen in the value of β_0. The data indicates that GG_{WP} had 6.7 more skid in terms of GN, followed by the CS_{LM} with 7.5, FM with 13.4, CS_{RJ} with 13.6, GG_{CL} with 17.3, and finally CS_{HQ} with 42.4 more GN. The only surface type that had a lower friction relative to the dense coarse mix was CS_{RF}. It should be emphasized that CS_{RF} is a very distressed chip seal whose extensive aggregate loss had left the binder exposed at the surface. The parameter associated to each surface type is consistent with what one would expect would be the performance of the pavement. Depending on its condition and aggregate type and size, a good quality chip seal would have the highest friction, whereas a seal coat that has been severely distressed would be expected to show low skid. The center lane was found to have higher friction as compared to the wheel path, since in that section some early signs of bleeding were observed. After accounting for surface type, a tenth of a unit increment in the skewness of the profile increases the skid by 0.6 GN, whereas a unit increment in the kurtosis increases the GN by 1.9 units. Recall, skewness indicates the predominance of peaks or valleys, and kurtosis indicates the presence of extreme peaks/valleys or lack of them. Given these results, a predominance of peaks (positive texture, or positive skewness) and the presence of extreme peaks (positive kurtosis) creates more friction within each group that was defined in Model 2.

Chapter 7. Conclusions and Recommendations

From the linear regression between noise and texture, it was found that noise correlates the strongest with texture at wavelengths from 31.5 mm to 2.5 mm, which include the first decade of macrotexture. The correlation appears to be positive, indicating that pavements with a higher level of texture tend to generate more noise.

Based on the correlation mapping approach, across all different types of pavements sampled, TOMs had not only relatively lower texture, but also generated less noise given the same texture level. The two PFC pavements sampled in this study, though found by many previous works to be quieter compared to other pavement types, did not produce less noise in either the low or high frequency spectra. Moreover, given the same texture level of short and long wavelengths, the two PFC pavements generated more noise at both high and low frequency spectra, respectively. One of the seal coat surface pavement sections, which was located on US 84, behaved differently at the two frequency ranges. With the same level of long wavelength texture, it produced the highest level of low frequency noise, significantly higher than two other groups. When considering noise in the high frequency spectrum, however, its noise-texture correlation matched that of the quieter group, given the same level of short-wavelength texture. This further confirmed the idea that tire/road pavement noise is a superposition of noise generated by different mechanisms, independent of each other.

The correlation between noise and friction was found to be not significant, which is consistent with what many previous researchers have claimed and is a further indication that constructing a pavement that generates a low level of noise while providing sufficient skid resistance is viable, and a compromise does not necessarily have to be made between the two. However, this also means that using noise measurement as an alternative to friction measurement might not as simple as was expected.

The correlation between friction and texture also varies across different pavements and within similar pavement types. Between the two PFC pavements, the MPD did not differ much, but large differences were found in friction measurements from the GripTester. The two seal coat pavements had similar level of texture overall: while the IH-20 section did not have a sufficient measurement in friction, it performed slightly better in providing friction as measured by the BPT than did the US-84 section, which had very high friction levels measured by both the Micro-GripTester and the GripTester. The two TOM pavements differed significantly in terms of texture level, GN, and BPN.

Overall, the evaluated TOM pavements tended to generate the lowest level of noise, while providing moderate to high level of friction. If this pattern is confirmed in future studies, this mix type can be a competitive choice for pavement selection. The PFC evaluated provided a good level of friction in general as well, while being slightly louder as compared to TOM. Neither PFC nor

TOM had much macrotexture, but their ability to provide skid resistance is satisfactory as compared to dense-graded mixes. Novachip and seal coat also had the characteristic of providing good friction with low texture level, though they were relatively loud as compared to the two previous types. Moreover, since only one of each type was sampled, it is premature to draw a general conclusion simply based on the current data. Type C dense-graded pavements seemed to generate less noise given the texture level, but their texture did not provide as much friction as the other types of pavements did.

Some of the findings from this research study are consistent with what previous researchers have proposed or discovered: for example, the positive correlation between low frequency noise and long wavelength texture and the negative correlation between high frequency noise and short wavelength texture. But there are also findings that contradict previous research conclusions, such as PFC pavements being relatively loud, and some findings are even counterintuitive, such as the negative correlation between friction and texture in some cases. These conflicts may be due to other pavement factors not accounted for, such as age, stiffness, surface thickness, etc. Keeping track of at least the year each pavement was constructed might be a sensible approach for further analysis, as many of the pavement characteristics evaluated in this study are time dependent.

The poor correlation between friction and texture, found in the first analysis done, was partially due to the mismatch between the measurement location for the friction and the texture measuring equipment. To overcome that problem, texture and friction measurements were simultaneously collected at highways speeds and on the same wheel path, resulting in a much higher correlation utilizing the new equipment developed at the University of Texas at Austin (the LLS). Effective prediction models for pavement skid resistance in terms of GN were developed as a function of texture statistics using this new dataset. The major advantages of the equipment developed can be summarized as follows:

- The LLS eliminates the uncertainty that may arise given a time gap between the data collection for pavement texture and skid.
- Both types of data (skid and texture) are collected on the same wheel path.
- The equipment has been proven to work at the same speed at which the locked wheel testers operate (80 km/h or 50 mph).
- The laser sensor used is powerful enough to capture the full spectrum of macrotexture and a few wavelengths within the microtexture spectrum.

In addition, this additional study on skid and texture demonstrated that texture summary statistics computed using high-definition texture profile instrumentation have a statistically significant influence on pavement skid resistance and can be used for prediction of friction with a high degree of accuracy. In fact, these technological advances allow for the development of predictive friction models more powerful than previously possible. Based on the analyzed data, there appears to be a clear relationship between the texture summary statistics and friction; however, this relationship is not unique and depends on the mixture type. Strong correlation can be found between these two factors, but texture statistics alone can explain only up to 56% of the variance within the skid resistance of asphalt pavements when all mixtures are considered together. Nonetheless, accounting for the surface type and clustering pavement sections based on the pavement material increases the explanatory power of texture statistics as high as 98%. Furthermore, the results have indicated that, out of all the texture statistics computed, $RMS, SV6$, and PSD_{int} constitute the best combination of summary statistics to predict friction when surface type is unknown. However, when surface information is included, kurtosis and skewness were found to be the best statistics for predicting friction.

To further improve this study, the sample size should be expanded to include more pavement surfaces and material types. Additionally, using information to characterize the surface type of roads, such as aggregate gradation and type parameters or maximum nominal aggregate size, could help improve the predictive power of the models. Some of these parameters can be found within the specifications of each pavement mixture, but metrics would vary based on the specifications from each state. The information that is typically lacking is the aggregate type and source, which has been demonstrated to have a significant effect.

Appendix A: Sampled Pavement Images

Pavement sections used for the analysis shown in Chapter 5

Location:
San Antonio
Right Wheel Path

Mix Design:
Open Graded
Novachip

Location:
Bryan
Right Wheel Path

Mix Design:
Dense Graded
Type C – Seal Coat

Location:
Brownwood
Right Wheel Path

Mix Design:
Dense Graded
Type C

Location:
Austin
Right Wheel Path

Mix Design:
Open Graded
PFC

Location:
Brownwood
Right Wheel Path

Mix Design:
Dense Graded
Type D

Location:
Austin
Right Wheel Path

Mix Design:
Thin Overlay Mix

Location:
Austin
Right Wheel Path

Mix Design:
Thin Overlay Mix

Pavement sections used for the analysis shown in Chapter 6.

Surface Type: Dense Coarse Mix ($\boldsymbol{\beta_0}$)

Number of Sections: 2

Range in MPD : 0.49 – 0.72 mm

Surface Type: Dense Fine Mix ($\boldsymbol{FM}$)

Number of Sections: 1

Range in MPD : 0.41 – 0.42 mm

Surface Type: Dense Fine Mix ($\boldsymbol{FM}$)

Number of Sections: 1

Range in MPD : 0.22 – 0.25 mm

Surface Type: Gap Graded Mix ($\boldsymbol{GG_{CL}}$)

Number of Sections: 2

Range in MPD : 2.17 – 2.31 mm

Surface Type: Gap Graded Mix ($\boldsymbol{GG_{WP}}$)

Number of Sections: 2

Range in MPD : 1.94 – 2.18 mm

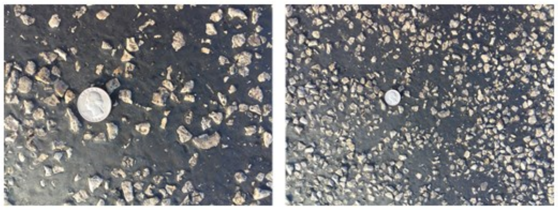

Surface Type: Heavily Distressed Chip Seal ($\boldsymbol{CH_{FR}}$)

Number of Sections: 2

Range in MPD: 1.11 - 2.06 mm

Surface Type: Chip Seal ($\boldsymbol{CH_{HQ}}$)

Number of Sections: 2

Range in MPD : 1.53 – 1.60 mm

Surface Type: Chip Seal ($\boldsymbol{CH_{LM}}$)

Number of Sections: 1

Range in MPD : 1.90 – 1.96 mm

Surface Type: Chip Seal ($\boldsymbol{CH_{RJ}}$)

Number of Sections: 1

Range in MPD : 0.51 – 0.58 mm

Appendix B: Additional Plots of Texture

PFC	SH 195	S1	19.65	20.89
		S2	17.99	
		S3	22.15	
	US 181	S1	19.21	22.38
		S2	19.98	
		S3	26.54	
	IH 20	S1	26.26	24.18
		S2	22.91	
		S3	21.29	
Type C	SH 36	S1	20.42	20.72
		S2	21.30	
		S3	19.34	
	US 84	S1	31.76	35.35
		S2	37.12	
		S3	35.51	
PFC	FM 1431	S1	18.47	17.92
		S2	17.05	
		S3	16.80	
TOM	RM 12	S1	25.02	19.85
		S2	15.29	
		S3	17.96	
TOM	FM 1626	S1	14.89	15.70
		S2	14.48	
		S3	16.09	

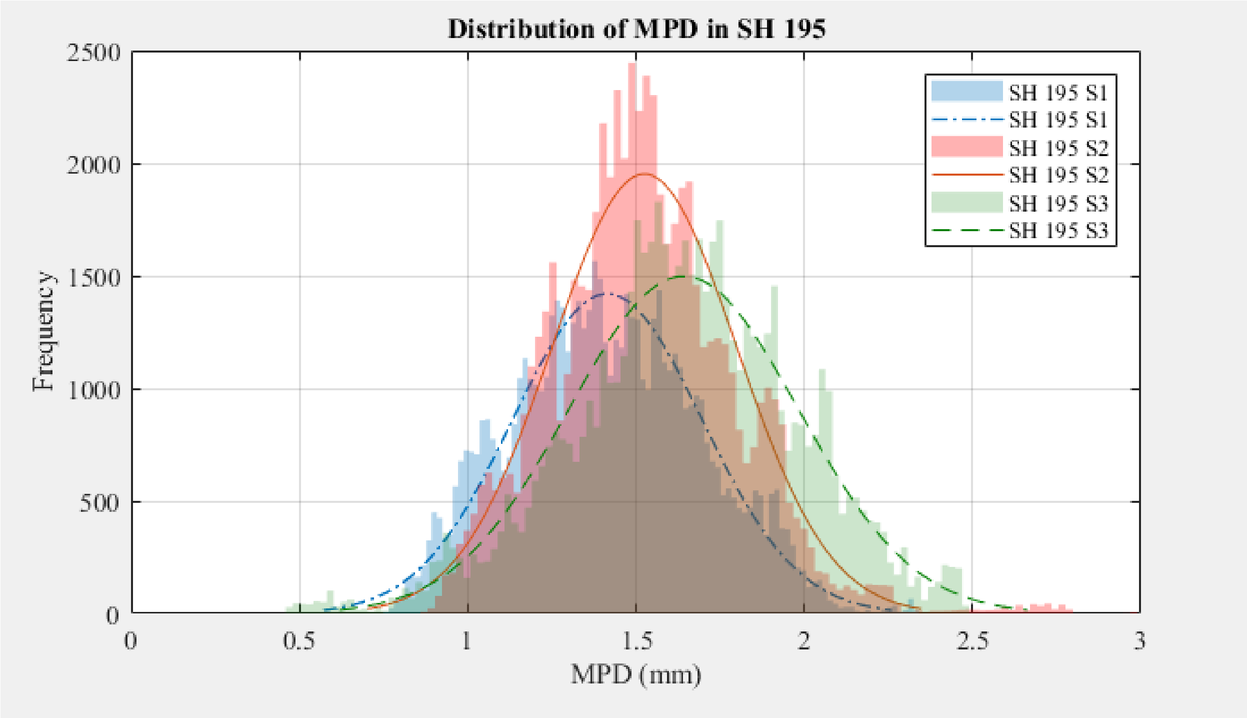

S1: Mu 1.41376, sigma 0.27775; **S2**: 1.53345, sigma 0.275931; **S3**: 1.61906, sigma: 0.358639

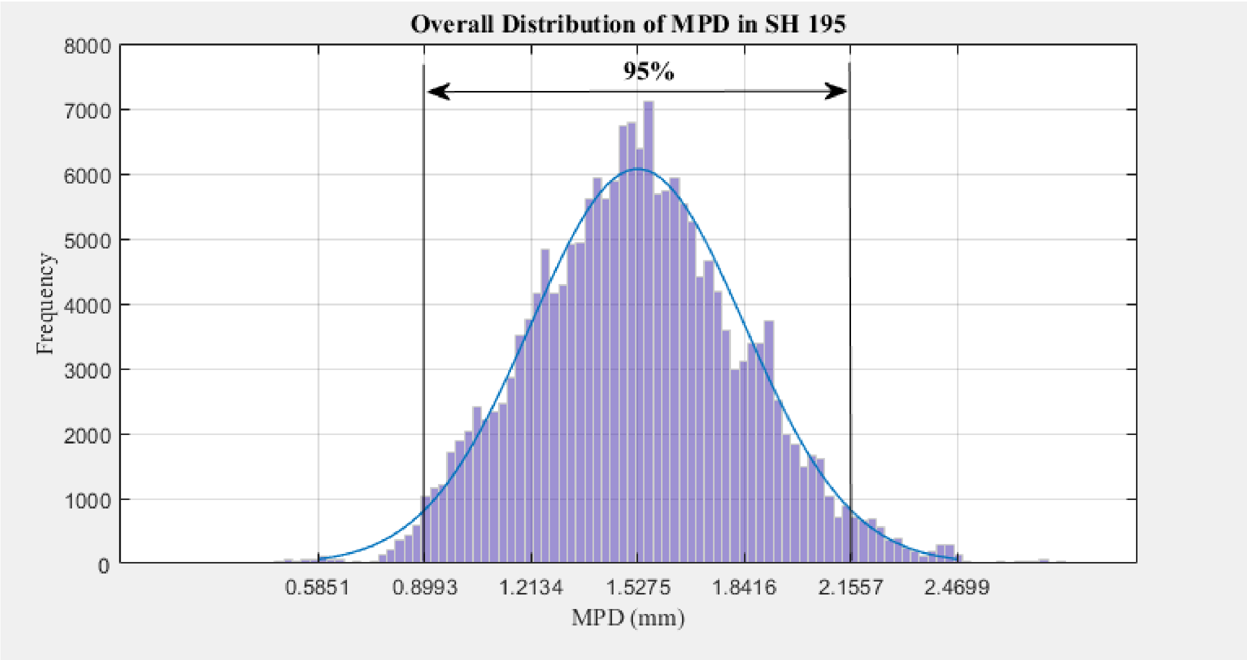

Mu= 1.5275, sigma= 0.314126

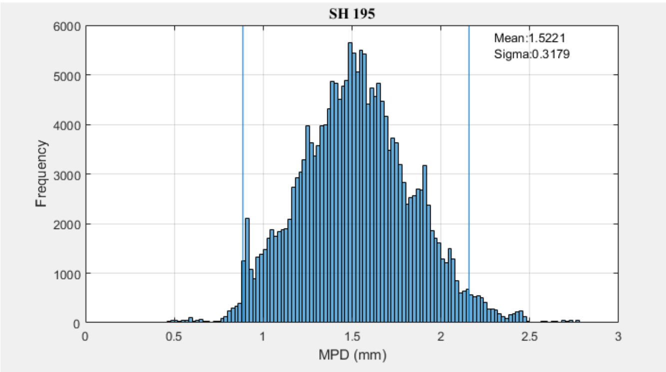
SH 195
Mean:1.5221
Sigma:0.3179
Frequency
MPD (mm)

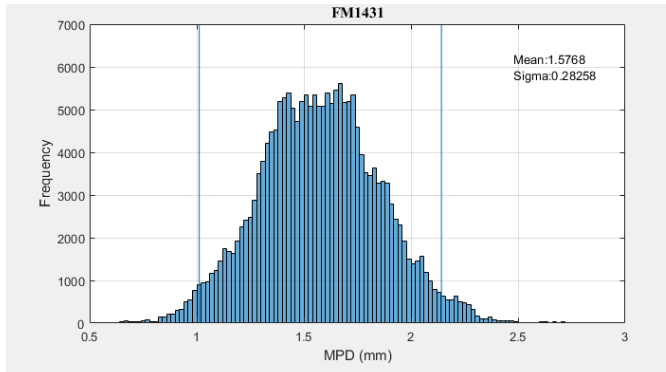
FM1431
Mean:1.5768
Sigma:0.28258
Frequency
MPD (mm)

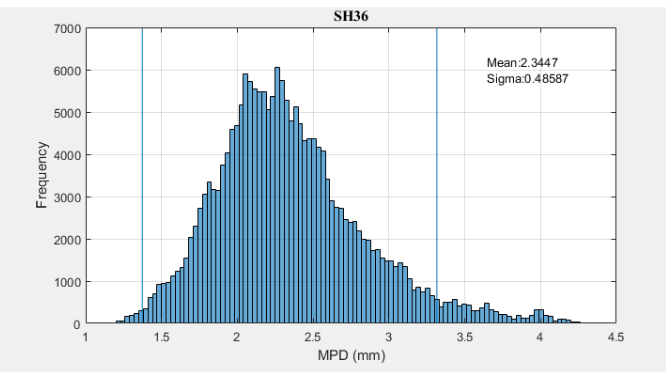
SH36
Mean:2.3447
Sigma:0.48587
Frequency
MPD (mm)

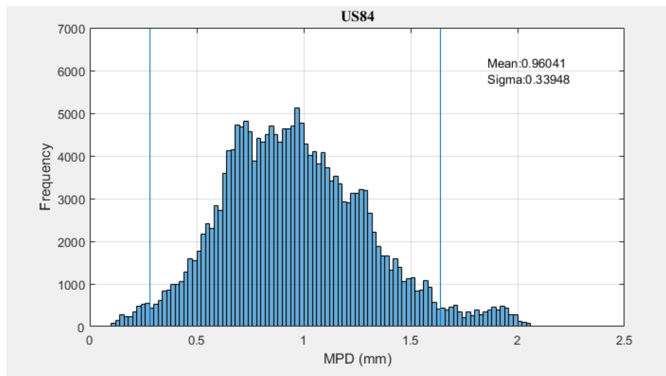
US84
Mean:0.96041
Sigma:0.33948
Frequency
MPD (mm)

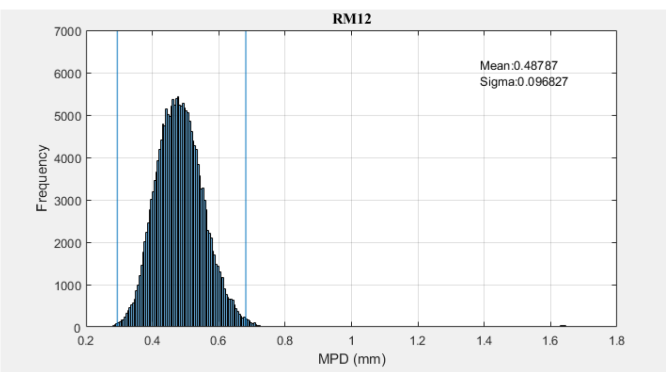
RM12
Mean:0.48787
Sigma:0.096827
Frequency
MPD (mm)

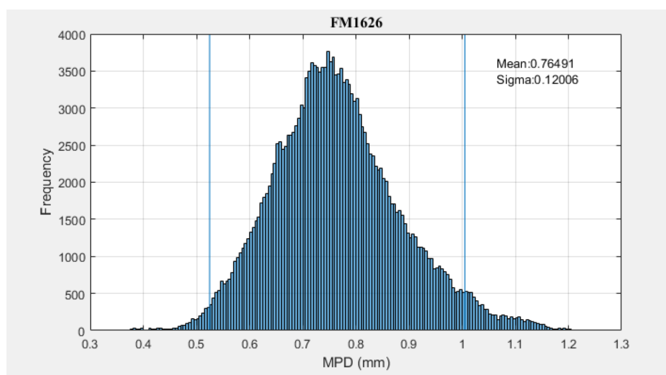
FM1626
Mean:0.76491
Sigma:0.12006
Frequency
MPD (mm)

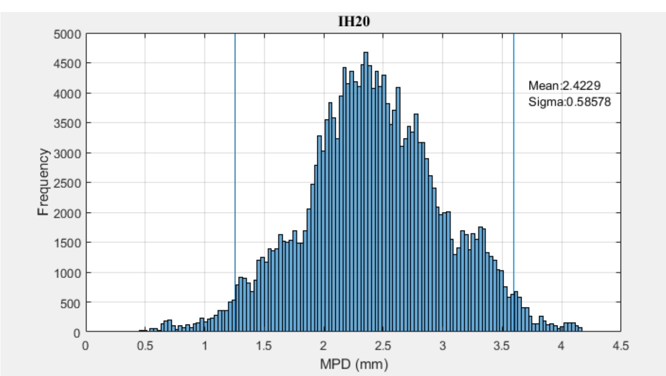
IH20
Mean:2.4229
Sigma:0.58578
Frequency
MPD (mm)

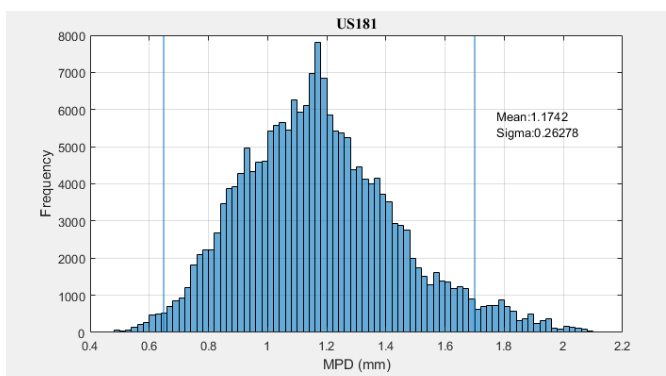
US181
Mean:1.1742
Sigma:0.26278
Frequency
MPD (mm)

References

Abbott, P. G. S., & Phillips, M. (1996, September). Vehicle noise levels derived from the statistical pass-by method and road surface texture. In NOISE CON (pp. 217-222).

Ahammed, Mohammad & Tighe, Susan. (2010). Pavement surface friction and noise: Integration into the pavement management system. Canadian Journal of Civil Engineering. 37. 1331-1340. 10.1139/L10-076.

American Association of State Highway and Transportation Officials (AASHTO). (2008). AASHTO Guide for Pavement Friction, first ed., Washington DC.

American Association of State Highway and Transportation Officials (AASHTO). (2015). Standard method of test for measurement of tire/pavement noise using the on-board sound intensity (OBSI) Method, first ed., Washington DC.

American Association of State Highway and Transportation Officials (AASHTO). (2015). Standard method of test for determining the influence of road surfaces on traffic noise using the continuous flow traffic time-integrated method (CTIM), first ed., Washington DC.

Anfosso-Lédée, F., & Do, M. T. (2002). Geometric descriptors of road surface texture in relation to tire-road noise. *Transportation research record*, *1806*(1), 160-167.

ASME B46.1 (2009). Surface Texture (Surface Roughness, Waviness, and Lay) (ASME).

ASTM E1845 (2009). Standard Practice for Calculating Pavement Macrotexture Mean Profile Depth. American Society for Testing and Materials (ASTM).

ASTM E1911 (2009). Standard Test Method for Measuring Paved Surface Frictional Properties Using the Dynamic Friction Tester. American Society for Testing and Materials (ASTM).

ASTM E1960 (2015). Standard Practice for Calculating International Friction Index of a Pavement Surface. American Society for Testing and Materials (ASTM).

ASTM E2157 (2015). Standard Test Method for Measuring Pavement Macrotexture Properties Using the Circular Track Meter. American Society for Testing and Materials (ASTM).

ASTM E2380 (2015). Standard Test Method for Measuring Pavement Texture Drainage Using an Outflow Meter. American Society for Testing and Materials (ASTM).

ASTM E303 (1998). Standard Test Method for Measuring Surface Frictional Properties Using the British Pendulum Tester. American Society for Testing and Materials (ASTM).

ASTM E867 (2012). Standard Terminology Relating to Vehicle-Pavement Systems. American Society for Testing and Materials (ASTM).

ATCO Noise Management (n.d.). Environmental Noise Control. Environmental Management Authority.

Baran, R. G., & Henry, J. J. (1983). *Tire noise and its relation to pavement friction* (No. HS-037

873).

Berglund, B., Lindvall, T., & Schwela, D. H. (2000). New WHO guidelines for community noise. noise & vibration worldwide, 31(4), 24-29.

Bernhard, R, Wayson, R.L. (2005). An introduction to tire/pavement noise of asphalt pavement. Institute of Safe, Quiet and Durable Highways, Purdue University.

Birkner, C., Adesiyun, A., Greene, M., Conter, M., Haider, M., Schmidt, B., Sandberg U., Scharnigg, K., (2016) ROSANNE Final summary report. ROSANNE Deliverable D6.1

Braun, M. E., Walsh, S. J., Horner, J. L., & Chuter, R. (2013). Noise source characteristics in the ISO 362 vehicle pass-by noise test: Literature review. *Applied Acoustics*, *74*(11), 1241-1265.

Brüel & Kjær (1993). Sound Intensity. Copenhagen.

Cerezo, V., Viner, H., Greene, M., Schmidt, B., and Scharnigg, K., (2015). Analysis of data from the first round of tests and initial development of the common scale. ROSANNE Deliverable D1.2

Chandler, J. W. E., Phillips, S. M., Roe, P. G., & Viner, H. E. (2003). Quieter concrete roads: construction, texture, skid resistance and noise. TRL report, 576.

Choubane, B., Holzschuher, C.R., and Gokhale, S. (2004). Precision of Locked-Wheel Testers for Measurement of Roadway Surface Friction Characteristics. Transportation Research Record, 1869.

De Fortier Smit, A. (2008). *Synthesis of NCAT Low-Noise HMA studies.*. Auburn: National Center for Asphalt Technology, pp. NCAT Report 08-01.

Descornet, G. (1989). A criterion for optimizing surface characteristics. *Transportation Research Record*, (1215).

Domenichini, L., Fracassa, A., Torre, F.L., Loprencipe, G., Ranzo, A., & Scalamandrè, A. (1999). Relationship between road surface characteristics and noise emission.

Elsenaar P, Reichert J, Sautery R. Transp. Res. Rec. 1977; 622: 1-25. European Environment Agency. (2019). Exposure of Europe's population to environmental noise

Flintsch, G.W., McGhee K.K., Izeppi, K.L., and Najafi, S. (2012). The Little Book of Tire Pavement Friction.

Federal Highway Administration (1980). *Highway Noise Fundamentals, Noise Fundamentals Training Document*. Washington D.C.: US Department of Transportation.

Gottaut, C., Goubert, L. (2016). Texture-based descriptors for road surface properties and how they can be used in the appropriate standards. ROSANNE Deliverable D4.2

Graf, R.A.G., Kuo, C.-., Dowling, A.P. & Graham, W.R. (2002), "On The Horn Effect of a Tyre/road Interface, Part I: Experiment and Computation", Journal of Sound and Vibration, vol. 256, no. 3, pp. 417-431.

Greene, M., Viner, H., Cerezo, V., Kokot, D., Schmidt, B., (2014). Definition of boundaries and requirements for the common scale for harmonization of skid resistance measurements. ROSANNE Deliverable D1.1

Haider, M., Descornet, G., Sandberg, U., & Pratico, F. G. (2007, September). Road traffic noise emission: recent developments and future prospects. In Proc. 4th Int. SIIV Congress.

Hall, J.W., K.L. Smith, J.C. Wambold, T.J. Yager and Z. Rado (2009). Guide for Pavement Friction. NCHRP Web-Only Document 108. National Cooperative Highway Research

Program, Washington, D.C. Harland, D. G. (1974). Rolling noise and vehicle noise (No. 652 Lab Rpt.).

Hayes, G. G., Ivey, D. L., & Gallaway, B. M. (1983). Hydroplaning, hydrodynamic drag, and vehicle stability. In *Frictional Interaction of Tire and Pavement*. ASTM International.

Heckl, M. (1986). Tyre noise generation. Wear, 113(1), 157-170.

Henry, J.J. (2000). Evaluation of Pavement Friction Characteristics. NCHRP Synthesis 291. National Cooperative Highway Research Program, Washington, D.C.

Hoerner, T., Smith, K., United States, & Applied Pavement Technology, I. (2002). High performance concrete pavement: pavement texturing and tire-pavement noise. Retrieved from http://hdl.handle.net/2027/uc1.31822036169753

ISO 11819-1 (1997). Acoustics – Method for Measuring the Influence of Road Surfaces on Traffic Noise – Part 1: Statistical pass-by Method. International Organisation for Standardisation (ISO), Geneve, Switzerland

ISO 11819-2 (1997). Acoustics – Method for Measuring the Influence of Road Surfaces on Traffic Noise – Part 2: Close Proximity Method. International Organisation for Standardisation (ISO), Geneve, Switzerland.

ISO 13473-4 (2008). Characterization of pavement texture by use of surface profiles – Part 4: Spectral analysis of surface profiles. International Organisation for Standardisation (ISO), Geneve, Switzerland.

Kandhal, P. S. (2004). Asphalt pavements mitigate tire/pavement noise. *Hot Mix Asphalt Technology*, *9*(2), 22-31.

Kogbara, R.B., Masad E.A., Kassem, E. Sparpas A.T. Anupam, K. (2016). A state of art review of parameters influencing measurements and modeling of skid resistance of asphalt pavements. Construction and Building Materials 114 602–617.

Kouchaki, S., Roshani, H., Hernandez, J.B., Prozzi, J.A., *Field Investigation of Relationship Between Pavement Surface Texture and Friction*, 97th Annual Meeting of the Transportation Research Board, Washington, DC, January 7-11, 2018.

Kragh, J., Skov, R., Oddershede J., (2015). Report on the analysis and comparison of existing noise measurement methods for noise properties of road surface. ROSANNE Deliverable D2.3

Kuijpers, A., & Van Blokland, G. (2001, August). Tyre/road noise models in the last two decades: a critical evaluation. In *INTER-NOISE and NOISE-CON Congress and Conference Proceedings* (Vol. 2001, No. 2, pp. 2494-2499). Institute of Noise Control Engineering

Liu, Qingfan, and Shalaby, Ahmed. "Relating Concrete Pavement Noise and Friction to Three-Dimensional Texture Parameters." International Journal of Pavement Engineering 18.5 (2017): 450–458. Web.

Loprencipe, G. and Cantisani, G. (2013). Unified Analysis of Road Pavement Profiles for Evaluation of Surface Characteristics. Modern Applied Science, 7(8).

Mahmoud, E., Gates, L., Masad, E., Erdoğan, S., and Garboczi, E. (2010). Comprehensive Evaluation of AIMS Texture, Angularity, and Dimension Measurements. J. Mater. Civ. Eng., 22(4), 369–379.

Maguire, D.J., P.H.D. & Carme, C., P.H.D. (2015). "LOUDNESS tells you nothing", Ishn, vol. 49, no. 8, pp. 34.

Masad, E. (2005). Aggregate Imaging System (AIMS): Basics and Applications. Texas: Texas Transportation Institute. FHWA/TX-05/5-1707-01-1.

McDaniel, R. (2014). Hot Mix Asphalt Surface Characteristics Related to Ride, Texture, Friction, Noise and Durability. West Lafayette.

McGhee, K. (2012). Virginia quiet pavement study. SURF, Norfolk, VA.

Meyer, W. E., Hegmon, R. R., & Gillespie, T. D. (1972). Locked-wheel pavement skid tester correlation and calibration techniques. *NCHRP Research Results Digest*, (38).

Miller, T., Swiertz, D., Tashman, L., Tabatabaee, N. and Bahia, H. (2011). *Characterization of Asphalt Pavement Surface Texture*. Madison: Transportation Research Board.

National Academies of Sciences, Engineering, and Medicine (NASEM) (2009). *Guide for Pavement Friction*. Washington, DC: The National Academies Press.

Ohiduzzaman, M., Sirin, O., Kassem, E. and Rochat, J. (2016). State-of-the-Art Review on Sustainable Design and Construction of Quieter Pavements—Part 1: Traffic Noise

Measurement and Abatement Techniques. Basel: Molecular Diversity Preservation International and Multidisciplinary Digital Publishing Institute (MDPI).

Ongel, A., & Harvey, J. (2010). Pavement characteristics affecting the frequency content of tire/pavement noise. *Noise Control Engineering Journal*, *58*(6), 563-571.

Rasmussen, R., Benhard, R., Sanberg, U., and Mun, E.P. (2007). The little book of quieter pavements. Washington, D.C.: U.S. Federal Highway Administration.

Rymer, B. C., Donavan, P., & Kohler, E. R. (2010). *Tire/pavement noise levels related to roadway friction improvement* (No. 10-2896).

Sandberg, U. (1980). Road surface influence on tire/road noise-Part I Descornet. *G., Sandberg, U: Road surface influence on tire/road noise-Part II VTI preprint*, (56).

Sandburg, U. (1998). Influence of Road Surface Texture on Traffic Characteristics Related to Environment, Economy, and Safety: A State-of-the-Art Study Regarding Measures and Measuring Methods, VTI Report 53A-1997, Swedish National Road Administration, Borlange, Sweden.

Sandberg, U. (1987), "Road traffic noise—The influence of the road surface and its characterization", Applied Acoustics, vol. 21, no. 2, pp. 97-118

Sandberg, U. (1982, May). Will tire/road noise limit future vehicle noise reductions? In *INTER-NOISE and NOISE-CON Congress and Conference Proceedings* (Vol. 1982, No. 2, pp. 127-130). Institute of Noise Control Engineering.

Sayers, M.W., Gillespie, T.D., and Paterson, D.O. (1986). Guidelines for Conducting and Calibrating Road Roughness Measurements. Work Bank Technical Paper Number 46. The World Bank, Washington, D.C.

Seong, J. C., Park, T. H., Ko, J. H., Chang, S. I., Kim, M., Holt, J. B., & Mehdi, M. R. (2011). Modeling of road traffic noise and estimated human exposure in Fulton County, Georgia, USA. Environment international, 37(8), 1336-1341.

Serigos, P., De Fortier Smit, A. and Prozzi, J. (2014). Incorporating Surface Microtexture in the Prediction of Skid Resistance of Flexible Pavements. *Transportation Research Record: Journal of the Transportation Research Board*, 2457(1), pp.105-113.

Serigos, P., Buddhavarapu, P., Gorman, G., Hong, F. and Prozzi, J. (2016). *The contribution of Micro and Macrotexture to the Skid Resistance of Flexible Pavement*. Austin: Center for Transportation Research, Report No. SWUTC/16/600451-00085-1.

Smit, A., Prozzi, J., Manuel, T., Natalia, Z. and Buddhavarapu, P. (2016). *Designing Quieter Pavement Surfaces*. Austin: Center for Transportation Research, Technical Report No: 0-6819-1.

Texas Department of Transportation (n.d.), 3D Texture Measurement: "Development and Field Evaluation of a Texture Measurement System Based on Continuous Profiles from a 3D Scanning Instrument".

Thomas, L. (2008). MK2 D-type Maintenance Manual. Issue 4, Findlay, Irvine Limited, Scotland.

Van Keulen, W., Duškov, M (2005). Inventory study of basic knowledge on tyre/road noise. IPG Report DWW-2005-022, Delft, the Netherlands.

Wambold, J. C., Antle, C. E., Henry, J. J., Rado, Z., Descornet, G., Sandberg, U., Gothié, M. and Huschek S. (1995). International PIARC Experiment to Compare and Harmonize Skid Resistance and Texture Measurements (Paris: PIARC) Publication number 01.04.T.

Zeller, P. (2009). Handbuch Fahrzeugakustik (Handbook vehicle acoustics). *Vieweg+ Teubner, Wiesbaden*.

Zuñiga Garcia, Natalia (2017). Predicting Friction with Improved Texture Characterization. University of Texas at Austin.